Lehigh University
Lehigh Preserve

Theses and Dissertations

2019

An Investigation of Enhanced Additive Manufacturing Incorporating Spatial Performance Property Control throughout Printed Products

Alaauldeen Ali Duhduh
Lehigh University

Follow this and additional works at: https://preserve.lehigh.edu/etd

 Part of the Mechanical Engineering Commons

Recommended Citation
Duhduh, Alaauldeen Ali, "An Investigation of Enhanced Additive Manufacturing Incorporating Spatial Performance Property Control throughout Printed Products" (2019). *Theses and Dissertations*. 5555.
https://preserve.lehigh.edu/etd/5555

This Dissertation is brought to you for free and open access by Lehigh Preserve. It has been accepted for inclusion in Theses and Dissertations by an authorized administrator of Lehigh Preserve. For more information, please contact preserve@lehigh.edu.

An Investigation of Enhanced Additive Manufacturing Incorporating Spatial Performance Property Control throughout Printed Products

By

Alaauldeen Duhduh

Presented to the Graduate and Research Committee

of Lehigh University

in Candidacy for the Degree of

Doctor of Philosophy

in

Mechanical Engineering

Lehigh University

May 2019

Approved and recommended for acceptance as a dissertation in partial fulfillment of the requirements for the degree of Doctor of Philosophy.

_____
Date

_____
Dissertation Director: Dr. John P. Coulter

_____
Accepted Date

Committee Members:

_____
Committee Chair: Dr. John P. Coulter

_____
Dr. Raymond Pearson

_____
Dr. Sabrina Jedlicka

_____
Dr. David Angstadt

_____
Dr. Majed Alsarheed

ACKNOWLEDGMENTS

A PhD journey is long and includes many obstacles, without support from family and friends, this would have not been possible.

I have to start by thanking my parents (Ali Abdullah Dahdoh and Fatimah Ali Arishi) who have showed me great strength and support throughout my time at Lehigh. I would like to thank my brothers and sisters who have always been there for me.

I would like to thank my wonderful wife Somaya Rajhi, who has shown great strength and support taking care of our kids (Tameem and Sadeem).

I would like to greatly thank my advisor Dr. John Coulter, for his advises and support throughout the years. I have learned a lot from him and he was there for me through the ups and downs.

I would like to thank all my committee members for their advices and guidance. I would like to special thank Dr. Raymod Pearson, who helped me learned a great deal about polymer crystallization.

I would like to thank Mr. Eli Towne and Mr. Dick Towne for their help in the machine shop.

I would like to thank all the department supporting staff (Brianne Lisk, Jennifer Smith, Allison Marsteller and JoAnn Casciano)

I would like to thank all the previous and current members of the manufacturing science laboratory.

Table of Contents

List of Tables:

List of Figures:

ABSTRACT

The overall objective of this research is to investigate and develop a novel additive manufacturing technique that enables additive manufacturing to make products with customizable and gradient properties to match the consumer's needs. This research intends to expand the capability of additive manufacturing by tuning melt rheology. A novel technique called "4D Rheo-Printing" was developed to deliver intelligent printing and melt control of 3D printed parts. This technique has the ability to control the melt flow of each single strand during the printing process and to manipulate the quality of 3D printed parts.

Additive manufacturing (AM) is revolutionizing the way in which products for a variety of applications are designed and manufactured, AM parts are built from the ground up layer upon layer. For polymer based AM, the 4D Rheo-Printing technique expands on this concept by precisely tuning the material properties within each polymer strand of the built up part. This technique adds tunable control of melt rheology and morphology of 3D printed polymeric parts, resulting in tunable mechanical, thermal and biodegradation properties of semi-crystalline polymers.

Using the 4D Rheo-printing technique, shear rate can be tuned precisely at the head of the printer using a rotating nozzle. As a result of shear, molecular orientation and crystallization kinetics can evolve and be controlled to achieve desired outcome. Also, the viscosity of the melt can be tuned by controlling shear rate using the 4D Rheo-Printing technique to enable 3D printing of different materials with single extrusion head. The system can also be used to induce shear rate in order to align fibers to enhance the mechanical properties of 3D printed parts.

The work outlined in this dissertation highlights my contribution to the advancement of the science and technology related to additive manufacturing. These contributions include the design and development of the “4D Rheo-Priting” technique to tune the properties of 3D printed parts, whether by inducing molecular orientation and crystallization kinetics or by printing different materials using single extrusion head.

CHAPTER 1: INTRODUCTION

Additive manufacturing (AM) is revolutionizing the way in which products for a variety of applications are designed and manufactured. For polymer extrusion based additive manufacturing, we have expanded on this concept by developing a novel additive manufacturing technique that is called "4D Rheo-Printing" which enables precise material and physical property control within each deposited polymer strand of the built up structure. This technique adds tunable control of melt rheology which plays a significant role in determining the final mechanical, thermal and biodegradation properties of polymeric products. Shear rate, melt temperature and stage temperature are precisely control in the printing head to optimize and tune the molecular orientation and crystallinity that evolve during the printing process.

It is known that the crystallization of semi crystalline polymers depends strongly on the thermal processing conditions. In 3D printing, melt temperature and stage temperature can strongly effect the overall crystallinity of final products. Printing on a heated bed will not just help parts to stick to the stage but it will increase the overall crystallinity. The longer it takes to print a part on a heated bed the more crystallinity that part will have. Theoretically, the heated bed should be set at the crystallization temperature (Tc) in order to allow the maximum formation of nuclei and accelerate growth of spherulites [1]. The rate of crystallization drops dramatically below the glass transition temperature as the molecular motion becomes so sluggish.

Previous studies performed on different thermoplastic materials have shown that imposing shear rate can orient the macromolecules chains, which enhances the crystallization kinetics and crystal structure of semi crystalline polymers [2–5] thus,

polymeric products properties such as mechanical, physical, and biodegradation properties will be influenced [6]. High shear rate has shown to influence the crystallizations process by facilitating the formation of primary nuclei while very low shear rate has shown no effect on kinetics [4].

The 4D Rheo-printing technique can also be used to manipulate the viscosity of the melt in order to print multiple polymers with single extrusion head. 3-D printing a couple of materials that have different melting temperatures into a single part is challenging, since the temperature of the nozzle has to be tuned constantly to match the melt temperature of the material being extruded to achieve a desired performance. Otherwise, over extrusion or under extrusion will occur due to the different viscosities of the materials. In this research, 3-D printing different materials with single extruder using the 4D Rheo-Printing technique is investigated.

1.1 Purpose of study

Additive manufacturing of plastic materials has been around for decades since 1980s. Since then, many advancements have been invented ranging from developing new materials to increasing the geometry precision of printed parts while increasing the printing speed. From a processing perspective, during the printing process, the changing of viscosity and the evolving of molecular orientation occur due to the shear rate caused by the flow. Also, the viscosity and the molecular orientation are usually uncontrollable, thus, undesirable properties might be obtained. Because of that, the 4D Rheo-printing technique was developed in order to purposely and precisely manipulate the melt rheology during the

printing process to tune the molecular orientation and crystallinity. Therefore, parts with controllable overall properties can be produced using additive manufacturing.

1.2 Research motivation

Additive manufacturing is a promising technology that can easily produce complex devices efficiently because of the nature of its process. It can be used to create objects that fit the consumer needs while no other technique can produce the same parts efficiently. In biomedical applications, additive manufacturing has been used to create tissue engineering, implants and drug delivery systems [7]. Specifically, when dealing with implants, if the parts need to be biodegraded at a specific rate, it has to maintain its mechanical properties and transform the stress gradually until no longer needed. Also, regarding implantable bone scaffolds, the bone will be attached to different parts of the body that have different properties such as cartilages and bones, thus, it is important to produce bone scaffold with properties that mimic the part that will be attached to it. Therefore, it is essential to have a manufacturing technique that can balance all the factors needed to produce successful implantable devices.

This research intends to expand the capability of additive manufacturing to produce precise geometry objects, by adding material property control for each single layer of the printed part to achieve high performance parts with tunable overall properties.

1.3 Methodology

The RheoPrinting concept is aimed at optimizing plastic material properties by controlling the temperature and shear rate history that the polymer melt experiences during the printing process. The nozzle of the 4D Rheo-Printer can rotate at different angular velocities (RPM) to induce varying shear rates as shown in **Error! Reference source not found.**. As a result, the formation and relaxation of the dynamically oriented chains can be tuned via precise shear and temperature control of the material passing through the device.

Axial and circumferential molecular orientation will initially be induced by the screw which mixes the material and pushes it down for extrusion. Additionally, the rotating nozzle induces stretching such as the one founded by Cao[8] to affect molecular orientation in the circumferential direction.

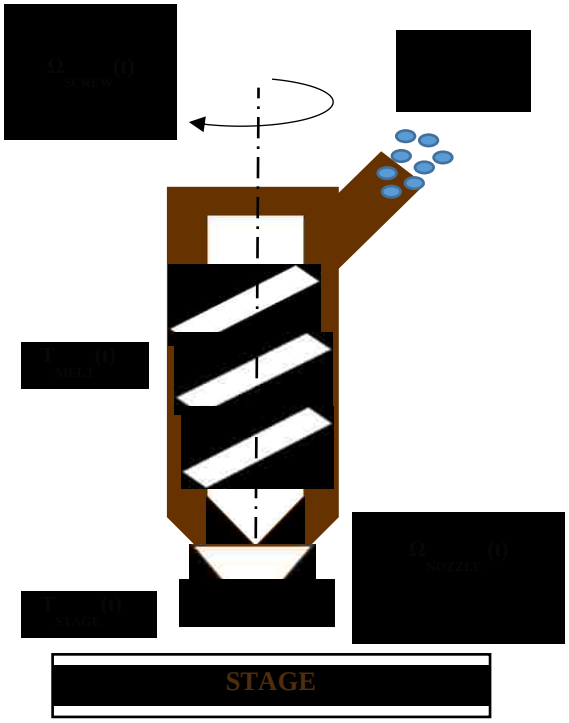

Figure 1-1: Diagram of the Rheo-Printer Concept.

1.4 Program objectives

- To theoretically and numerically investigate the possibility of expanding additive manufacturing to include control over localized product properties.

Prior to developing the 4D Rheo-Printing system, research analysis of the market needs of such system was conducted. Then, numerical simulations using Ansys fluent were conducted to ensure the feasibility of the new technology to manipulate the melt rheology. The results show that the rotating nozzle is capable of manipulating shear rate inside the printer head. Molecular relaxation analysis were also conducted to investigate the relaxation times of the used materials.

Moreover, Avrami analysis were conducted as well to investigate and understand the crystallization kinetics of the material.

- To design and develop a single nozzle system prototype to validate the theoretical system.

The 4D Rheo-Printing system was designed and developed based in the theoretical system. It was built with minimal necessary parts to minimize costs and weight. The system was designed to be used in extrusion based 3D printer with screw extruder, due to its many advantages, which will be discussed later. This system can also be incorporated in fused filament fabrication printers.

- To incorporate such system to actual 3d printers and to experimentally and analytically validate the benefit of the system.

The concept of the 4D Rheo-Printing system was validated experimentally. The experimental results proved the capability of the machine to tune the properties of the final printed parts by tailoring shear rate and thermal processing conditions. Furthermore, other significant capabilities of the machine was discovered and it was investigated as well.

1.5 Dissertation structure

This dissertation presents the design, development and validation (analytical and experimental) stages of the 4D Rheo-Printing system. It consists of eight chapters including the introduction. It is structured as follows:

- CHAPTER 2 details history of additive manufacturing, different types of additive manufacturing and their limitations, additive manufacturing materials, additive manufacturing applications and the challenges of additive manufacturing.
- CHAPTER 3 describes related scientific fundamentals of polymer melt rheology and morphology.
- CHAPTER 4 presents the design and development of the 4D Rheo-Printing system. It also presents the system as workable prototype for market evaluation.
- CHAPTER 5 investigates numerically the capability of the 4D Rheo-Printing system to tune the melt rheology of polymeric materials.
- CHAPTER 6 presents experimental results of the 4D Rheo-Printing system. It also contains experimental investigation of the crystallization kinetics of the PLA materials under quiescent conditions.
- CHAPTER 7 discusses market analysis and the feasibility of commercializing the described system.
- CHAPTER 8 presents conclusion regarding all the work completed and the impact of this research. It also presents future work and suggestions related to the 4D Rheo-Printing system.

CHAPTER 2:Background

2.1 Additive manufacturing technology

There are several polymer processing technologies currently in use. One of the most emerging technologies is additive manufacturing. Additive manufacturing also usually goes by 3-D printing is the process of creating objects layer upon layer [9]. It is also known as rapid prototyping and rapid manufacturing [10]. It works by transforming a digital 3-D model into a solid three-dimensional object. The process doesn't include any cutting or parts assembly, which is one of the main advantages of additive manufacturing. This enables additive manufacturing to produce parts with complex geometries that are hard or impossible to be produced with other manufacturing processes. Also, it allows the production of parts efficiently since no waste is produced by cutting compared to the other manufacturing processes.

The versatility of AM is seen in its ability to reproduce virtually any shape from a Computer-Aided Design (CAD) model. This process is in stark contrast to subtractive manufacturing, the process of producing parts through the removal of material seen in cutting and milling operations, which has traditionally dominated the manufacturing industry. AM is based largely around the 3D modeling CAD software, which can be performed through a variety of licensed software such as AutoCAD and SolidWorks. Open source CAD software is also available for users who do not have access to licensed software such as Google sketch and Free CAD. A typical 3D printer will only be compatible with a Stereo Lithography (STL) formatted file. The STL file is run through a

software called "slicer," which converts the model into a layered format and creates a G-code file containing instructions customized to a specific type of 3D printer [11]. At this stage, the file is ready for printing and when it is complete may require post processing to improve the overall quality of the piece.

This chapter provides an introduction into existing additive manufacturing technologies as well as current applications of these technologies.

2.2 Additive manufacturing processes

This section will cover a comprehensive overview of the different types of 3-D printing technologies that currently exists in the market.

Fused filament fabrication (FFF), also known as fused deposition modeling (FDM), was developed by Scott and Lisa Crump in 1989 with the term FDM trademarked by Stratasys. FDM is categorized as a material extrusion operation. Material is selectively dispensed through a nozzle or print head that moves in three dimensions to construct a part layer by layer. The extruded material is a thermoplastic filament, such as Acrylonitrile Butadiene Styrene (ABS) or Polylactide (PLA).

Dual extruders can also be used to construct parts with two colors or create support material. Support materials are used to prevent the falling of overhanging parts. This temporary support structure can be removed manually or with chemical processing. With the use of support material, designs can become complex and contain interlocking, interlinking, and movable parts [15]. Overall, FDM is a very affordable and versatile technique. The major drawbacks of this method are rough surface quality of and micro-

gaps that exist between the layers and that can result in leakage. The diagram detailing the process can be found in Figure 2-1.

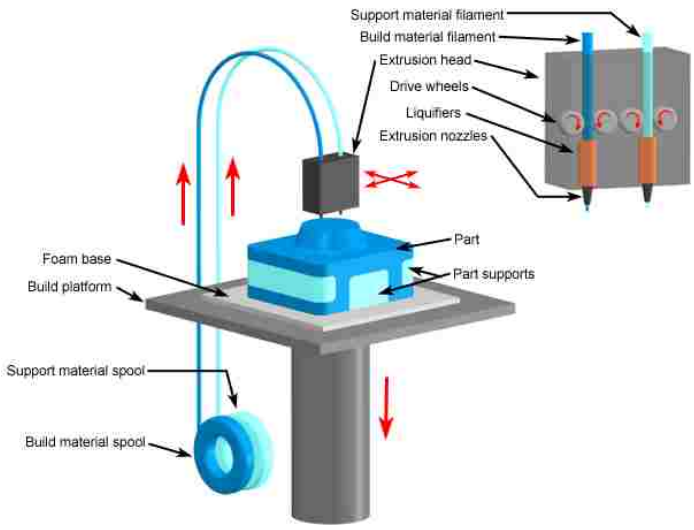

Figure 2-1: Schematic diagram of the FDM process.

Another extrusion-based 3D printers are the one developed in this study which is equipped with screw extruder. The main benefit of this printer over FFF is that it enables the use of different variety of materials in their granulated form. It also cut one of the manufacturing processes of FFF, which is the filament fabrication. As a result, parts can be built cheaply. This type of printers is also able to print big parts more efficiently since it is able to increase the flow rate dramatically. In this case, it will increase the layer thickness and limit the number of layers used to fabricate an object and therefore reduce printing time. One of the limitations of this technique is that the diameter of the layer thickness can fluctuate during the printing process due to the feed rate not being consistent. This will be discussed broadly later in the next chapters. A diagram of this technique is shown in Figure 2-2.

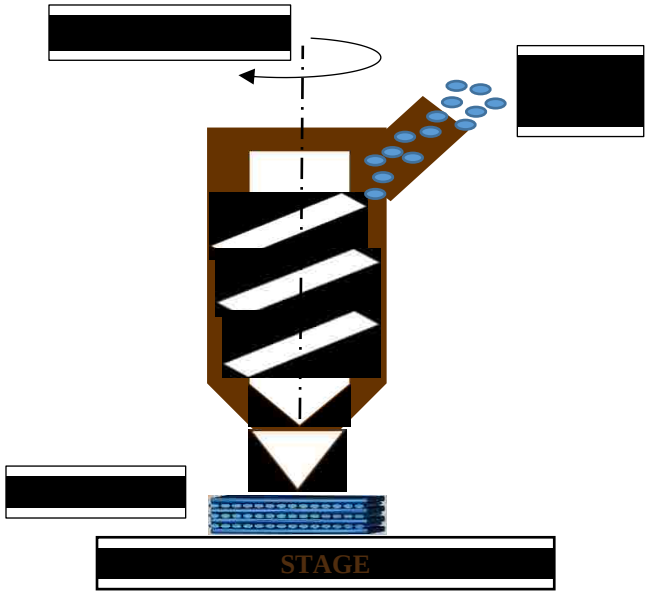

Figure 2-2: Diagram extrusion-based printer with screw extruder.

Selective laser sintering (SLS) was invented at the University of Texas at Austin by Joe Beaman and Carl Deckard in 1986 [12]. SLS is categorized as a powder bed fusion process which produces objects from powdered materials using one or more lasers to selectively fuse or melt the particles at the surface, layer by layer, in an enclosed chamber. The SLS process uses a bed of small particles made of plastic, metal, ceramic, or glass. The plastic particles used in SLS can only be selected from a few polymers, such as nylon and polystyrene. The interior of the printer is heated up to just below the melting point of the powder of your choice. The printer then spreads out an incredibly fine layer of this powder and a high-power laser traces one layer at a time, fusing the small particles. The rest of the particles not hit by the laser continue to remain loose [11]. A new layer of loose particles is added to the surface by a roller and are ready for tracing. After the printing job is finished, post processing is required to remove the un-sintered powder. A key advantage to SLS is that there is no need for support material, since the sintered nylon is suspended in a powder

which acts as its own support. Designs can become complex and contain interlocking, interlinking, and movable parts. The diagram detailing the process can be found in Figure *2-3*.

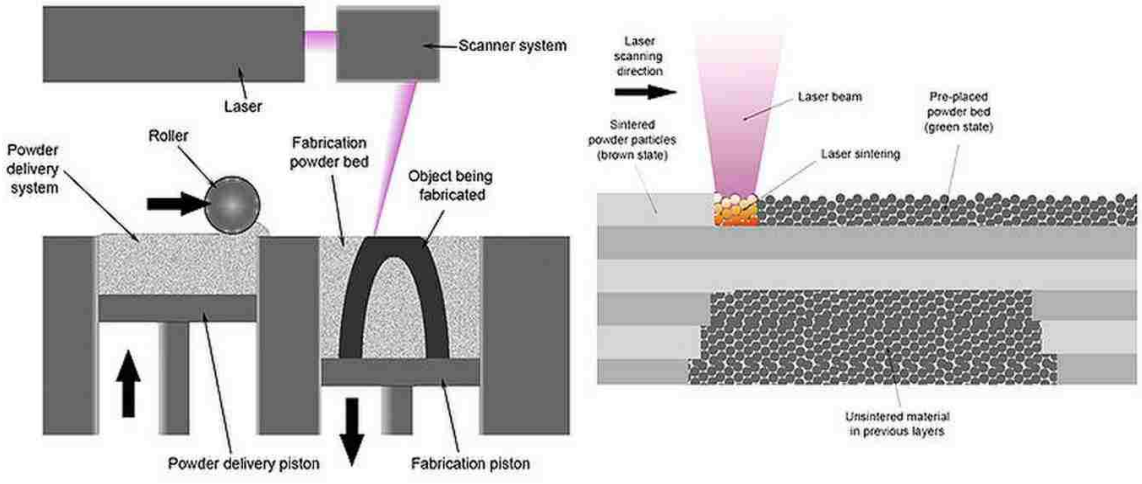

Figure 2-3:Schematic diagram of selective laser sintering [5].

Stereolithography(SLA) was developed by Charles Hull in the 1986 who is also the founder of 3D Systems [13]. SLA is categorized as a vat photo polymerization process where liquid photopolymer in a vat is selectively cured by light-activated polymerization. The SLA process takes place in a large tank and begins with a layer of liquid polymer spread over a platform. In the SLA system, a laser travels through the liquid photo-resin, curing the part while the rest of the layer stays liquid. The platform is then lowered and the next layer is drawn directly on top of the previous one. Support material for overhanging parts is needed and will then be removed manually during post processing. Design freedom for this technology is somewhat limited due to the support material. SLA only works with polymers and resins, not metals. The main advantages of materials printed with SLA are

smooth surfaces and high about of detail. The major drawback to SLA is the manual removal of support structures and a lot of finishing. The diagram detailing the process can be found in Figure 2-4.

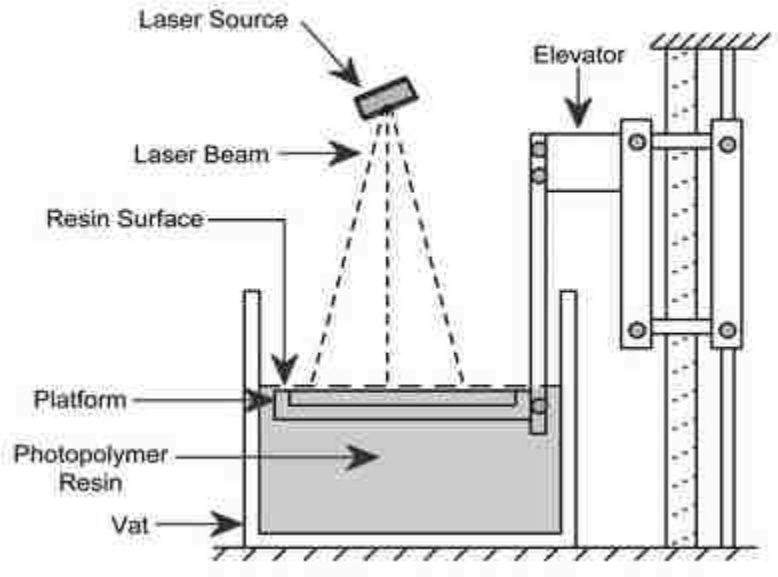

Figure 2-4: Schematic diagram of SLA printing process [14]

Another type of printers is called direct energy deposition (DED) or direct metal deposition. This type of printers is commonly used to make objects out of metals and alloys. Also, it can make parts out of glass and ceramic but it is not common for that [15]. In addition to making new objects, these types of printers can add materials to existing objects [16]. This type of printers is commonly utilized to repair existing parts. The process of DED is similar to the material extrusion discussed previously, where there is a nozzle that supply the material. The nozzle supplies the material in a wire form, and there is a beam used to melt the material which is supplied by an electron beam projector. The nozzle and

the beam projector move together and follow the shape of the object being fabricated. A schematic diagram of the direct energy deposition process is shown in Figure 2-5.

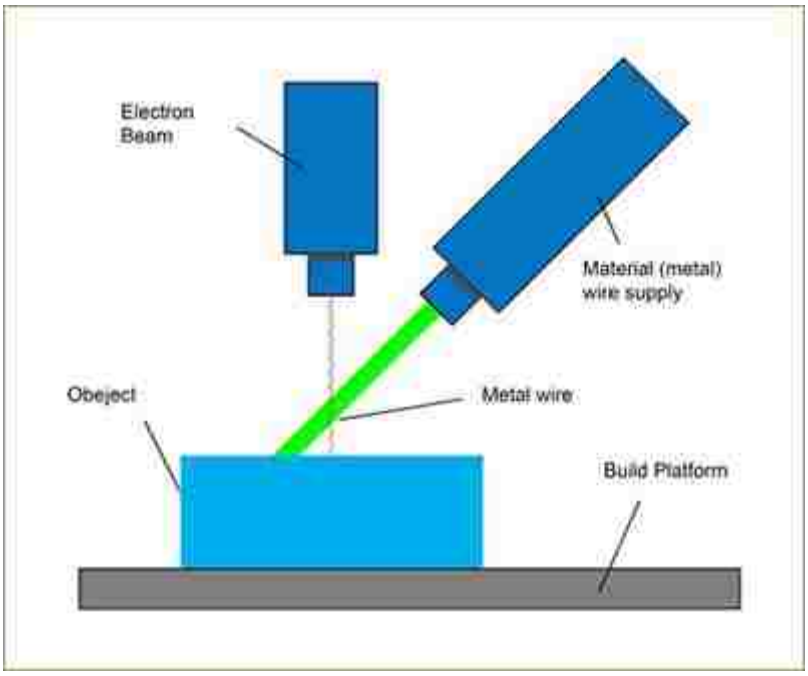

Figure 2-5: Schematic diagram of Direct Energy Deposition [17].

2.3 Additive manufacturing materials

Additive manufacturing uses different materials to create objects. Materials such as thermoplastics polymers, metals, ceramics and biochemical have all been used to fabricate objects. Thermoplastic polymers such as Acrylonitrile butadiene styrene (ABS), Polylactic acid (PLA) and Polycarbonate (PC) are the most used materials in additive manufacturing.

2.4 Additive manufacturing applications

Additive manufacturing has been used to fabricate products in many fields such as automotive, aerospace, dental and medical industries. AM allows engineers to design and create new objects that were hard to produced.

The automotive industries use additive manufacturing to make concept models and prototypes. For example, the car's dashboard was designed with the help of 3D prototypes to make sure it fits perfectly. Lately Mercedes-Benz started 3d printing spare parts for classic models [18]. Usually cars manufacturers stop production of spare parts for cars after 10 years of last production, since it costs them a lot to store these spare parts and the demand is low to justify the increase of storage costs. So, using 3D printing is a smart move to fabricate spare parts for classic cars on demands to eliminate waste and reduce storage costs.

In the aerospace industry, the use of AM is increasing to produce parts for many reasons such as efficiency and weight reduction. Not long time ago, AM has been used only for prototypes in the aerospace industry. GE Aviation has developed a fuel nozzle using 3D printing as shown in Figure 2-6. These nozzles used to be assembled out of 20 parts, with additive manufacturing it was reduced to just one part [19], which saves a lot of time and energy.

Figure 2-6: GE Additive fuel nozzle [20].

One of the application of additive manufacturing in the dental industries is the use of 3D printers to make Invisalign® braces, which is one of the most popular 3D printed products that is used to correct bites instead of the metal braces. These types of braces allows for continent and flexibility which traditional braces didn't have, since they can be assembled or removed at any time. Also, each aligner is customized for an individual.

In the medical industry, the use of 3D printing is very promising and developments in this area are progressing rapidly. Some of the most popular applications of AM in the medical industry are shown in Figure 2-7. Customized hearing aids are 3dprinted to fit the patient ear because every patient has different ear canal. Customized Knee replacements have also been 3D printed. It can be customized to fit more like the natural knee which reduces the surgery time, because less bone cutting is required, and makes it less painful

for the patient [21]. In the medical industry, additive manufacturing holds a great promise compared to traditional manufacturing processes since it can build customized medical parts in real time with less costs.

Figure 2-7: 3-D printed medical parts.

Another promising area for additive manufacturing is in the manufacture of tissue engineering scaffolds. Tissue engineering and 3D printing are very important to the future of medicine for many reasons such as:

1. Shortage of available organ donors [22].

   Tissue engineering and additive manufacturing have the potential to be able to make organs on demands.

2. Rejection of donated organs.

Sometimes when a patient gets an organ from a donor, the patient's immune system recognizes the organ as foreign and tries to reject it. That is not an issue in tissue engineering since the cells were taken from the same patient. Additive manufacturing has been used to create biomaterial tissue scaffolds. The scaffold is one of the three crucial components in the process of engineering a successful tissue, the other two of which are the cells themselves and growth-stimulating signals. "Scaffolds, typically made of

polymeric biomaterials, provide the structural support for cell attachment and subsequent tissue development" [23]. Tissue scaffolds help to promote the integration of the engineered tissue into the existing component of the body that it is implanted into. They provide a framework to contain the cells while they grow, as well as promote a direction for growth of the cells, so that the engineer tissue patch can become biologically fused with the body part. "Without a foundation to support and guide cells in a path specific to the target organ, it is nearly unattainable to generate functional tissues" [24]. In addition, for tissue scaffold to serve the previously mentioned purposes, the tissue scaffold should also biodegrade at a rate equivalent to the growing or the healing rate of the organ. Tissue scaffolds are designed with pores to "maintain optimal nutrient supply, gas diffusion, active cell proliferation and metabolic waste removal" [24]. Additive manufacturing allows for better design flexibility and properties control which ensure the manufacture of successful scaffolds.

2.5 Factors affecting Additive manufacturing parts properties

3-D printing has been used mostly to fabricate prototypes because of its poor final product properties. Many researchers have been studying the factors that affect the properties of the 3-D printed final products to achieve the required mechanical properties and the performance criteria. Factors such as extrusion rate, nozzle height from the bed, nozzle temperature, bed temperature and raster angle are expected to have an effect on the mechanical properties, optical properties, dimensional accuracy and the biodegradation rate of the final product. It is very important to know which factors have the most effect on

the 3-D printed products quality since 3-D printing holds great promising in many areas such as medical field.

Extrusion rate and nozzle height from the bed were found to affect the dimensional accuracy. As the extrusion rate increases the material width coming out of the nozzle will increase [25]. Also, raising the nozzle height from the bed will result in thinner printed lines. Every polymer will behave differently, even the same polymer from different suppliers will behave differently. In order to find the optimum line width, trial and error might be performed. Extrusion rate also affects the viscosity of the polymer. Since polymers are non-Newtonian shear thinning, any increase on extrusion rate will result in more shear and less viscosity which will affect the properties of the 3-D printed parts. Since shear rate induces molecular orientation, and molecular orientation is known to affect the mechanical properties, optical properties, and biodegradation rate of fabricated parts. A study was conducted to study the effect of the printing speed on maximum stress [26]. It was found than as the printing speed increases, the maximum stress increases Figure 2-8 [25]. A hypnosis was suggested that the reason of this increase in maximum strength is due to adhesion between the small filaments constituting the infill is better because the material has had less time to cool down between each passage with the faster printing speed [25].

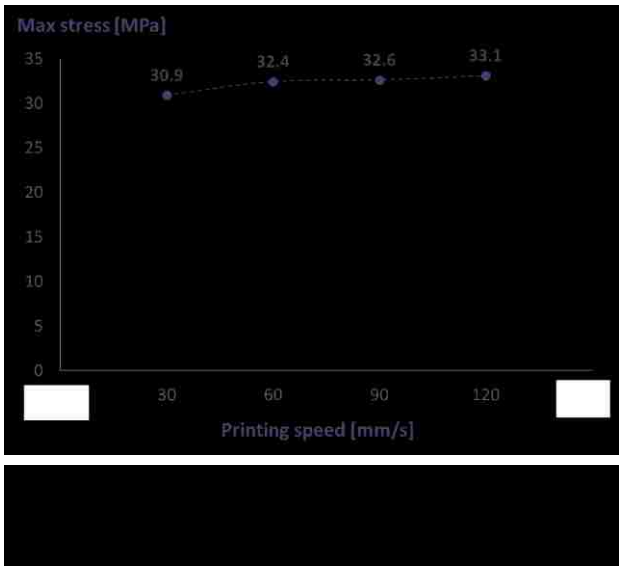

Nozzle Temperature is a very important factor to consider because it affects the flow rate Figure *2-9* [27]. Lower temperature than the polymer melt temperature might result in no flow issues. On the other hand, a temperature higher than the melting point of the polymer might result in material degradation and also a viscosity that is lower than needed which will affect the quality of the print. Moreover, different nozzle diameters require different nozzle temperatures. A 0.2 nozzle diameter will require less polymer viscosity to extrude material than 0.8 nozzle diameter.

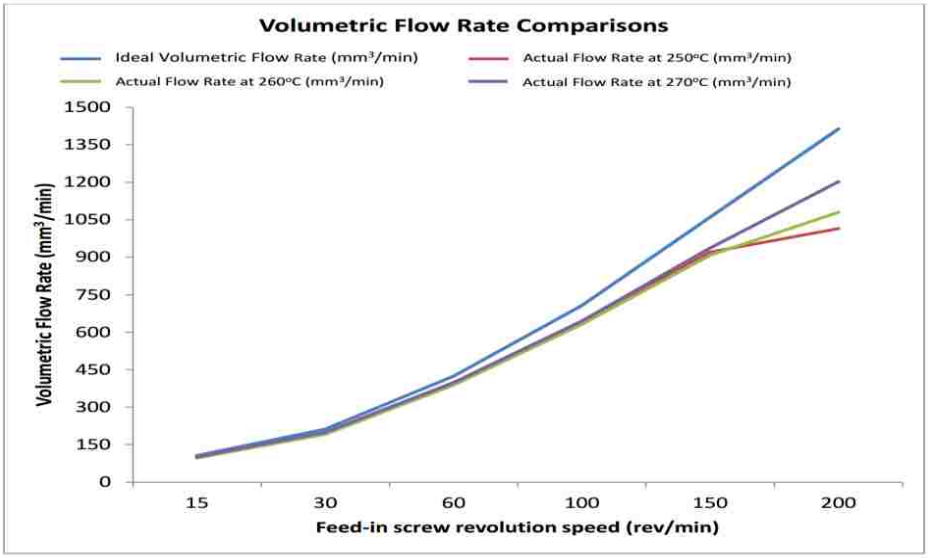

Figure 2-9: Flow rate vs screw speed.

After extrusion, the material is directly exposed to the room temperature which will affect the print quality. In order to reduce the effect of room temperature on print quality and to help the material stick to the stage, a heated bed should be used. Heated beds are used to allow the material to stick to the bed, also, it allows for crystallinity enhancement when dealing with semi crystalline polymers.

Raster angle has also an influence in the mechanical properties of the 3-D printed parts. A study was performed to study the effect of raster angle and layer thickness on the mechanical properties of the products [28]. They collected samples with raster angles of 0″ /90″, 30″ /60″ and 45″ /´45″. The study was conducted using PEED samples. The maximum mechanical strength was found at 0/90 raster angle while the lowest mechanical strength at 30/60 Figure 2-10 [28].

Factors		Tensile strength (MPa)	Bending strength (MPa)	Compressive strength (MPa)
Layer Thickness (μm)	200	40.1	52.1	53.6
	300	56.6	56.1	60.9
	400	32.4	48.7	54.1
Raster Angle (°)	0°/90°	56.6	56.1	-
	30°/−60°	41.8	48.5	-
	45°/−45°	43.3	43.2	-

Figure 2-10: The influence of different raster angles and layer thickness on the mechanical properties.

2.6 Investigation of targeted process

2.6.1 Extrusion based 3d printers.

The targeted AM processes to be modified in this project are extrusion-based 3D printers. As mentioned earlier extrusion based 3d printers extrude polymeric materials through a nozzle. There are two types of them, one that used filaments which is called FFF, and the other uses pellets instead of filaments, which is equipped with screw extruder. The latter technique has an advantage over FFF since it cuts one of the manufacturing processes which is the filament fabrication. As a result, parts can be produced efficiently. The technique that was investigated, developed and modified in this project is the extrusion based 3D printers equipped with screw extruders.

2.7 Additive manufacturing challenges

Challenges present opportunities. Despite all the advantages of AM, it still has its challenges which are the followings:

- Lower performance of products compared to traditional manufacturing processes.
- Lack of material property control.
- Inability to locally control melt rheology and morphology.

These challenges are the motivation of my work. According to literatures, there are many factors that have been proven to affect the properties of the printed parts as mentioned earlier in this chapter, most of these literatures focused on enhancing the properties of the whole printed part. In this project, we are investigating the capability of AM to tune the material properties for each single layer within one part.

CHAPTER 3: Related Scientific Fundamentals

The structure of this chapter is organized as follows: First, an introduction to polymers and polymer melt rheology. Then, molecular structure of polymers is introduced and the different characteristics of each one. After that, theoretical approaches that are used to investigate the crystallization kinetics and relaxation times of molecules are investigated. Then, a detailed description of characterization techniques that are used to characterize polymer crystallinity is explained. After that, the proposed innovation is described.

3.1 Related processing issues

3.1.1 Polymer melt rheology

Polymers are long chains molecules with high molecular weight, because of that the term macromolecules is usually used to indicate polymeric materials [29]. Polymers can be classified to three groups thermoplastics, thermosets and elastomers [30].

Thermoplastic materials can be melted and solidified by heating and cooling repeatedly. The molecules in thermoplastics are held together by weak secondary bonds or molecular forces; the secondary bonds can be broken when the material is heated above its melting point. The focus of this study is on this type of materials.

Thermosets materials form chemical crosslinks, these crosslinks reaction bind the polymer molecules together in three dimensional network [31]. Thermosets may soften when reheated but they will not melt again. Figure *3-1* demonstrates the viscosity temperature behavior of thermoplastics and thermosets. The viscosity of thermosets will start dropping when the material is heated such like thermoplastics until it reaches a certain

point where crosslinks reactions begin. Eventually, the viscosity starts to increase with increasing heat because the crosslinks binds the molecules together and limit their movements [31].

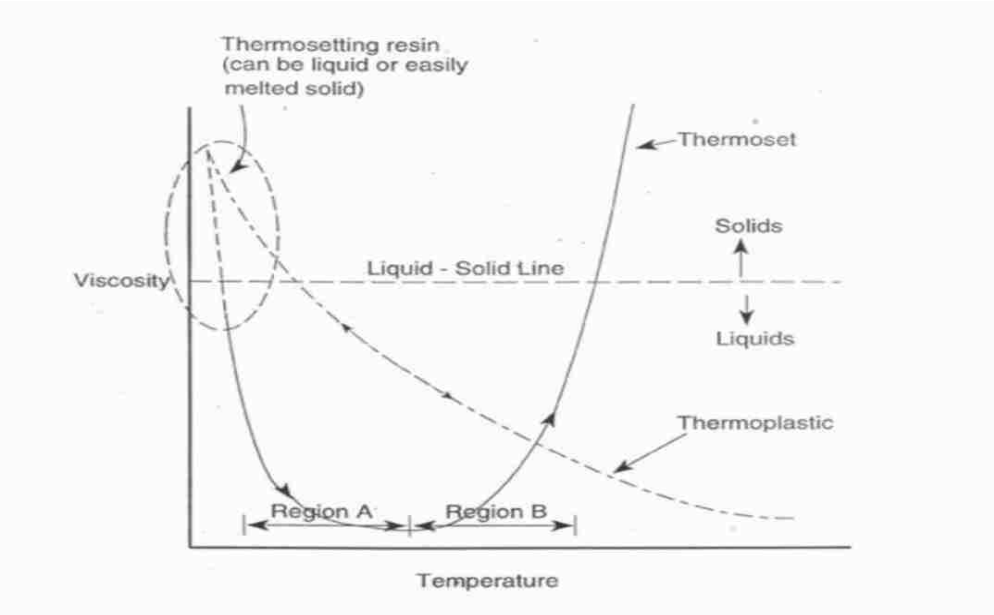

Figure 3-1: Viscosity vs temperature behavior for thermoplastics and thermosets [3].

Elastomers are the materials that can be stretched to over twice their regular length and then when released they can return to their original length. They can be either thermoplastics or thermosets [31]. Elastomers have few strong interactions between molecules and have flexible molecules chains. Figure *3-2* demonstrates the stress strain behavior of elastomers compared to other plastics.

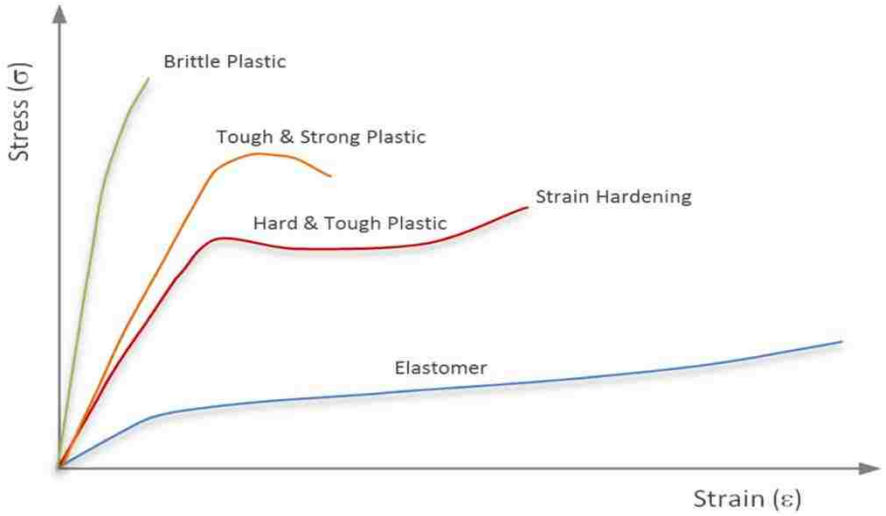

Figure 3-2: Stress strain curve of polymers [32].

3.1.1.1 Non-Newtonian fluids

Viscosity is the resistance to flow, and it is defined by shear stress over shear rate. Fluids can be classified based on their viscosity behavior with shear rate and temperature to two types Newtonian and Non-Newtonian fluids. The viscosity of Newtonian fluids is constant with changing shear rate. On the other hand, the viscosity of Non-Newtonian fluids is affected by shear rate in addition to temperature. Non-Newtonian fluids can be shear thinning or shear thickening. Figure *3-3* illustrates the difference between shear thinning (Pseudo Plastics Non-Newtonian), shear thickening (Dilatant non-Newtonian) and Newtonian fluids [33]. The focus of this research is on Pseudo Plastic Non-Newtonian or shear thinning materials.

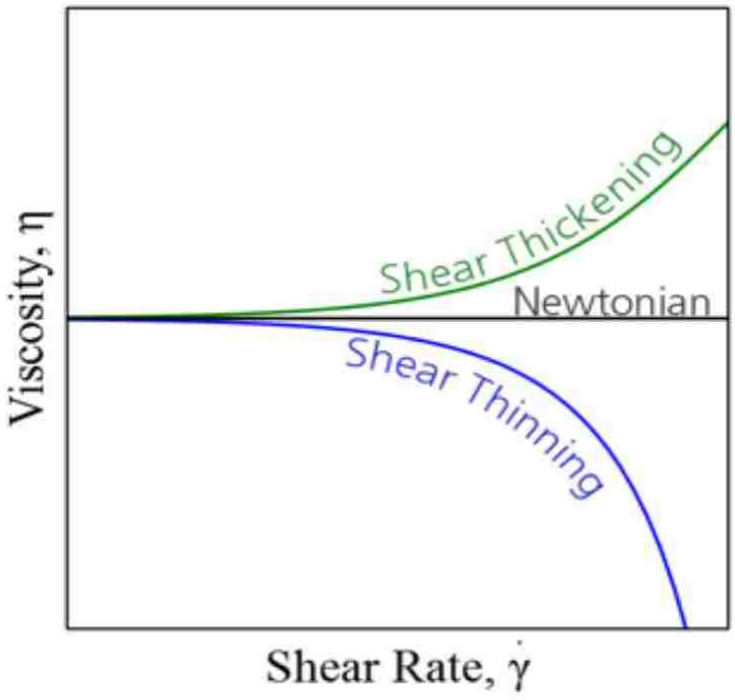

Figure 3-3: Viscosity vs. Shear rate comparing Newtonian, shear thinning and shear thickening fluids [34].

Shear rate causes the molecular chains to orient in Pseudo Plastics Non-Newtonian fluids which allows them to pass each other freely. As a result, viscosity drops and the entanglement is reduced. At very low and very high shear rate, Non-Newtonian shear thinning materials typically acts as Newtonian as shown in figure 4; their viscosity will be independent of shear rate [35].

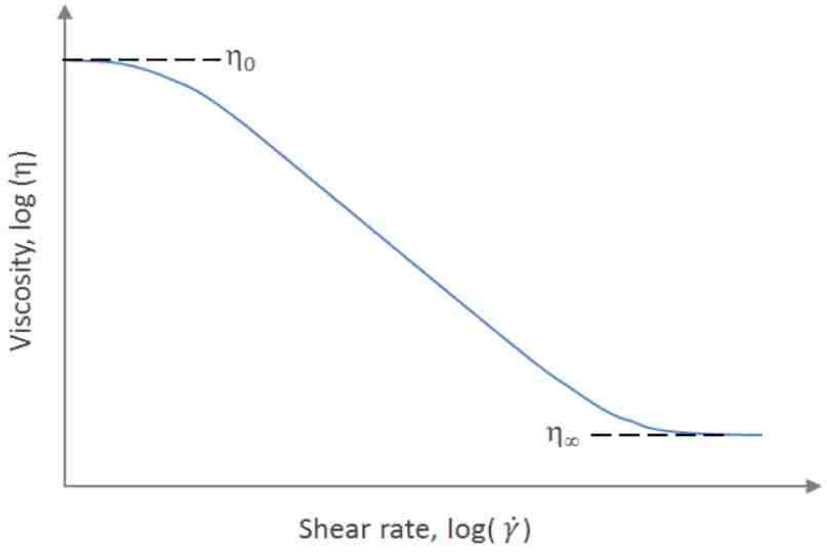

Figure 3-4: The effect of shear rate on viscosity of Pseudo plastics non-Newtonian fluids.

3.1.1.2 Viscoelastic behavior

Viscoelasticity is the property of the material that exhibit both viscous and elastic behavior. Polymers are viscoelastic, their mechanical properties change with temperature as the material undergoes a transition between different physical states [36]. Figure 5 shows the five distinct regions of viscoelasticity of an amorphous polymer with (Tg = 363 K). It shows the stiffness of the polymer when undergoes different temperatures.

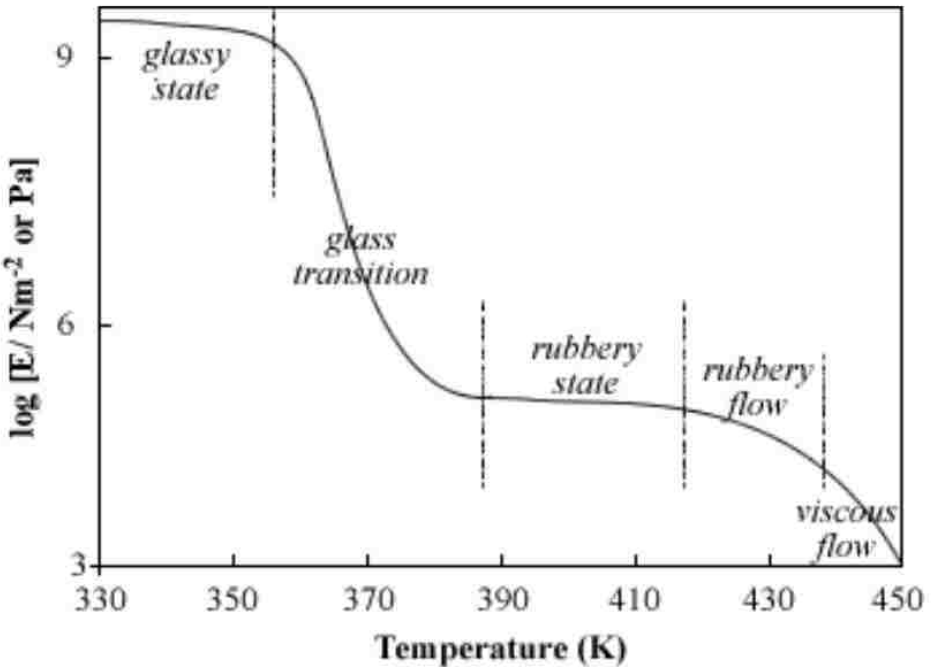

Figure 3-5: Viscoelastic behavior of an amorphous polymer [36].

At low temperature below the glass transition temperature, the modulus is high and the material acts as elastic solid. As the temperature goes above the glass transition temperature, the molecules will start to move slightly and that results in a decrease in the modulus.

After the glass transition region comes the rubbery region or rubbery plateau where the modulus remains constant, the appearance of rubbery plateau is the result of entanglements or crosslinks [37]. The rubbery plateau is also related to the degree of crystallinity of polymers, where the behavior of a modulus as a function of temperature of a semi crystalline polymer is similar to that of a high molecular weight amorphous polymer [37].

After the rubbery plateau region comes the rubbery flow region and viscous flow region respectively. The modulus decreases one order of magnitude in the rubbery flow region with increasing temperature, while in the viscous flow region a noticeable drop in the modulus is observed.

The shape of the curve shown in Figure *3-5* is similar for all amorphous polymers [36]. Crystalline materials behave differently with temperature as shown in Figure *3-6*. A fully crystallized polymer does not go thorough glass transition temperature, it will act as elastic solid until the temperature reaches the melting temperature.

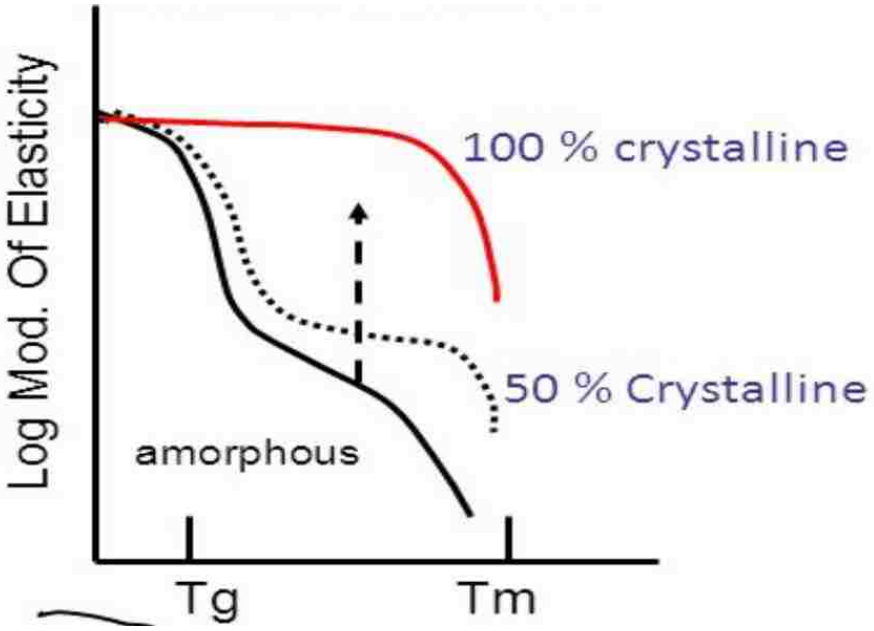

Figure 3-6: Viscoelastic behaviors of amorphous, semi crystalline and crystalline polymers [38].

3.1.2 Molecular orientation and relaxation

3.1.2.1 Introduction

Polymers are long chain molecules and their molecular structure dictates their characteristics properties [39]. It is well established that molecular orientation and relaxation play a significant role in determining end use properties of polymeric materials such as mechanical, optical and biodegradation properties [40,41]. Also, it is known that molecular orientation is obtained due to shear rate during polymer flow. Then, if viscosity is low enough after shear flow, chain molecules will relax which means they will go back to their original shape [42].

3.1.2.2 Theoretical approaches

3.1.2.2.1 Reptation and chain motion

The reptation theory was first introduced by deGennes and then it was extended to the tube model by Doi and Edward [43]. It describes the motion of a molecule that is entangled with other neighboring molecules [44], where the motion of an entangled polymer molecule looks like the motion of a polymer in a tube [43] as shown in Figure *3-7*.

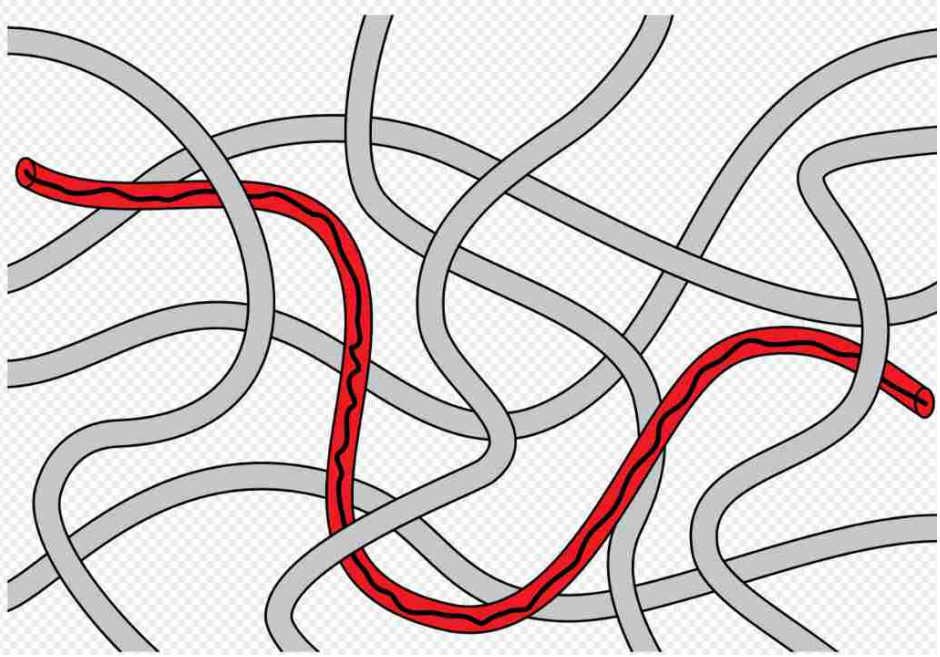

Figure 3-7: Model for reputation [45].

The tube model assumes that the chain moves randomly along the tube and the motion of each molecule is independent of the neighboring molecules. Also, it assumes that the lateral motion can be neglected [43].

3.1.2.2.2 Molecular relaxation times

There are several models to estimate the relaxation times of polymers such as rouse model and Doi-Edward model. Rouse model is best used for polymers with low molecular weight, since it can't predict the relaxation of polymers with high molecular weight. On the other hand, Doi-Edward model can be used to predict the relaxation of polymers with high molecular weight [46] [47]. As stated before, Doi-Edward model is based on Reptation theory where the motion of a molecule is restricted by the neighboring molecules. The relaxation time can be calculated using the following formula: [47]

$$\tau = \frac{15Me\eta 0}{\pi 2\rho RT}$$

Where,

$\eta 0$: zero shear viscosity.

Me: Molecular weight between entanglements.

ρ: Density

R: Ideal gas constant

T: temperature

3.1.3 Crystallinity

3.1.3.1 Introduction

Thermoplastic polymers can have different varieties of microstructures such as amorphous, crystalline and semi-crystalline.

An amorphous polymer is composed of randomly aligned polymer molecules and it doesn't contain any crystalline region. Moreover, amorphous polymers have flexibility and elasticity due to their random molecular alignment. Amorphous materials go through the second order transition which is the glass transition temperature [29]. The glass transition temperature (Tg) is defined as the temperature in which the material will transform from glassy to rubbery while heated; it constitutes the most important mechanical properties of amorphous polymers.

Crystalline polymers have an ordered molecular structure compared to the amorphous polymer as shown in Figure *3-8*. Their structure gives them their strength and

rigidity [48]. They are known to exhibit the first order transition known as melting. Figure *3-9* demonstrates the melting temperature of crystalline materials and the glass transition temperature of an amorphous material.

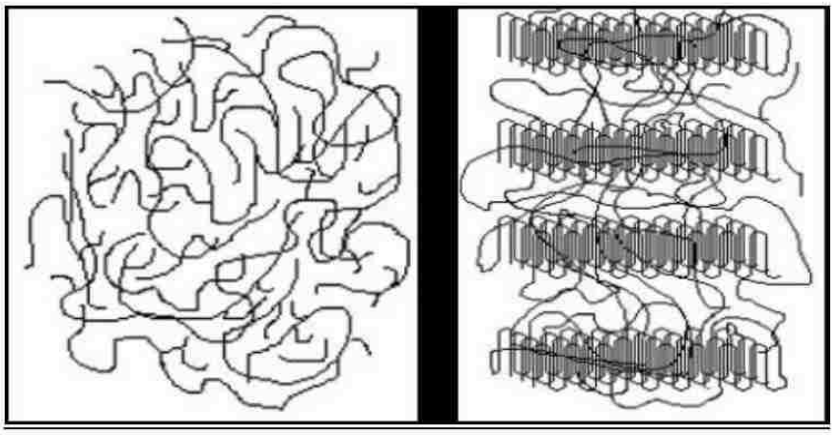

Figure 3-8: Left, an amorphous region. Right, semi crystalline region that contains an amorphous and crystalline structures [49].

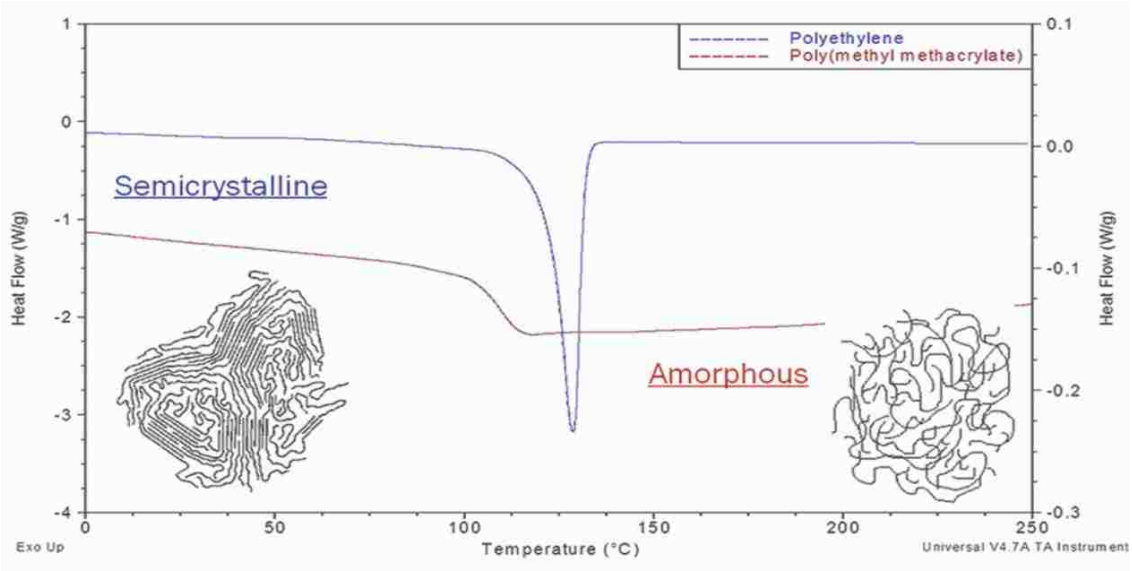

Figure 3-9: DSC of a melting endothermic of crystalline polymer and glass transition of an amorphous polymer [39].

The microstructure of semi crystalline materials contains both crystal and an amorphous structure as indicated in Figure *3-8*. Thus, semi crystalline polymers exhibit both glass transition temperature and melting temperature. The glass transition temperature is usually higher in semi crystalline polymers relative to the amorphous polymers. Since semi crystalline polymers contain both amorphous and crystalline structure, their characteristics properties highly depend on their degree of crystallinity, size and orientation of their molecular chains.

3.1.3.2 General characteristics properties of amorphous and crystalline polymers

Amorphous polymers exhibit different characteristics than crystalline polymers Table *3-1*. Table shows general characteristics of amorphous vs crystalline polymers. Regarding the properties of semi crystalline polymers, the properties will depend greatly on the amount of crystallinity. If the amount of crystallinity is high, the material will show characteristics similar to the crystalline polymers and vice versa.

	Amorphous Polymers	**Crystalline Polymers**
Appearance	Transparent	Opaque
Toughness	Higher Toughness	Lower Toughness
Shrinkage	Low Shrinkage	High Shrinkage
Glass Transition Point	Sharp Glass Transition Temp.	Less Sharp Glass Transition Temperature
Melting point	No Melting Point	Melting Temperature

Table 3-1: Amorphous vs Crystalline Polymers

As shown in Table *3-1*, amorphous materials exhibit different characteristics than crystalline materials. Amorphous polymers are the right choice when flexibility is required

due to its high toughness; where toughness is the ability to bend without breaking. On the other hand, when hardness is required, crystalline polymers are the right choice. It is important to select the correct types of plastics based upon the requirement of the applications.

3.1.3.3 Factors affecting polymer crystallization

Crystallization is the process of forming crystals. From a thermodynamic perspective, every system is trying to lower its energy. Crystallization causes the entropy to decrease since there is a considerable ordering of polymer crystals, and also the enthalpy decreases as well during the crystallization, which can be explained by Gibbs free energy as shown in equation [30]. The Crystallization becomes favorable when the amount of change in enthalpy is greater than that of the entropy change, since it will cause a lower value of G.

$$\Delta G = \Delta H - T.\Delta S$$

For any phase transformation to occur, the value of ΔG should be negative under constant temperature and pressure. The crystalline state exists at lower free energy below the melting point, while above the melting point, the liquid state exists at lower free energy as shown in Figure 3-10 [50]. Also, the equilibrium occurs at the melting point.

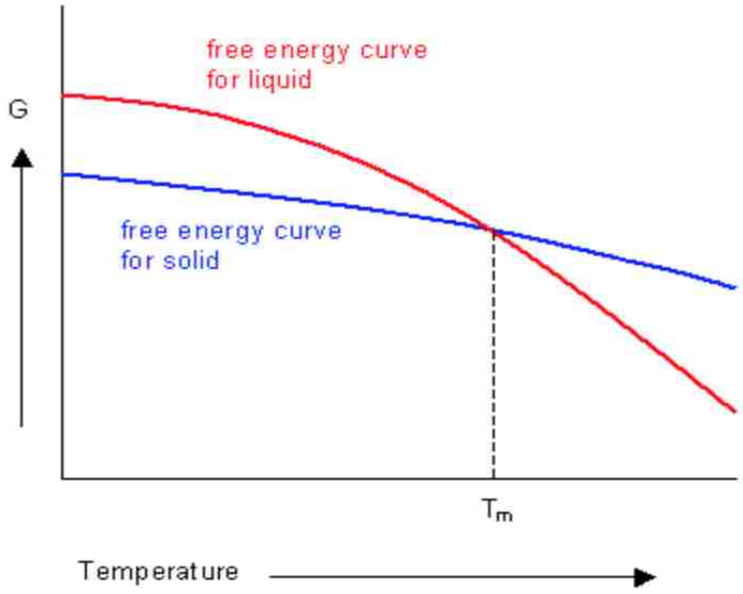

Figure 3-10: Changes of Gibbs free energy at different temperatures.

Crystallization in polymers consists of two steps: The first step is nucleation sites formation, which is the starting point of forming crystals [51]. The likelihood of forming nucleation increases as the temperature goes further below the melting temperature or by introducing external pressure, which causes the equilibrium state to be destabilized [52]. In order to form stable nucleation sites, the energy barrier has to be overcome as shown in Figure 3-11 [53].

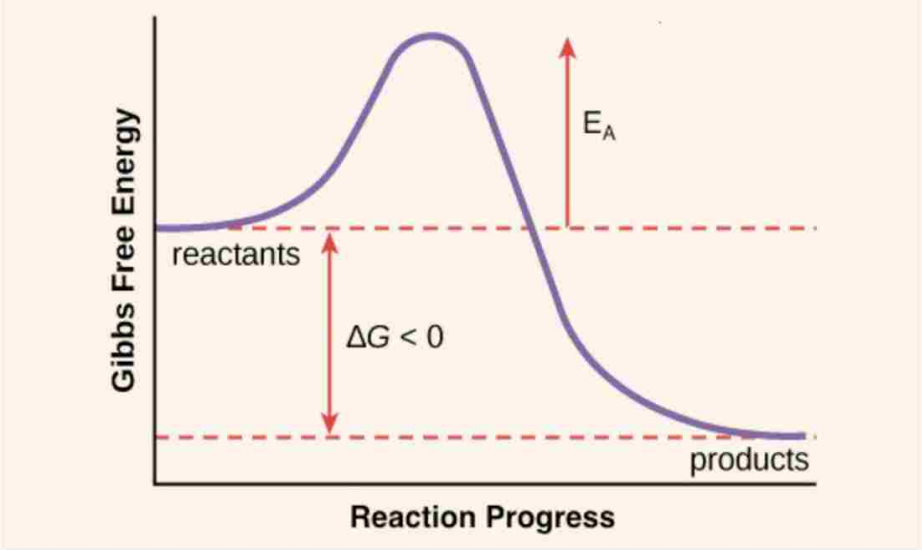

Figure 3-11: The variation of free energy to form primary nuclei.

The second step is growth rate, which is the process of growing crystals from the nucleation sites. The growth rate becomes faster around the crystallization temperature, which is a temperature between the melting temperature and the glass transition temperature. A typical crystallization rate of polymers is shown in Figure 3-12. The crystallization occurs between Tm and Tg, above Tm, there is no crystallization occurs, and below Tg, no crystallization takes place because of the higher viscosity that restricts the molecular movement.

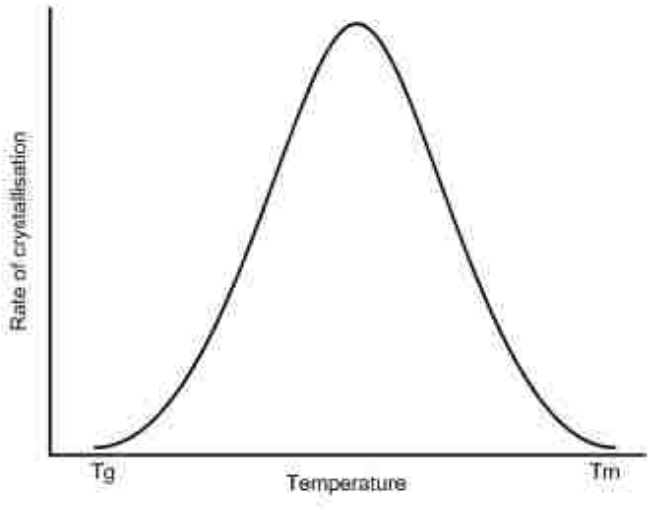

Figure 3-12: Typical crystallization rate for polymers at different temperatures [54].

In order to control the crystallization kinetics of polymers and influence the overall final crystallinity, one should control the two components that control the crystallization kinetics, which are nucleation sites formation and growth rate. Generally, there are several methods that can be used to control the crystallization kinetics of polymers [51]:

- Methods that require physical manipulation such as controlling shear rate and thermal history of the polymer melt during manufacturing, this study will focus on this type of manipulation.
- Methods that require adding chemicals such as adding nucleating agents.

The crystallization process in 3D printing is complicated since it includes both isothermal and non-isothermal crystallization. During the printing process inside the head of extrusion-based 3D printers, the crystallization process is non-isothermal since the material is exposed to shear rate and temperature as a function of time. Once the material is printed on a heated bed, usually it takes a few minutes to finish the print depending on the sample size, in this case, the crystallization process is isothermal. Another factor that

influences the crystallization of 3D printed polymers is the cooling rate, which starts when the material exits the nozzle until it is printed on the heated bed.

3.1.3.3.1 Shear rate

Shear rate plays a critical role in determining the final properties of semi-crystalline polymer products during polymer processing such as injection molding, extrusion and extrusion-based 3D printing. The effect of shear rate on polymer crystal can be summarized as follows:

- Enhancing the crystallization kinetics [5]. As stated before, the crystallization kinetics consists of two steps, the formation of primary nuclei and the growth rate. Several studies have shown that shear rate can influence the formation of new primary nuclei which result in faster crystallization kinetics [1,55]. Moreover, a study that was conducted by Roberto Pantani and his group [56] has shown that shear rate has an effect on both nucleation site formation and growth rate.
- Increasing the number of nuclei which decreases the size of crystallites [2].
- Changing crystal morphology from spherulite to oriented crystal like shish kebab Figure 3-13 [5].

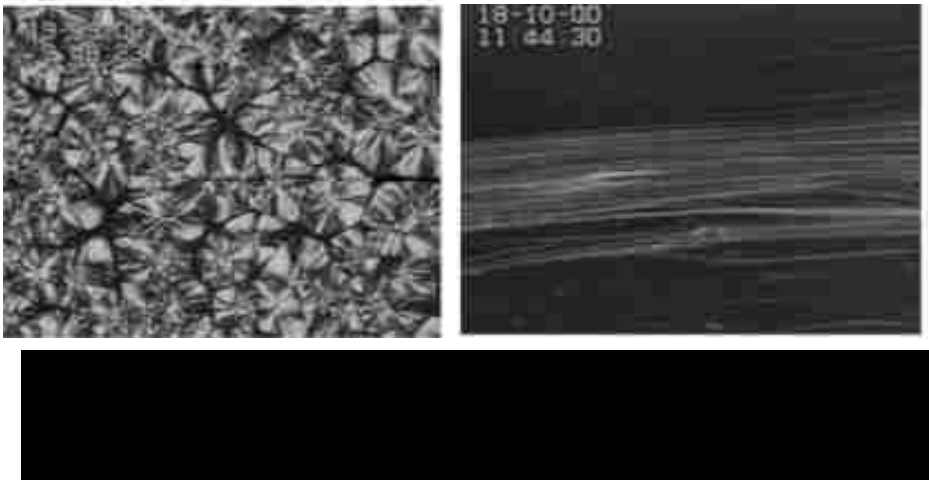

Figure 3-13 shows the effect of shear rate on polymer morphology. Polymers usually crystallize into spherulite under quiescent conditions. On the other hand, when polymers are exposed to high shear rate, their chains get stretched and then shish kebab structure gets formed.

3.1.3.3.2 Cooling rate and temperature

Cooling rate has also shown to influence the effect of shear rate on both crystallinity and molecular orientation. For amorphous polymers, high cooling rate tends to lock in more of the orientation caused by flow while slow cooling rate will allow most of the molecular orientation to relax [33]. On the other hand, for semi crystalline polymers, slow cooling rate will allow crystals to grow resulting in higher crystallinity compared to fast cooling rate.

Mostly during polymer processing, factors such as temperature, cooling rate and shear rate have shown to influence the crystallization process, and changing one of these factors affects the influence of the other factors on the crystallization process. For example, at low cooling rate, shear rate can induce the formation of additional nuclei which enhances

the crystallization kinetics [2]. On the other hand, at high cooling rate, shear rate will not have sufficient time to induce the formation of additional nuclei. Generally, when dealing with slow to crystallize polymers, a moderate to high cooling rate will result in mostly an amorphous structure [57]. However, even when no crystals have grown because of the high cooling rate, several studies have shown that the cooling rate influences the nucleation rate. Moreover, after isotherm the material for long amount of time, the DSC curve showed no influence by the cooling rate[57]. In other words, the influence of the cooling rate on the nucleation rate was dissipated by the long isotherm time.

Semi crystalline polymers such as PLA are known for their slow crystallization rates. The temperature at which the material during processing stays the longest time is critical to allow crystals to grow and to influence the final overall crystallinity. It is know that the highest crystallization rate occurs around the crystallization temperature as shown previously in Figure 3-12. Also, in the case of PLA, when isotherm at higher temperatures, the material tends to form α crystal structure [58]. On the other hand, at lower temperatures below 100 ºC, only α' can be formed under quiescent conditions [3]. The main difference between α and α' crystal structure is that α' has loose chain packing while α crystal structure has more ordered chain packing. Several studies have shown that at lower temperatures, strong shear rate can influence the formation of α crystal structure [3,58].

3.1.3.4 Theoretical approaches

The microstructure formed during the melt processing of polymers determines the final properties of the part such as mechanical, thermal and biodegradation properties. Thus, much attention has been given to the microstructure that is formed into the part

caused by shear flow. Even though the literature on shear induced crystallization is large, it is rare to find papers that discuss both experimental results and the models used to predict such results.

Most of the discussions on polymer crystallization usually is conducted or investigated under quiescent conditions which means the absent of shear. Under these conditions the rate is based on idealized conditions such as isothermal crystallization where the temperature, shear flow and pressure are constant [59]. Experimental studies conducted on polymer melt have shown that shear rate can significantly enhance the crystallization kinetics [60]. One study that was conducted to investigate the effect of shear flow on isotactic polypropylene crystallization kinetics have shown that shear flow increased both the number of nuclei and the rate of crystallization dramatically [1], and the results are shown in Figure *3-14*.

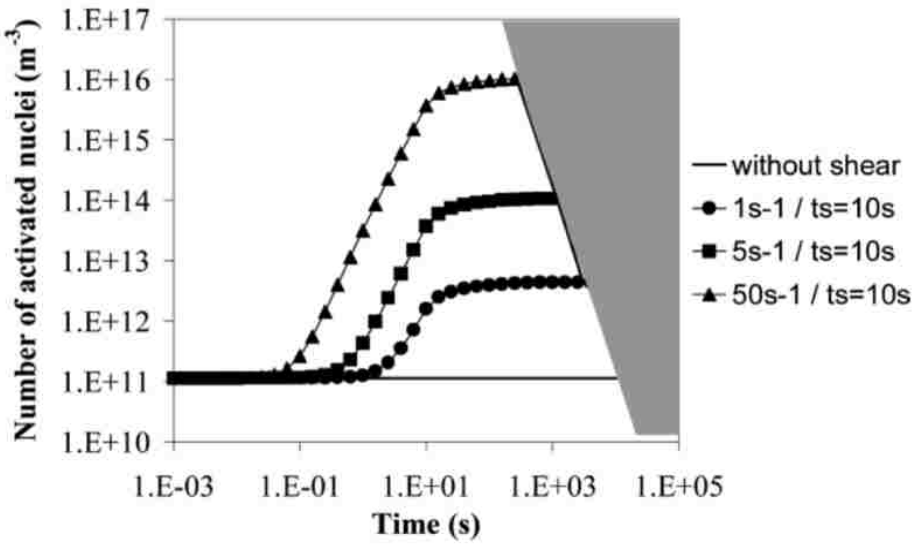

Figure 3-14: Calculate number of nuclei increase in a PP melt at different shear rate.

As shown in the previous figure, the number of activated nuclei increased with increasing shear rate. Also, the duration of shear rate has shown to influence the number of activated nuclei as shown in Figure *3-15*.

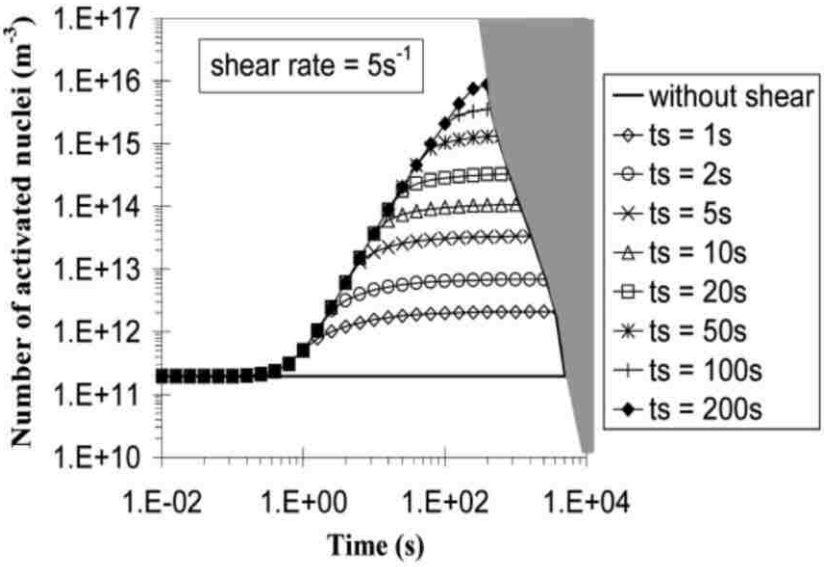

Figure 3-15: Calculated number of activated nuclei for different shear as a function of time.

- Avrami equation

Avrami theory is usually used to model the kinetic of isothermal crystallization. The avrami theory can also be used to predict the non-isothermal crystallization kinetics as shown in the following equation [29].

$$1 - X(t) = \exp(-Zt\, t^n)$$

Where X(t) is crystallization kinetics. Zt is the crystallization rate constant which is temperature dependent, it involves both nucleation and growth parameters; n is an integral [61].

3.2 Resultant impacted product attributes

The stereochemistry and thermal history dictates the final mechanical, physical, optical and biodegradable properties of polymeric products. One of the most emerging and studied bio materials is PLA, PLA is biodegradable and biocompatible polymer and it is widely used in medical applications [7]. It can be amorphous or semi crystalline based on its stereochemistry and how it is processed. Its mechanical properties and biodegradation rate are highly dependent on its amount of crystallinity.

3.2.1 Mechanical properties

The mechanical properties of PLA is dependent on its molecular weight, since the molecular weight determines the amount of crystallinity that can be achieved by the material. The mechanical properties that are mostly reported are focused on tensile strength, tensile modulus and ultimate strain. Tensile modulus of PLA has shown to increase by factor of 2 when the molecular weight is increased from 50 to 100 kDa [7].

3.2.2 Biodegradation

Biodegradation can be defined as the erosion of a material. It is the way that a material can be naturally decomposed by its environment, weather through interactions with certain bacteria or fungi, or through absorption into the waste system of the human body in the case of implanted materials. “It is now widely recognized that along with the importance of synthetic polymers possessing long-term stability, there is also a need for polymers that break down in a controllable manner. Biodegradable macromolecules can be

tailored specifically for controlled degradation under the inherent environmental stress of biological systems" [62].

Generally, biodegradation can occur either with or without the assistance of enzymes, but the project focuses on materials that biodegrade without the use of enzymes. Biodegradation without the use of enzymes is mainly a chemical reaction that is dictated by the processes of hydrolysis and oxidation. In materials that biodegrade in this manner, hydrolysable and oxidizable linkages can be found in the polymer main chain. During the first phase of biodegradation of these materials, water penetrates the material and breaks down the hydrolysable bonds in the long main chain of the polymer, resulting in shorter chains or oligomers [49]. Progressive degradation thus changes the microstructure of the bulk material through the creation of pores through which oligomers can escape [63]. Then, the shorter chains are further degraded through hydrolysis and oxidation, resulting in monomeric acids. These acids can then be metabolized, resulting in carbon dioxide and water. This release of oligomers and monomers from the bulk material is what causes the weight loss of the material. Because of this, the best way to monitor the level of degradation of a polymeric material is by monitoring the weight of the material. This process that results in the reduction of molecular weight of the material can be classified as erosion. Figure 3-16 shows the reduction over time for molecular weight, strength and mass [64]. As described earlier, the molecular weight starts decreasing first, followed by strength and then mass.

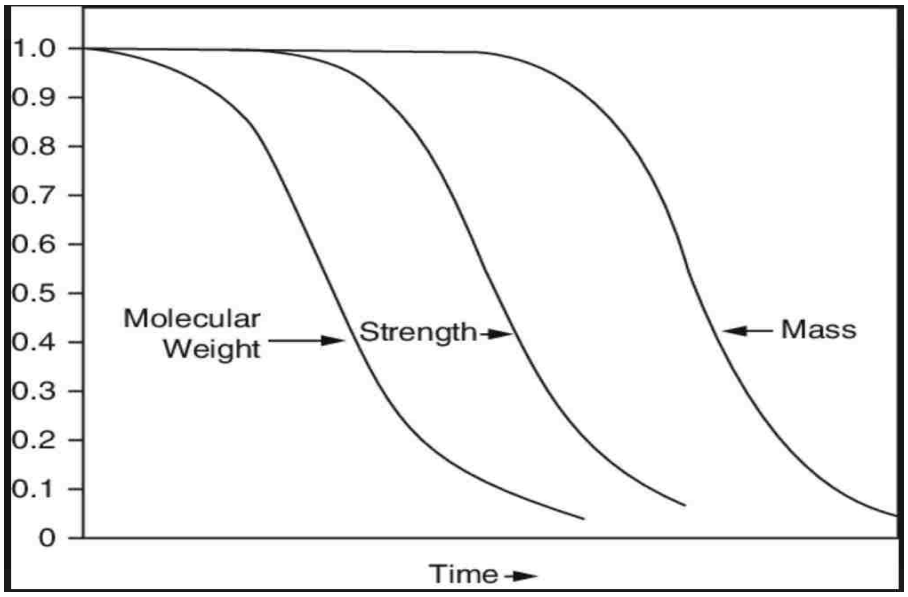

Figure 3-16: The reduction of polymer molecular weight, strength and mass over time.

Biodegradable polymeric materials can be classified based on the two types of erosion that they experience during the degradation process. These two main types of erosion are heterogeneous surface erosion and homogeneous bulk erosion. Materials and products that experience heterogeneous surface erosion solely lose material from the surface, and reduce in size while still maintaining their geometric shape [63]. On the other hand, homogeneous bulk erosion materials will generally maintain their shape and size during degradation, as the erosion of these products is not restricted to the surface of the product. An illustrative comparison of these two processes can be seen in Figure 3-17 [63].

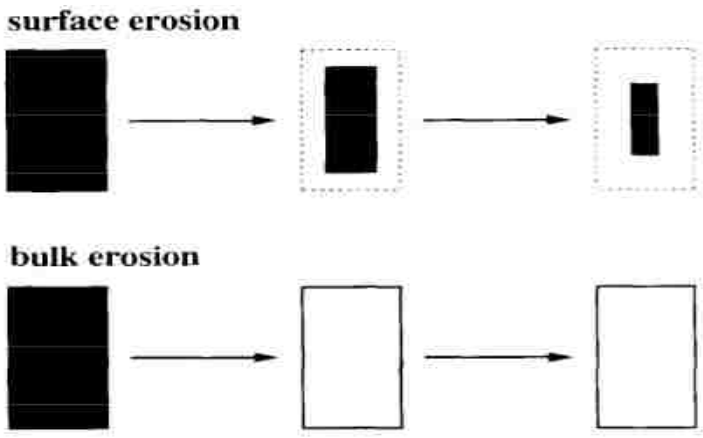

Figure 3-17: Schematic illustrative comparison of heterogeneous surface erosion and homogeneous bulk erosion.

It is important to keep in mind that most polymers cannot be completely categorized by either type of erosion. Erosion in itself is a more complex process that is dependent on factors such as material swelling as it absorbs water, morphological changes in the material during the process, and dissolution and diffusion of the oligomers and monomers as the polymer degrades [63]. Despite the complexity of this process, it is important to be able to control or predict degradation in order to ensure success in the application of biodegradable polymeric materials. That way, the correct material that exhibits the appropriate type of erosion can be utilized for an application. For example, in tissue engineering, properties such as porosity and surface conditions affect the performance of tissue scaffold implants, so it is important to know how the porosity and surface will be affected by degradation.

Since passive biodegradation by erosion is caused by hydrolysis of individual molecular chains, the molecular orientation and crystallinity of a material has an effect on this process. The rate of degradation is influenced by many characteristics of the polymer, including morphology, chain orientation, and initial crystallinity [65]. Amorphous

materials are composed of randomly oriented, loosely packed polymer chains that can easily slip past each other. On the other hand, crystalline materials are composed of densely packed molecules that are aligned in a more orderly fashion. In a semi crystalline biodegradable polymer such as PLA, water first penetrates the amorphous phase since its easier to break down the amorphous phase compared to the crystalline phase. Because of that, the amount of crystallinity increases because of the degradation of the amorphous phase before it decreases again when the crystalline phase starts degrading.

3.3 Standard methods to characterize polymer chains orientation

There are a couple of characterization techniques that can be used to investigate the polymer chain orientation such as optical birefringence, DSC and XRD. DSC thermal analysis can be used to investigate the glass transition temperature of a polymer. The glass transition temperature is influenced by a couple of factors such molecular weight and free volume.

3.3.1 DSC

Differential scanning calorimetry (DSC) is a thermo analytical technique used to study the thermal transition temperatures and transition enthalpies of a polymer. It measures the difference in the amount of heat that is required to raise the temperature of a sample and a reference as a function of temperature. The reference pan is empty.

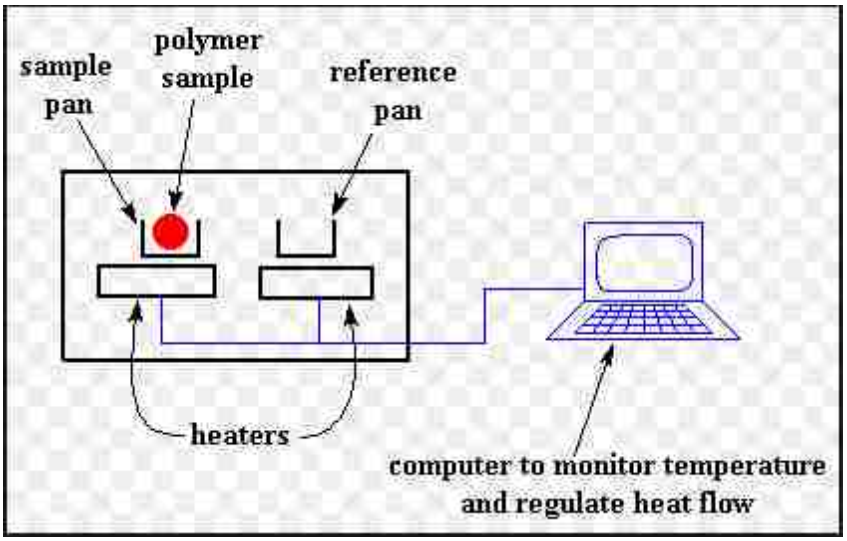

Figure 3-18: DSC process

The heaters try to heat the two pans at a constant rate. Although, it takes more heat to raise the temperature of the pan that has a sample on it compared to the empty one.

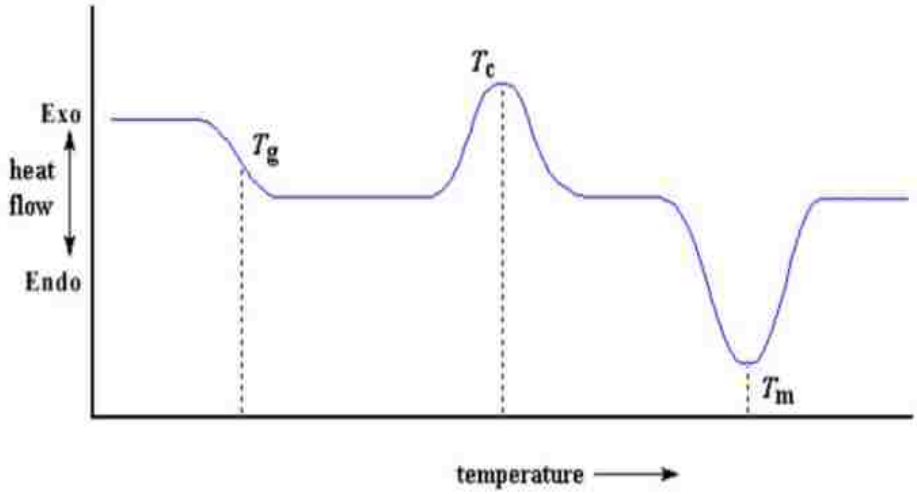

At the crystallization temperature the sample releases heat (Exotherm) due to the molecules arranging themselves and no longer in their random configuration so the heaters will not have to put out much work in order to keep the temperature of the pan rising. On the other hand, at the melting temperature the sample absorbs heat (Endotherm) in order to melt the material and heaters have to put a lot of heat in order to melt the material and keep the temperature of the pan rising.

3.3.2 X Ray Diffraction (XRD)

X ray diffraction is a characterization technique used to get information about the structure of crystalline and semi crystalline materials [66]. It is also used to determine the degree of crystallinity of polymers. X ray diffraction uses Brags law to calculate the distance between two layers of atoms or molecules. The Braggs law is shown in Figure 3-20 and equation.

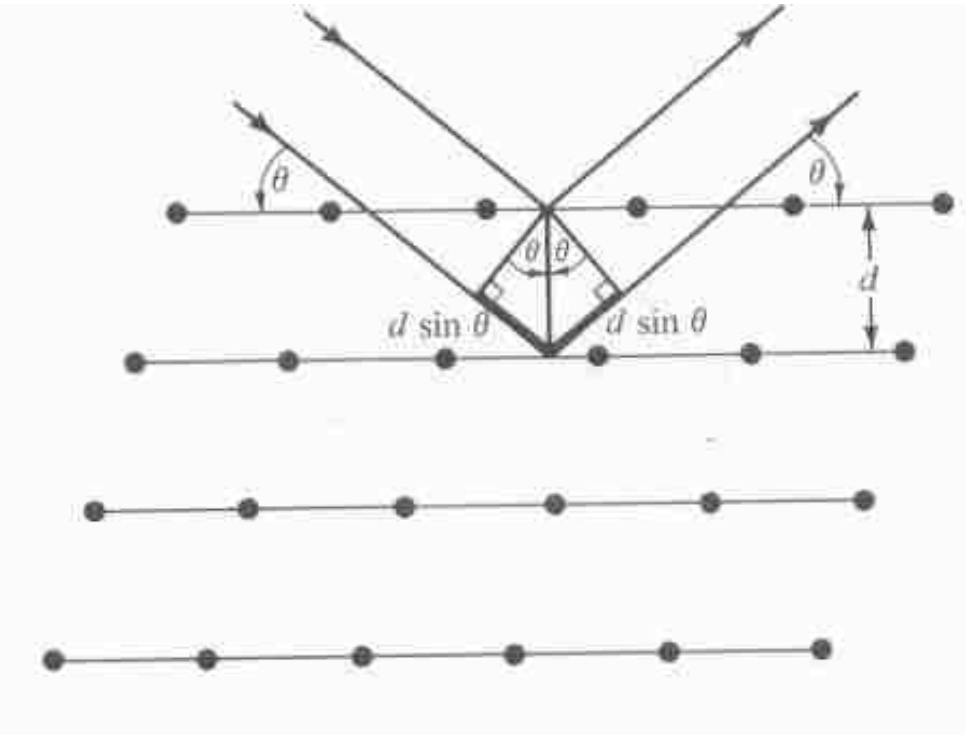

Figure 3-20: Bragg's law

$$n\lambda = 2d \sin\theta$$

Where n is an integer, λ is the wavelength of X rays, d is the spacing between the crystal planes and Θ is the angle between incident beam and the normal to the reflection lattice plane.

3.4 Proposed additive manufacturing innovation

The possibility of controlling the final morphology of additive manufactured polymeric parts is an interesting topic. As stated in this chapter, polymers are long chain molecules and their final properties are highly influenced by their molecular structure, and their molecular structure is dependent on the processing conditions such as thermal history

and shear rate. Thus, by precisely controlling thermal history and shear rate, the final properties of polymeric parts can be tuned. Additive manufacturing parts are built from the ground up layer upon layer, which allows the control over shear rate and thermal history for each single layer. As a result, parts can be manufactured with tunable molecular structure for optimized performance.

In this project, shear rate will be controlled inside the extrusion head of 3D printers, since according to many literature studies as stated in this chapter, shear rate can influence the formation of primary nuclei and accelerate the crystallization kinetics, resulting in higher overall crystallinity. Also, shear rate is controlled without affecting the flow rate of the extruded material.

Extrusion based additive manufacturing contains both non-isothermal and isothermal crystallization. During the extrusion process, when the material is inside the extrusion head and when it is being printed into a heated bed, the process is non-isothermal crystallization. Then, when the parts are printed on a heated bed and usually it takes a few minutes to a few hours to finish the print depending on the part size, the process in this case is isothermal crystallization. It is important to understand the influence of each case to be able to customize the final properties of printed parts.

CHAPTER 4: Design and Development of Rheo-Printing System

4.1 Introduction

The design and development of successful products require a clear understanding of the problem to be solved. In this project, in order to understand the problem, knowledge of basic science principles such as 3D printing, melt rheology and polymer extrusion should be obtained. Then, a detailed design should be sketched to match the parts to be used. In other words, there are some parts to be bought such as actuators and motors. Therefore, the design should consider the dimensions of the parts to be assembled. In addition, each project has a certain or limited budget. So, during design and development, budget should be taken into account.

The main goals of the machine to be designed were to be able to use pellets instead of filaments, and to precisely control shear rate of the polymer melt. In order to achieve these goals, extruder based printer with screw extruder was designed and developed to be able to use polymer pellets and have access to different varieties of materials. Also, the nozzle was designed to allow high speed rotation to precisely control shear rate of the melt. Two prototypes were developed of the 4D Rheo-Printing system. The first prototype didn't work properly but it gave us a better understanding of the problems and how to solve them. Also, porotype 2 is the one that is currently being utilized to manipulate melt rheology and morphology of additive manufactured polymeric parts.

This chapter discusses the designs of the 4D Rheo-Printing system including designs, thermal control system, and motion control system. Moreover, the problems that were faced will be discussed as well as how they were solved.

4.2 Design of the Rheo-Printing System

4.2.1 Prototype 1

4.2.1.1 Introduction

Prototype 1 was developed in the beginning of this research. The extruder barrel used in this prototype was provided by Professor John Coulter which he had for a long time along with funnel and the heaters. The other parts were designed and developed in our manufacturing laboratory. This prototype didn’t work well due to the different inner diameters of the barrel which will be explained later. A brief explanation of prototype 1 is reported.

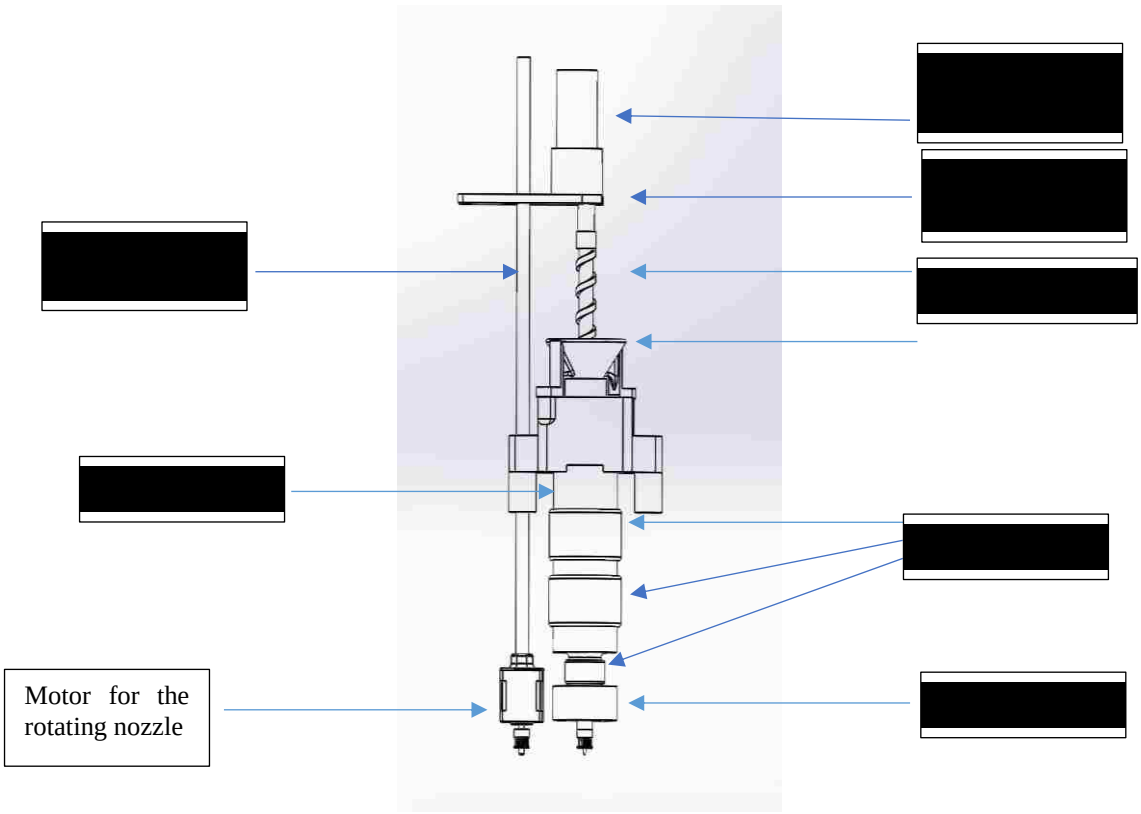

Figure 4-1: A Schematic diagram of prototype 1.

4.2.1.2 Design of the extruder body or barrel of Prototype 1

The extruder body is the main structure of the system, where all the other components where designed to retrofit. As mentioned earlier, the extruder body was provided by Professor John Coulter and it is a part of a Newbury vertical injection molding model no. 45-3-5408-0, it is shown in Figure *4-2*. Figure *4-2* shows a picture of the inside of the extruder body.

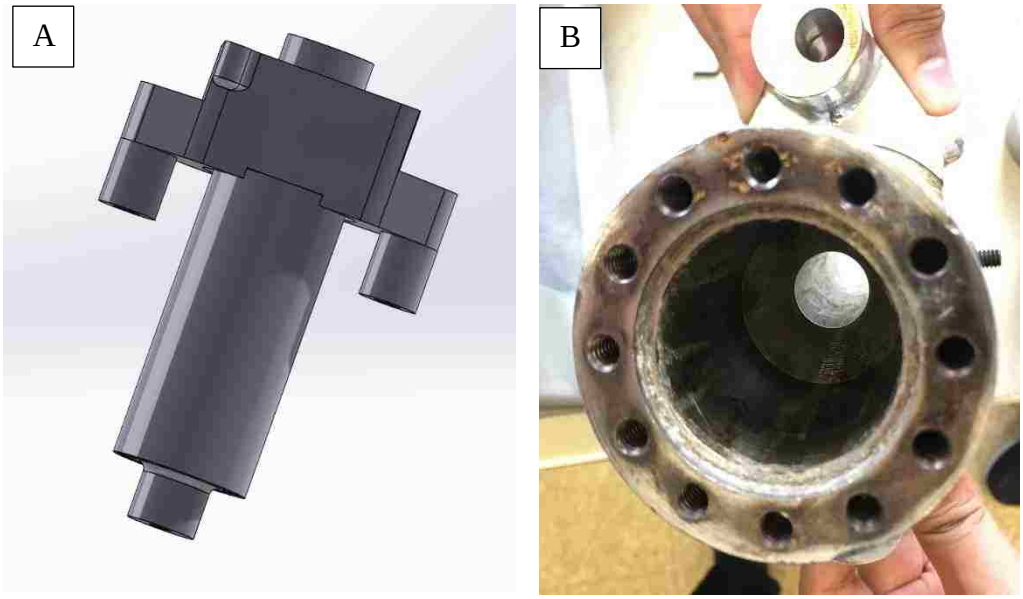

Figure 4-2: A) A schematic diagram of the extruder body. B) A picture showing the inside of the extruder body.

The extruder body is 7.5 inches long. The inner of the extruder body is composed of two different diameters as shown in figure 2b. The larger inner diameter is 1.5 inches and 3 inches long while the small inner diameter is 0.75 inches and it is 4.5 inches long. These differences in diameter caused an issue of no extrusion which will be discussed later.

4.2.1.3 Design of the screw extruder

The screw was designed to fit the small inner diameter of the barrel. The screw that was designed for prototype 1 is shown in Figure *4-3*.

Figure 4-3: Extruder screw of Prototype 1

The screw extruder is driven by a DC motor. The motor utilized for this purpose is a Pittman 12-Volt DC motor. The rate of rotation of the motor can be controlled by the amount of electrical power applied to it. The motor also features two threaded holes on both sides of the motor's shaft to aid in the mounting of the motor.

A mounting plate was designed and developed in order to hold the DC motor in place as shown in Figure *4-4*.

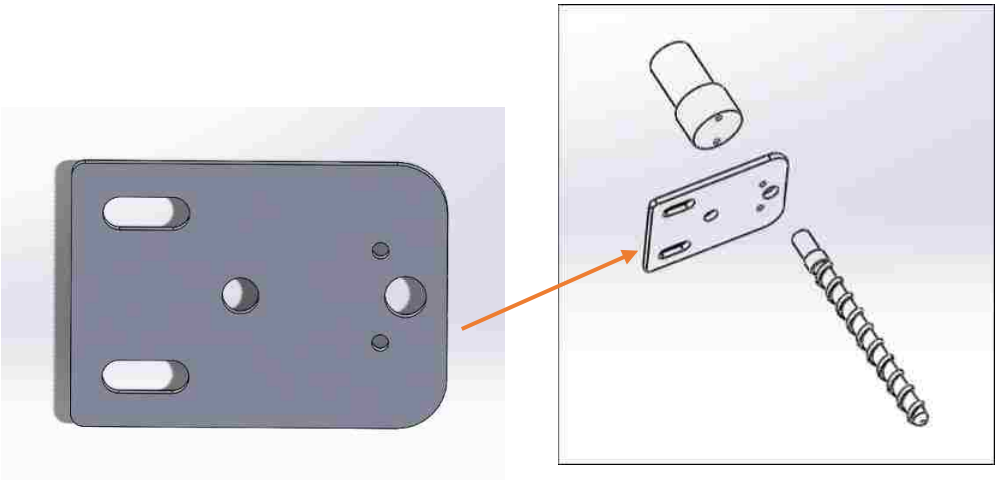

Figure 4-4: Extruder screw mounting plate.

There are a couple of important features of the mounting plate. First, the bore in the middle of the plate is used to mount the extruder screw, the DC motor, and the motor utilized to rotate the tip. There is a threaded shaft that goes through the middle bore and is held in place by means of a nut, the placement of the extruder screw can be adjusted through this shaft. Second, the two small mount bores and the larger bore in between them, which are used to fix the motor with the screw. The small bores are aligned with the threaded holes in the DC motor to fix the DC motor in Place. The DC motor's shaft goes through the larger hole to be mounted into the screw.

4.2.1.4 Design of the nozzle assembly

The nozzle assembly of prototype 1 consists of three parts Nozzle Mount, Bearing and Nozzle head as shown in . The main purpose of the nozzle assembly is to allow rotation

of the nozzle tip in order to tune shear rate of the polymer melt. The nozzle assembly was custom designed and developed for the purpose of experimentation at Lehigh University.

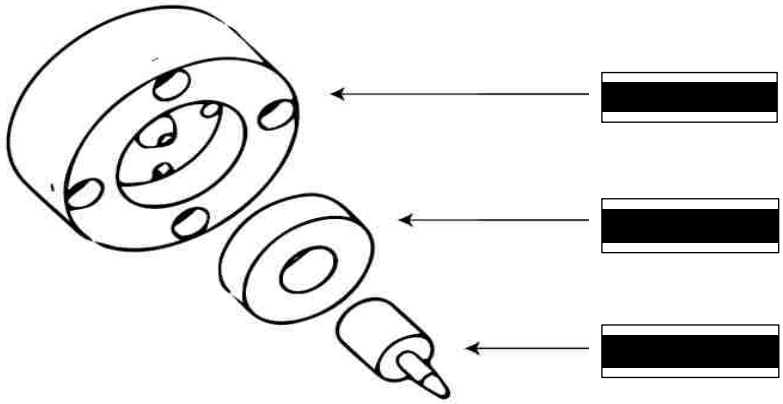

Figure 4-5: Nozzle assembly used to allow nozzle tip rotation.

The nozzle mount is used to connect the bearing and the rotating nozzle to the extruder body. It should hold everything in place while allowing the movement of the rotating nozzle and preventing leaks. The ball bearing is press fitted into the nozzle mount and the nozzle tip is press fitted into the bearing. A bottom view of the nozzle mount is shown in Figure *4-6*.

Figure 4-6: Bottom view of the nozzle mount.

There are couple of features included in the design of the nozzle mount. At the outer edge of the nozzle mount, there are four counter bored holes. These holes are aligned with threaded holes in the extruder body in order to allow the nozzle assembly to be mounted to the extruder body. Moving inwards, there are four smaller bores which allow for access to the back of the bearing in order to remove the bearing easily if needed. Moving inward again, there is a circular channel which were designed in order to fit an O-ring to prevent polymer flashing between extruder body and the nozzle mount. Then finally, there is the channel where the polymer melt goes through and moves from the extruder body to the rotating nozzle.

The radial motion of the nozzle is driven by an electric motor and gear system which are shown in figure 1. The electric motor features four threaded holes at the corners that allow for an easy mounting of the motor. A customized motor mount plate was designed and developed to utilize the four holes and hold the motor in place Figure *4-7*.

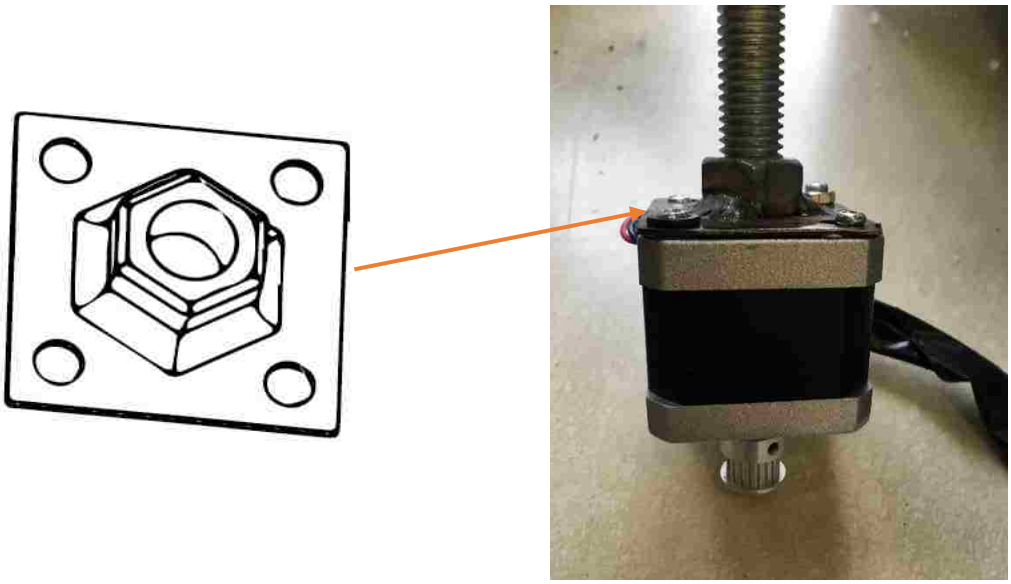

Figure 4-7: Motor mount plate that was customized to hold the electric motor responsible of rotating the nozzle.

In order to rotate the nozzle, a set of gears are used, one gear is connected to the nozzle tip and the other one is connected to the shaft of the electric motor. The two gears are driven by a timing belt which can be seen in Figure *4-8* which shows the final image of prototype 1.

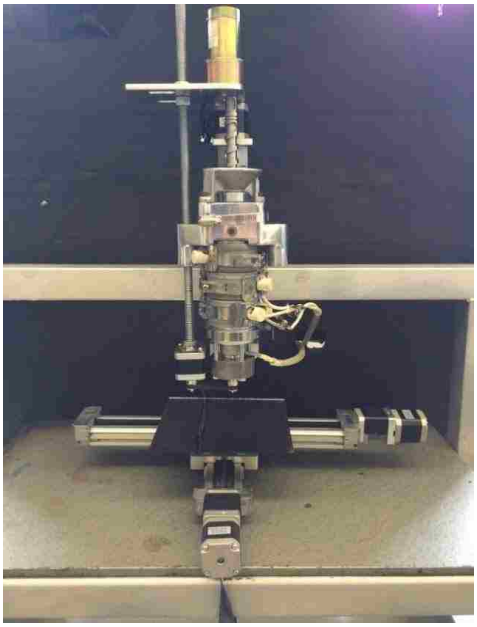

Figure 4-8: Initial prototype 1 manufactured at Lehigh University.

4.2.1.5 Discussion and conclusion

The designing and development of Prototype 1 began after a clear understanding of the problem that we were trying to resolve. Polymer melt rheology and morphology were investigated first as discussed in the previous chapter in order to understand the properties that this system would be designed to manipulate and how to accomplish such design to do that.

The first parts that were developed in prototype 1 were the nozzle assembly in which the melt manipulation would be induced. High temperature ball bearing was obtained and the design of the nozzle tip and the nozzle mount were developed to assure easiness of the press fitting of the assembly parts. Early design of the nozzle mount was developed without 4 counter holes to have access to the back of the bearing in order to remove it. After doing some testing, the bearing had to be removed for reasons to be

explained later. But, it was not possible to remove the bearing without causing damage to the nozzle mount with the equipment that we have in the lab. So, adding 4 counter holes to be able to remove the bearing easily was necessary. The O-ring was used in order to prevent polymer flashing between the nozzle mount and the extruder body.

Once all the parts of the extruder were assembled. The heating system was tested with incorporation of material. The heaters were old since they came with the extruder body. One of the heaters was missing insulation wires. Several attempts were conducted to test the heaters but unexplained short circuit were experienced. Eventually, it was found that one heater was shorted so it was removed from the set. The other heaters were able to work.

The materials used during the first testing was polymethylmethacrylate (PMMA) acrylic resin. The polymer resin was fed into the funnel, polymer resin wasn't able to go down the screw. The resin accumulated around the screw in the funnel and it caused the screw to jam and the DC motor to overheat. In order to solve this, polymer resin was fed slowly into the funnel so the screw can move them down to the barrel instead of filling the funnel with polymer resin at once. I kept filling polymer resin but nothing came out of the nozzle, with time the motor started to overheat as the necessary torque to rotate the screw kept increasing as the polymer is filling the extruder. The nozzle was removed to see if polymer would be extruded out of the extruder. It started flowing gradually as shown in Figure *4-9* and the DC motor didn't work as hard to rotate the screw.

Figure 4-9: Polymer flowing out of the extruder after removing the nozzle.

At this time, the problems that were preventing polymer melt form being extruded out of the nozzle were clear. The first problem was the funnel not able to move polymer resin into the barrel smoothly without causing screw jamming. The second problem was as polymer melt fill the extruder which took a long time because of the larger diameter of the extruder body, the DC motor had to work hard as it required more torque to rotate the screw due to the large amount of polymer inside the extruder. Due to the large diameter of the extruder body, the polymer near the wall get to the melt temperature while the one near the core stayed solid. It was clear that another extruder body had to be designed and developed for this specific application where it would be able to work homogenously with the screw

in order to melt the polymer and push it down for extrusion. A better functioning funnel that can transition polymer resin into the barrel had to be developed.

4.2.2 Prototype 2

4.2.2.1 Introduction

Valuable knowledge and better understanding of the issues accompany the design of the extruder system have been gained from prototype 1. Most of the issues that were preventing the extruder from working properly were known and needed to be solved in order to achieve workable prototype. Prototype 2 was developed in order to solve the issues faced in prototype 1. Also, some of the parts used in prototype 2 were developed for prototype 1. The main components to be designed for prototype 2 carefully are the barrel, the screw extruder, nozzle assembly.

Two companies were contacted in order to develop a mini extruder for our system. The lowest cost was around $2500 for just the mini extruder (screw and barrel) without the other parts such as heaters, thermocouples, temperature controllers, motor, power supply and nozzles. Because of the high prices of the mini extruders and the limited budget we had, we decided to design and build the extruder in our lab.

4.2.2.2 Design of extruder

The hardware components of the mini extruder that was developed in this project is described in this section. The major components of the developed extruder are screw, barrel and funnel. The screw is the main component of the machine, since all other parts revolve around it. The rotation of the screw causes the material to move forward and

contribute to the heating of the material [67]. The barrel is the cylinder that surrounds the screw. The funnel or the feed hopper feeds the material to the extruder. A good functioning extruder should be able to convey granulate material from the feed hopper into the extruder, then, crush and move the material forward or downward as in our case for extrusion.

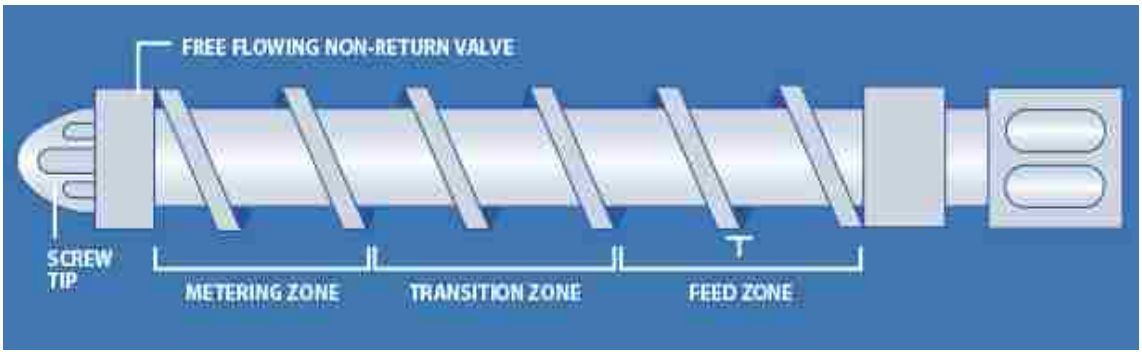

Figure 4-10: Three zones of general purpose screw extruder.

A proper extruder consists of three zones: the solid conveying zone, the melting or transitioning zone and the metering zone [68]. The three zones of the screw extruder is shown in Figure *4-10* [69].

The feed zone is responsible of transporting the polymer pellets form the feed hopper to the screw channel [68]. The polymer pellets must stick to the barrel slip on the screw in order for it to move forward [70]. High coefficient of friction between the barrel and the pellets must be maintained in order to build up pressure and move the solid pellets forward to the melting zone. A couple of solutions are usually used to achieve high coefficient of friction in the feeding zone such as internal screw cooling or grooving the surface of the barrel in the axial direction [68,70]. These solutions are typically used when dealing with materials that have low coefficient of friction. The melting zone is the zone

where the material gets melted. As it gets melted, the size of solid pellets shrink. So, the root of the screw should gradually become smaller in order to be able to move the material forward toward the metering zone. In the metering zone, the material should be completely melted. Also, this is the most important zone as it governs the output of the extruder [71].

The design of prototype 2 is shown in Figure *4-11*. The main differences between prototype 1 and prototype 2 are the barrel, the screw, the nozzle assembly and the extruder mount.

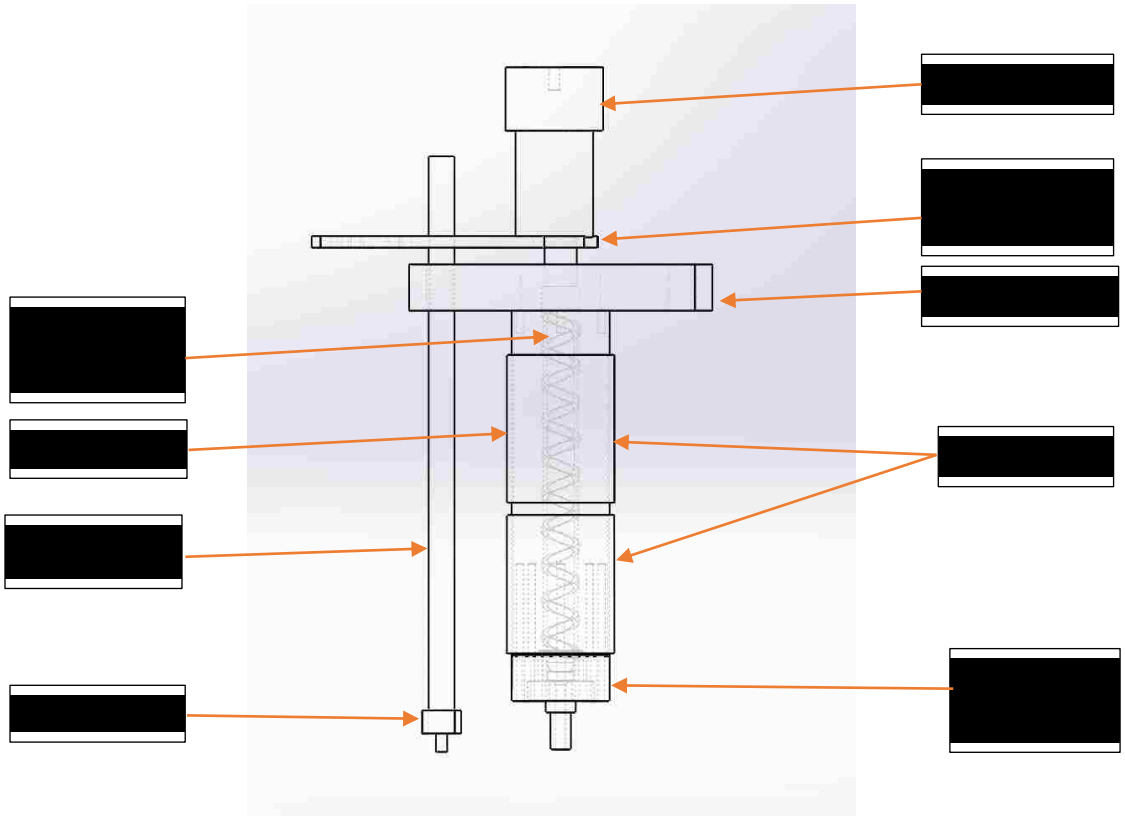

Figure 4-11: Schematic Diagram of Prototype 2.

The screw extruder developed for prototype 2 was designed with three zones. The length to diameter ratio (L/D) was designed to be 10/1 in order to minimize the weight of the mini extruder since it will be mounted in the z axis and the stepper motor should be

able to move it up and down during printing. The diameter was designed to be 0.75 inches which standard diameter for extruders according to literatures [68] and the length is 7.5 inches. The screw helix angle is 17.65° which is the typical helix angle used for general purpose extruders. The channel depth in the metering section was designed to be 0.06 which is the recommended depth for extruders with diameters less than 1 inch. Figure *4-12* shows the screw extruder developed for prototype 2. The barrel designed for prototype 2 is shown in Figure *4-13*.

Figure 4-12: Screw extruder designed and developed for prototype 2.

Figure 4-13: The extruder barrel designed for prototype 2.

The barrel was designed with distinct features. As seen on Figure *4-13*, on top of the barrel, there are threaded holes that were designed in order to hold the barrel to the extruder mount. The extruder mount was designed with holes where screws go through them and then into the threaded holes of the barrel Figure *4-14*.

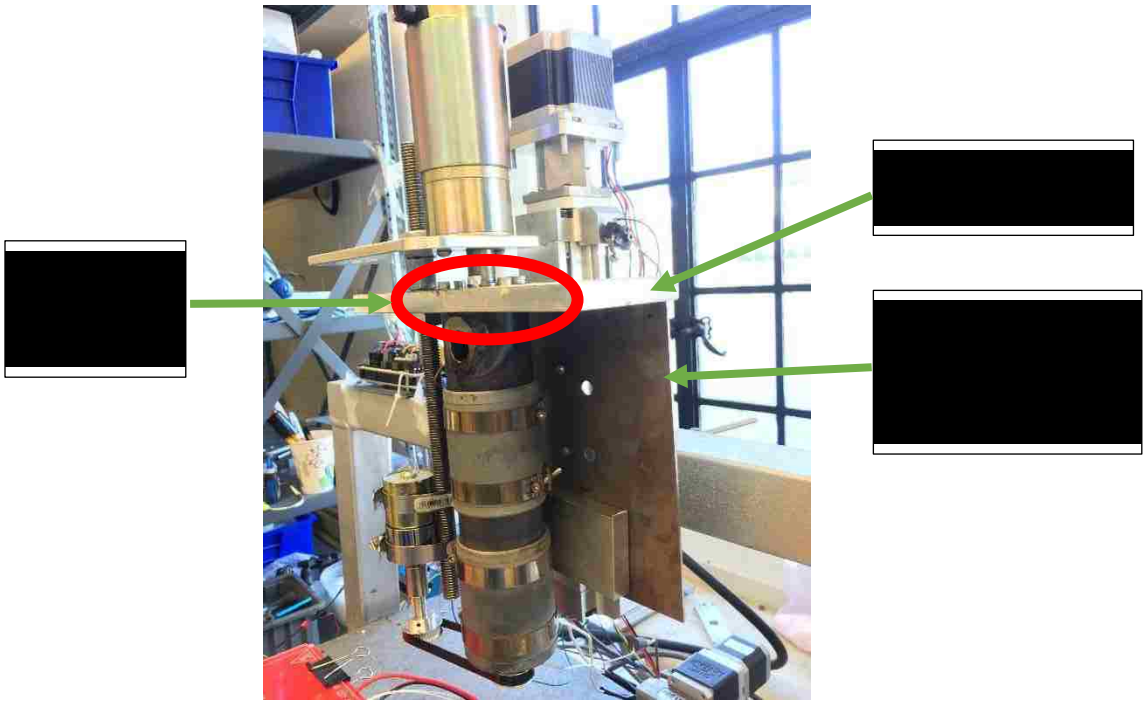

Figure 4-14: Screws used to attach the barrel to the extruder mount.

The extruder mount was designed with threaded holes in the back in order to be fixed to the Z axis mount. Figure *4-15* shows the screws that were used to fix the extruder mount to the Z axis mount. Also, it shows the screw used to attach the Z axis mount to the Z axis actuator.

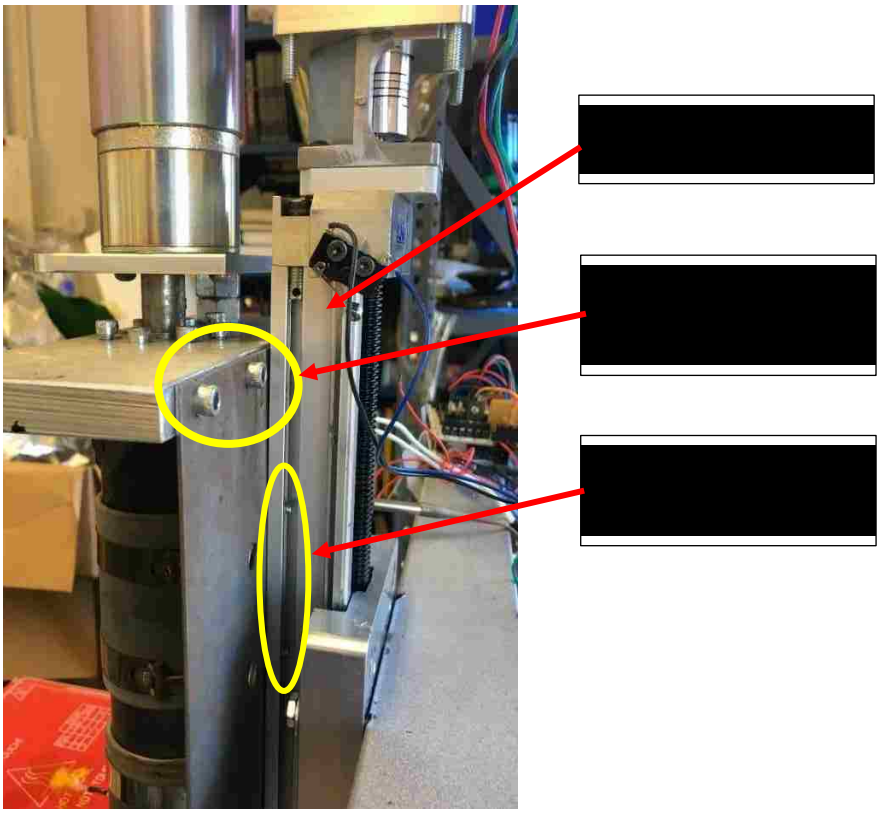

Figure 4-15: The attachment of the extruder mount to the Z axis mount and then to Z axis actuator.

Moving downward to the bottom of the barrel shown in Figure *4-13*, there is a counter bore hole and a couple of threaded holes that were designed to enable precise and tight fitting of the barrel to the nozzle mount to prevent shaking and leak. A bottom view of the barrel is shown in Figure *4-16* along with a top view of the nozzle mount that was designed to be attached to it. The difference in diameter between the counter bore hole and lip of the nozzle mount was set to be 2000 of an inch so it will allow easy installation and removal of the two parts. It is also important to note that the two parts are tightly screwed to each other to prevent leaks since difference of 2000 of an inch might cause polymer leaks depending on the viscosity of the material being used.

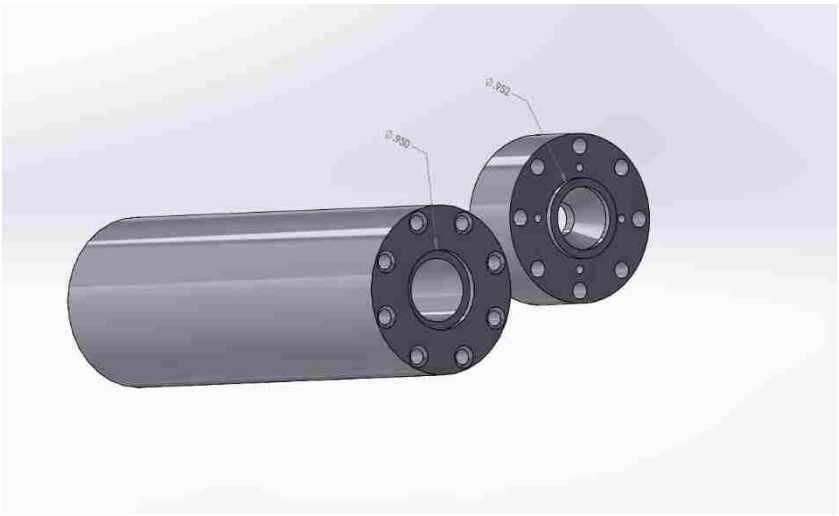

Figure 4-16: Bottom view of the barrel and top view of the nozzle mount.

4.2.2.3 Design of the nozzle assembly

The nozzle assembly was designed in order to allow manipulation of polymer melt by controlling the shear that the polymer melt experiences. Shear rate is controlled by the rotating nozzle developed in this project. The nozzle assembly of prototype 2 consists of nozzle mount, ball bearing, nozzle shaft and nozzle as shown in Figure *4-17*.

Figure 4-17: Parts of the nozzle assembly of prototype 2.

The nozzle mount is the main part that is responsible of attaching the barrel to the rotating nozzle. It is attached to the barrel through the outer counter holes as shown in Figure *4-17*. Moving inward, there are four holes that will give an easy access from the back to remove the bearing if needed to be replaced without causing damage to the other parts. Then, there is a counter hole where the rotating shaft of the nozzle will fit. The clearance between the outside diameter of the counter hole and the outside diameter of the rotating shaft of the nozzle should be able to perform two distinct features. First, it should allow the shaft to rotate freely. Second, it should prevent polymer from leaking between the counter cavity wall and the rotating shaft wall. According to literature on standard engineering tolerances [72], the minimum clearance between the shaft and the hole for our system should be .0010 inches and the maximum clearance should be 0.0034 inches to prevent shaking and to allow high speed rotations. The clearance between the rotating shaft and the hole was set to be 0.001 inches as shown in Figure *4-18*.

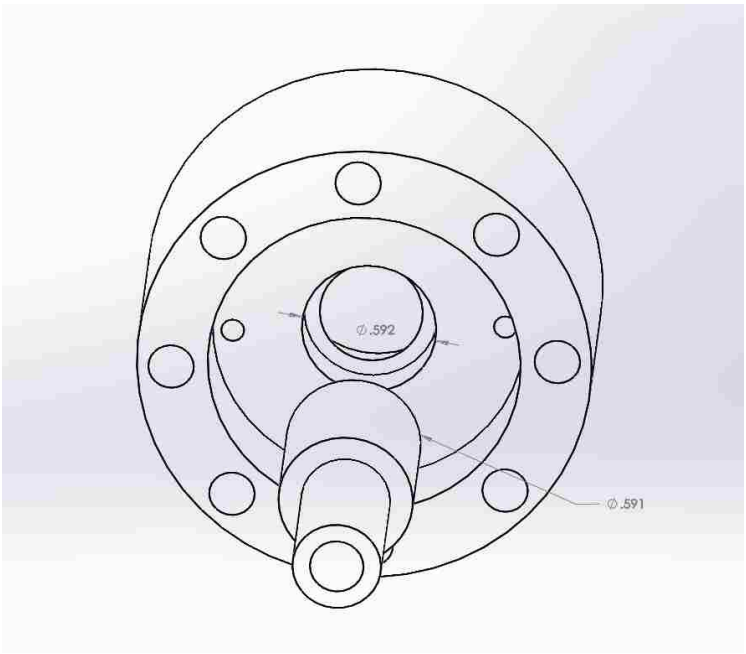

Figure 4-18: The clearance between the hole in the nozzle mount and the nozzle shaft.

The bearing used in prototype 2 is VXB brand model S62002ZZ high temperature 500 degrees stainless steel ball bearing. It can support axial and radial loads at high speeds. The bearing has 0.5905” inner bore, 1.3775” outer bore and has a 0.433” width. An important feature of this bearing is its dual-sided steel shielding that protects its high temperature lubricant from outside contaminants which will protect the bearing from contamination and failure in the event of a polymer flash. In order to assemble a functional bearing, the clearances between the bore of the bearing and the shaft, also, between the mount housing and the outside diameter of the bearing should be considered carefully based on the application and requirements. In this case where the expansion coefficient of the shaft and the housing are similar, the mount housing was designed to have 0.0005 inches less diameter than the outside diameter of the bearing. Also, the clearance between

the nozzle shaft and the bore diameter of the bearing was made to be 0.0005 as well as shown in Figure *4-19* [73].

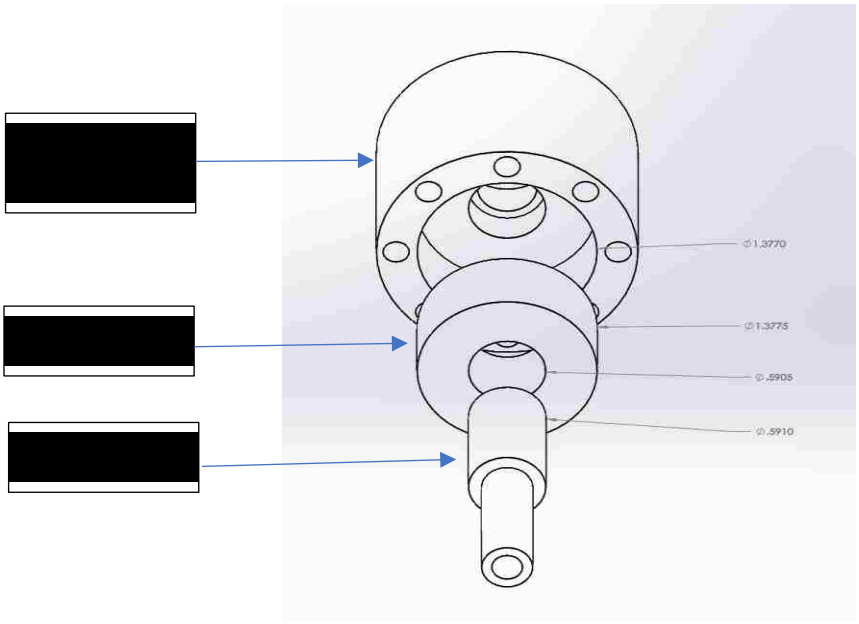

Figure 4-19: Clearances used to fit the bearing.

The inner of the nozzle shaft was designed to be threaded for an easily assembly of different nozzles. Nozzles with different diameters ranging from 0.2mm to 0.8 mm were bought for this project. Also, the outside diameter of the head of nozzle shaft was designed with consideration of the gear diameter that is used to rotate the nozzle. Figure *4-20* shows a view of the nozzle assembly fixed to the barrel and a bottom view of the mini extruder with gear and belt assembled to it.

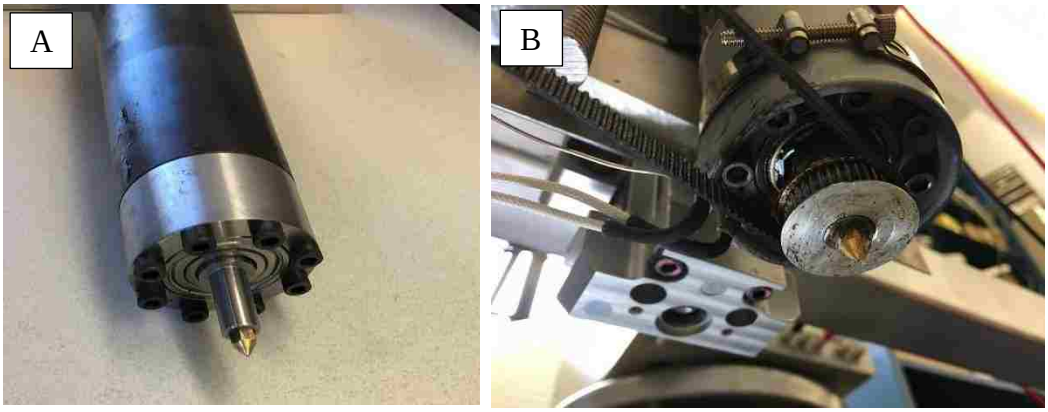

Figure 4-20: A) view of the nozzle assembly and the barrel. B) Bottom view of the mini extruder with gear and belt assembled to it.

4.2.2.4 Structural Base

The structural base is the main holder of all components. It supports all components of linear motions X, Y and Z. The structural base that was designed for use in prototype 2 is shown in Figure *4-21*. The base was designed out of steel and it was also designed to be able to support all components and minimize or prevent any vibration that may occur during the printing process. The four bore holes that are shown in the crossbeam were made to support the actuator that moves in the Z direction and holds the mini extruder with all its components.

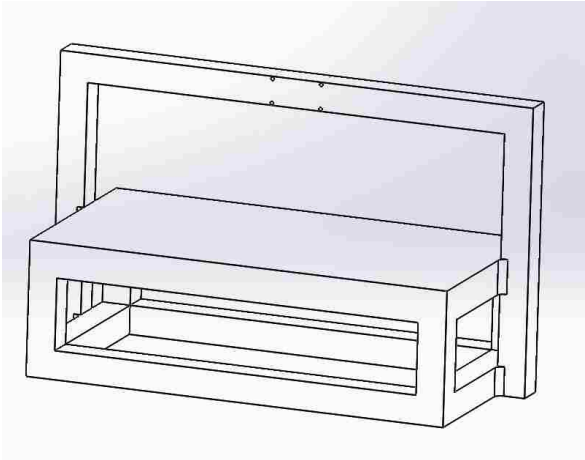

Figure 4-21: Diagram of the structural base of prototype 2.

4.3 Motion Control System

4.3.1 Axis control system

4.3.1.1 Hardware

Axis motion is the main feature that differentiates 3D printing from other manufacturing processes. It enables 3D printers to create objects that were impossible to be created otherwise. In our system, three dimensional linear actuators are responsible of the three-dimensional movements. Choosing the proper actuator is critical in order to achieve the desired performance and it requires a better understanding of the system requirements. The linear actuators used in our system were purchased from PBC linear which is an Illinois based manufacturer company. It has a precision of 50 microns. The Z axis actuator was chosen to be able to carry higher weight up to 20Ib since the mini extruder is mounted in the Z axis actuator as shown previously in Figure *4-15*. The linear actuators are held by the structural base as shown in Figure *4-22*. An aluminum adapter plate is bolted to the

crossbeam through the use of four mounting bore hole and then the Z actuator is attached to the adapter plate. The Y actuator is mounted to the platform of the structural base. An aluminum adapter is installed to the Y actuator. Then, the X actuator is mounted on top of the aluminum adapter plate perpendicular to the Y direction actuator.

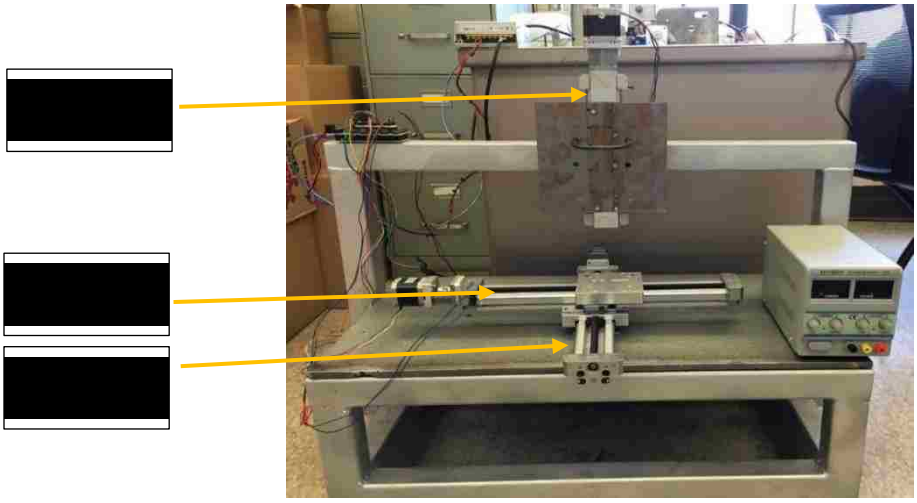

Figure 4-22: Three dimensional linear actuators.

The linear actuators use lead screws which translate the rotational motion of the stepper motors into liner motion. The stepper motor is connected to the lead screw of the linear actuator through motor mount and coupling as shown in Figure *4-23*. The stepper motors used for X and Y actuators are CNC Nema 17 2-phase stepper motors with a 0.2" diameter, 0.875" long shaft that is capable of rotating in 200, 1.8^{o} intervals or steps. The stepper motor used to move the Z actuator is CNC Nema 23 2-phase stepper motor with a 0.25" diameter, 0.875" long shaft that is capable of rotating in 200, 1.8^{o} intervals or steps.

This motor has a higher torque rating in order to be able move the higher load mounted to the actuator.

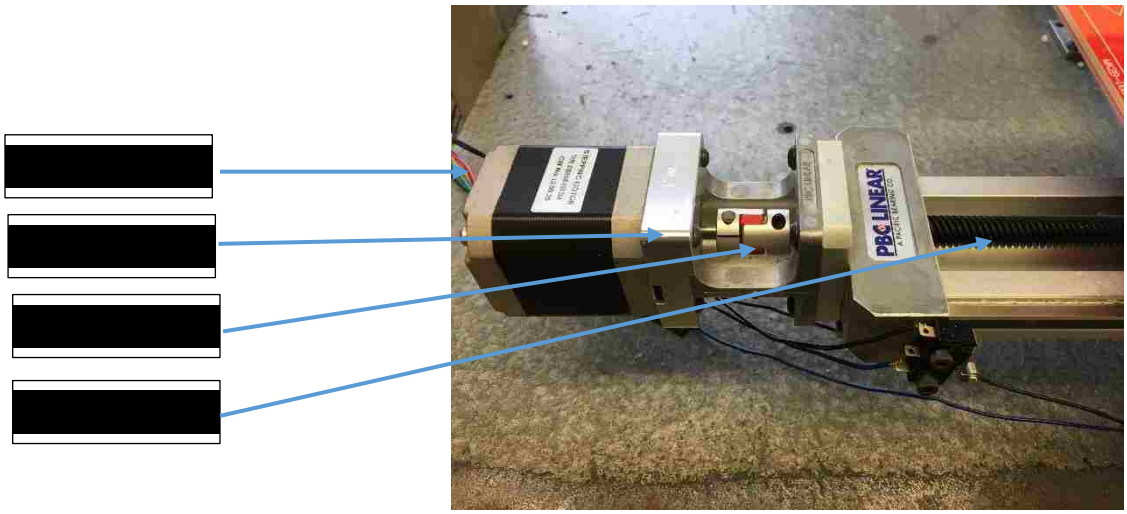

Figure 4-23: Mechanism of linear actuator connection to the stepper motor.

Extrusion based 3D Printers utilize different motional techniques to create objects such as Cartesian, Delta and Polar [74]. Cartesian printers move the stage in the Z direction and it moves the head in the X & Y directions. Brands such as Ultimaker and Makerbot use Cartesian technology. Delta printers move the head in all directions X, Y and Z while their stage doesn't move. The head of Polar printers move up and down while the stage can both rotate and move at the same time. The system we are using move the head in Z direction and the stage in X and Y direction.

4.3.1.2 Software

The hardware is of no value without a software and vice versa. The control kit used in prototype 2 is shown in Figure *4-24*. It includes Arduino 2560, 3D printer control board, power supply, stepper motors, end stops, wires, cable and Repetier host software.

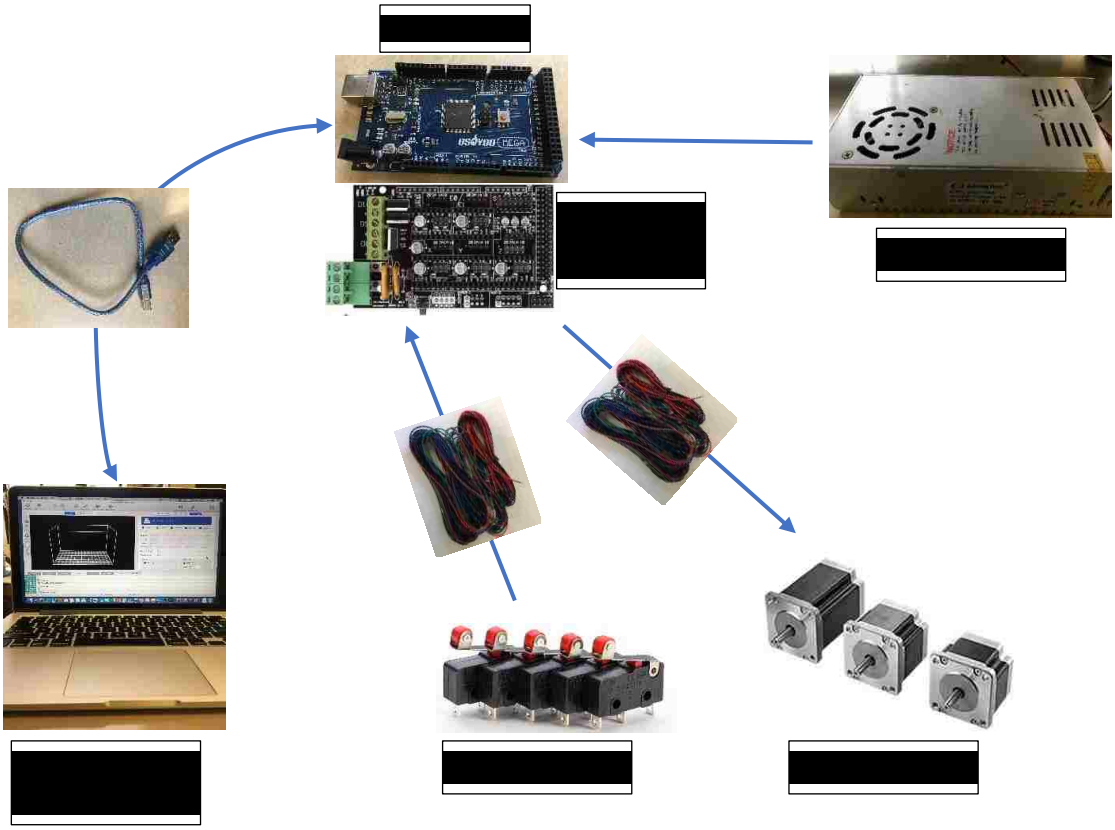

Figure 4-24: 3D Printer Control Kit.

The Arduino is an open source platform based on a simple input/output board [75]. It is connected to a computer through a USB cable where it allows the software and firmware to be uploaded to its memory.

The controller board sits on top of the Arduino, it is an adapter board and it delivers input to the stepper motors from the computer as G-code and from the end stops and then it give output to the stepper motor. Also, it allows communication between the software, the stepper motors and the end stops.

The Arduino Mega is powered through an external power supply. The power supply that is used is a 12-volt AC/DC. It gives power to the Arduino, the stepper motors that move the actuators and the end stops.

The software utilized is Repetier Host, it is a 3D printing software that supports windows, Mac and Linux operating systems [76]. It has a built in slicer where it allows the conversion of the STL file into G code. Moreover, the slicer cuts the model into horizontal layers and creates a path for the printer. Repetier Host is compatible with most firmware types, where firmware is the bridge that connects the software to the hardware [77]. The firmware translates the G-code sent by the software to the 3D printer. It tells the stepper motor how long it needs to turn in order to move the actuator for specific distance.

The linear actuators have to be calibrated with the stepper motors. The calibration is done through the firmware code in the customizable section of the code which is "Configuration H". The specifications of motors and linear actuators used are inputted to the "Configuration H" code. That way, the distance the actuators move is the distance required to make the desired shape. Otherwise, the print will be a mess and damage might occur to the printer due to the axis moving all over the place. Figure *4-25* shows an attempt to 3D print dog bone without proper calibration to the machine.

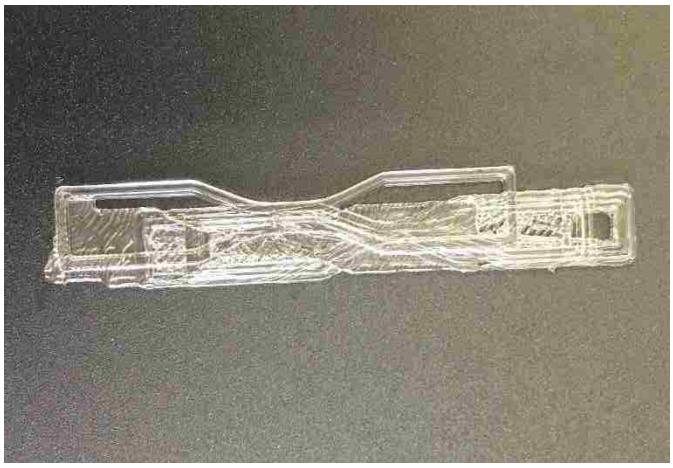

Figure 4-25: An attempt to 3D print a dog bone without proper calibration to the machine.

In order to resolve this issue, the steps per mm have to be adjusted from configuration H using the following steps.

1. Open the firmware and go to configuration H and then go to “axis steps per units”. Take the number for X axis. For ease of explanation, let’s assume the number is 43 steps per mm
2. Measure how far the machine moves. For example, order the machine to move an X amount of distance for example 100mm in the X direction. Then, using a caliber measure how far it really moves, let’s say it moved 55mm.
3. Divide the steps per mm found on the configuration H by the distance the machine actually moved when ordered to move for 100mm then multiply it by 100mm.

$$\frac{43\frac{steps}{mm}}{55mm} * 100mm = 78.18\ Steps/mm$$

4. Enter the new value into the firmware which is 78.18 in this case.

5. Order the printer to move 100mm again and measure how it really moved. If different than 100 mm, do the previous steps again.
6. Do the previous steps for Y and Z axis.
7. Save and upload the firmware to the Arduino.

When calibrating the Z axis, it is better to order the machine to move in the positive direction away from the stage. So, no risk of breaking the machine will occur if the head hits the stage. This step was learned the hard way where the machine was ordered to go 100mm in the negative Z axis. Then, it went unexpectedly way more than 100mm which caused the nozzle to hit the stage and break it.

4.3.2 Screw control system

The motor driving the screw has to rotate the screw at the desired speed. The speed should be constant since any fluctuations in speed will affect the thickness of the extruded road. The motor should also be able to supple the right amount of torque, since any changing in viscosity during extrusion will require different amount of torque in order to keep a constant rotational speed of the screw. Otherwise, the thickness of the extruded polymer will vary. Also, the screw control system should also be able to continuously adjust the screw speed if needed. The screw control system consists of DC motor and DC power supply.

The required torque to rotate the screw has to be calculated in order to choose the right motor for the application. The DC motor that is used to rotate the screw is PITTMAN

DC motor, the DC motor is shown in Figure *4-26*. This DC motor can produce torque of 2 lb.ft @ 161 RPM.

Figure 4-26: DC motor used for the screw extruder.

The power supply used is digital variable triple outputs linear type DC power supply, it is rated at 0-3- Volts @ 0-5 Amps. It is shown in Figure *4-27*. This DC power supply was chosen to have triple outputs, so, it will allow the wiring of the screw DC motor and the DC motor that rotates the nozzle.

Figure 4-27: DC Power Supply Controller.

The screw rotational speed is controlled manually by controlling the voltages. Also, any decrease in screw speed due to an increase in the viscosity of the melt, results in an increase in current, and hence torque. The motor torque increases to match that of the disturbance by the higher viscosity in order to keep rotating at the same rate.

4.3.3 Nozzle control system

The nozzle control system consist of DC motor, DC power supply, two gears and a belt as shown in Figure *4-28*. The DC motor used to rotate the nozzle is 12V and can rotate up to 550 RPM. It is powered through the same DC power supply utilized to rotate the motor of the screw extruder which was shown previously in Figure *4-27*.

The gears that are used have a ratio of 1 to 1, since the rotational speed of the nozzle was to be tested at lower speeds than 550RPM, and the DC motor is able to provide that

with the current setup. The gears ratio could be changed to 2 to 1 nozzle to motor, where the rotational speed of the nozzle can be increased to reach 1100 RPM if desired. The gears that are used were chosen to be aluminum instead of steel to decrease weight mounted on the Z actuator. The timing belt that is used has a pitch of 0.080” which match the pitch of the gears. It is dust free timing belt, to ensure clean print. It also can handle high temperature up to 180°C.

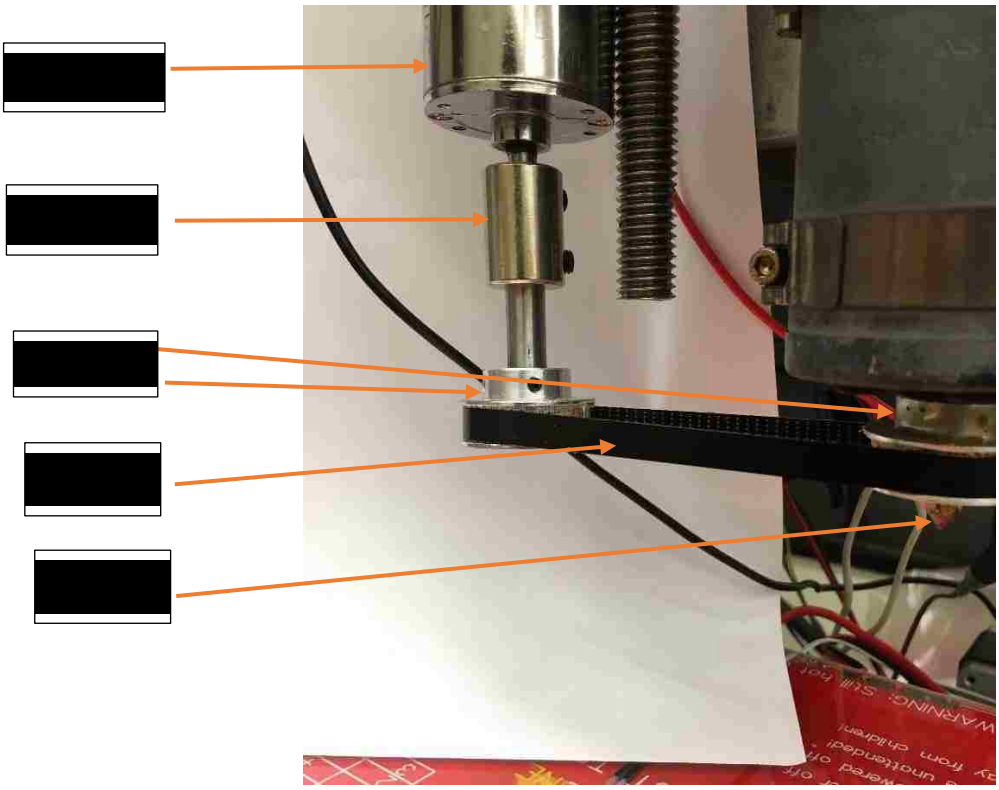

Figure 4-28: Components of nozzle control system.

A coupling was used to connect the DC motor to the gear, since the shaft housing of the gear has a larger diameter than the shaft of the DC motor.

4.4 Thermal control system

Band heaters were used to heat the extruder. Two heaters were used where one placed on the top and one on the bottom. The reason to use two small heaters instead of one big heater was to allow precise control of the polymer melt. In extrusion, the recommended feeding temperature usually is lower than the recommended nozzle temperature. For each band heater, there is a J type thermocouple used to measure the temperature of the extruder. Small holes are drilled into the extruder barrel and thermocouples are fitted into them to allow measurement of the extruder temperature as shown in Figure *4-29*.

Figure 4-29: Band heater and J type thermocouple.

Temperature controller is used to give power to the heaters and to allow communications between the heaters and the sensors used to measure the temperature which is the J type thermocouples. Through the temperature controller, the desired temperature can be set and also it can be changed during printing if desired. Although, it

takes some time to raise or lower the temperature. The temperature controller used is shown in Figure *4-30*, and it has two outputs where it can control up to two heaters.

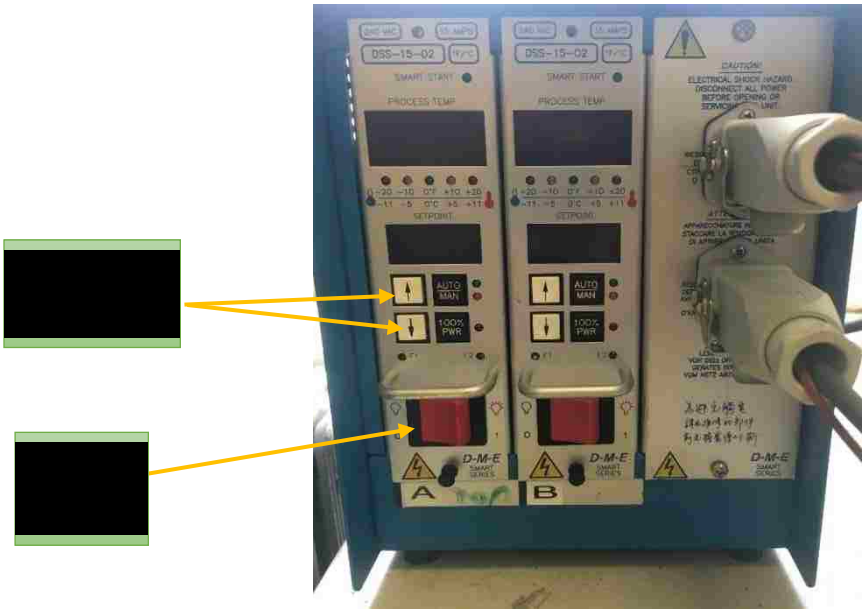

Figure 4-30: Temperature Process Controller.

4.5 Results and Discussion

Testing started after all parts were assembled together in prototype 2. First, the heaters were checked to make sure the melting temperature of the material to be tested can be achieved. PLA grade 3052D in form of Pellets were used in the first testing. Screw was set to run at 50 RPM. Then, the material was fed to the hopper. Unfortunately, the pellets

became partially melted and then got stuck into the hopper. As a result, pellets didn't move forward to feed the extruder.

Feed hoppers are used to hold pellets and feed them to the extruder. Usually the material flows by gravity from the hopper into the extruder. The temperature of the hopper should be lower than the glass transition temperature of the polymer. As in our case, the temperature was higher than the glass transition temperature. In order to solve this problem and after doing much research regrading this, there are a couple of techniques that were suggested to fix this issue. First, cool the hopper to a temperature below the glass transition temperature of the polymer being used. So, pellets will not get partially melted and then get stuck. Second, use vacuum hopper where the pellets will be sucked in, so, there is no time for them to be exposed to heat and get melted in the hopper. Since the previous two solutions would add more weight and complexity to the system, we decided to remove the hopper and use force to feed the material into the extruder in order to be able to test the functionality of the system. Figure *4-31* shows prototype 2 with and without the hopper.

Experimental testing was carried on again after removing the hopper. Pellets were fed directly into the extruder as shown in Figure *4-31*. After adjusting the temperature a couple of times, polymer extrusion through the nozzle was achieved. The main disadvantage of this solution is that constant feeding is required to keep extruding at the same rate. Otherwise, the layer thickness of the printed roads will vary.

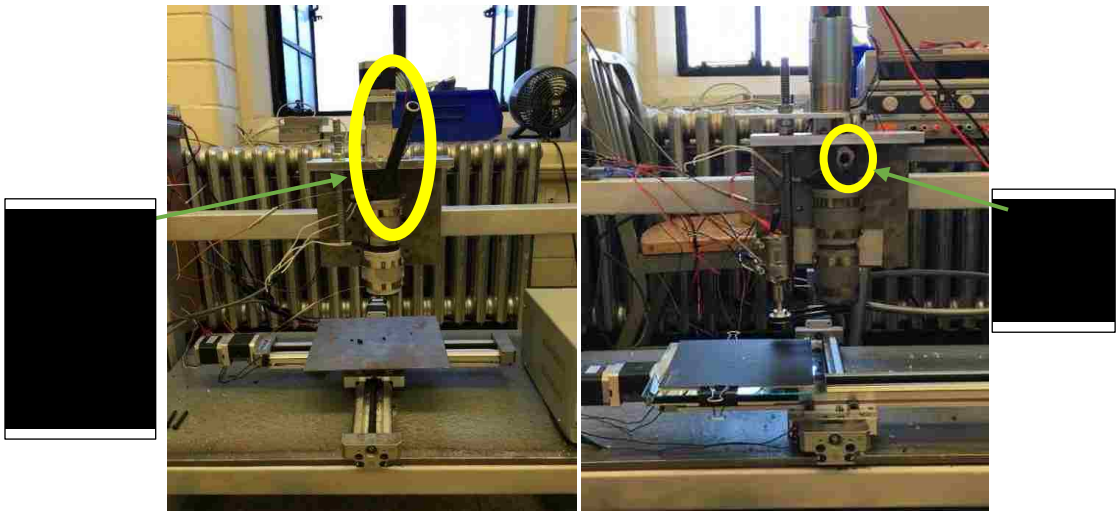

Figure 4-31: Before and after removing the hopper of Prototype 2.

The performance of the rotating nozzle was tested after polymer extrusion was achieved. The nozzle was adjusted to rotate at 100 RPM. It was found that the nozzle is rotating smoothly as there is some friction is preventing the nozzle from rotating at a constant rate. This issue was not evident when the parts of the nozzle assembly were put together as the nozzle was rotating smoothly. The issue was assumed to be caused by thermal expansion of the nozzle assembly parts which as a result caused the nozzle to not rotate properly. Therefore, the clearances of the assembly had to be adjusted. The clearance between the nozzle shaft and the nozzle mount housing shown in Figure *4-18* was adjusted to be 2000 of an inch instead of one thousand of an inch. Testing was carried on again after assembling the parts. The nozzle was rotating smoothly at this time.

The DC motor that rotates the screw started overheating after printing for 15 minutes or more. The reason it overheated because of its direct connection to the screw extruder. One solution was to design gears in order to,

1. Increase the torque and reduce the motor load.

2. Avoid the direct connection between the DC motor and the screw.

This solution would add weight to the Z axis actuator and the total weight limit of this actuator is almost used. Because of that, another solution had to be thought of. An external fan to cool the DC motor was used. It didn't add any weight to the Z axis actuator since it was fixed on the beam of the structural base shown in Figure *4-21*. The fan works well to cool the DC motor which prevented it from overheating again.

4.6 Conclusion

The 4D Rheo-Printing system is a novel technique that was developed to increase the potentials of 3D printing. It allows for precise melt rheology control. The system is extrusion based 3d printer with screw extruder that utilizes a rotating nozzle. The fourth dimension is dynamic melt rheology control during processing which is utilized with the screw extruder and the rotating nozzle. Extrusion based 3D printer with screw extruder was developed since it has many advantages over Fused Filament Fabrications (FFF). It cuts one of the processing steps of 3D printing which is the manufacturing of filaments. Therefore, parts can be printed with lower costs since pellets have also substantial lower costs than filaments. This types of printers also is ideal for those who are trying to use additives since they can be easily added. These types of printers also have higher flow rates compared to FFF. The rotating nozzle introduced in this system have many advantages which will be discussed in Chapter 6. The current version of the printer is shown in Figure *4-32*

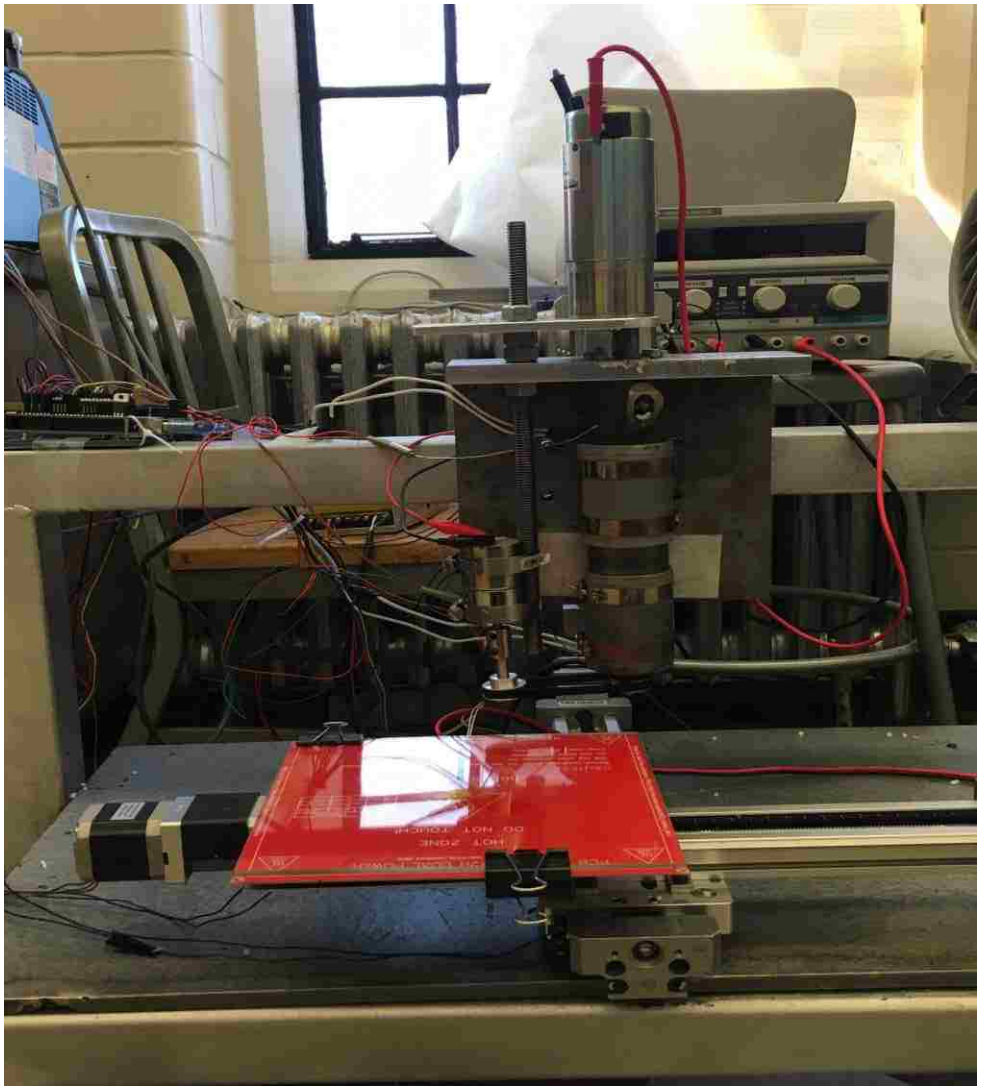

Figure 4-32: Current version of the 4D Rheo-Printer

CHAPTER 5: Analytical Investigation

5.1 Introduction

The main aim of the analytical investigation chapter was to investigate the melt rheology behavior of a commonly used polymer PLA under different processing conditions and to validate the novel concept.

Numerical simulations were first conducted to validate the 4D Rheo-Printing concept and compare it to traditional additive manufacturing techniques. The effect of the rotating nozzle on shear rate and viscosity was investigated numerically via ANSYS Fluent.

Once the material exits the nozzle in the case of extrusion based additive manufacturing, the main factors that influence its properties are cooling rate and stage temperature or ambient temperature. Therefore, in order to attain the final desired properties a precise control of cooling rate and ambient temperature has to be obtained after shearing the material. Polymers are long chain molecules and when they are exposed to shear rate, their molecules get stretched. Once shear rate disappears, the molecules go back to their original state. The speed or the time it takes them to fold back to their original state is called the relaxation time, which is dependent on the temperature. There are several models to investigate relaxation analysis of molecules which will be discussed in this chapter to have a better understanding of the material and how to cool it to achieve desirable outcome.

This chapter includes also crystallization kinetics analysis of the polymer to be used experimentally which is PLA. The crystallization kinetics is also dependent on the temperature and shear rate.

This chapter consists of three parts numerical simulation analysis, molecular relaxation analysis and crystallization kinetics analysis.

5.2 Numerical simulation (ANSYS Fluent)

The effect of the rotating nozzle on shear rate was studied numerically via simulation to:

- Validate the 4D Rheo-Printing concept.
- Compare the results to conventional extrusion based 3d printers.
- Establish a baseline of what angular velocity (RPM) is required to achieve the desired viscosity.

In this investigation, the nozzle was rotated at different angular velocities (RPM) and shear rate was documented. The geometry of the nozzle is the same used in fused deposition modeling printers with a nozzle tip diameter of 0.4mm as shown in Figure *5-1*.

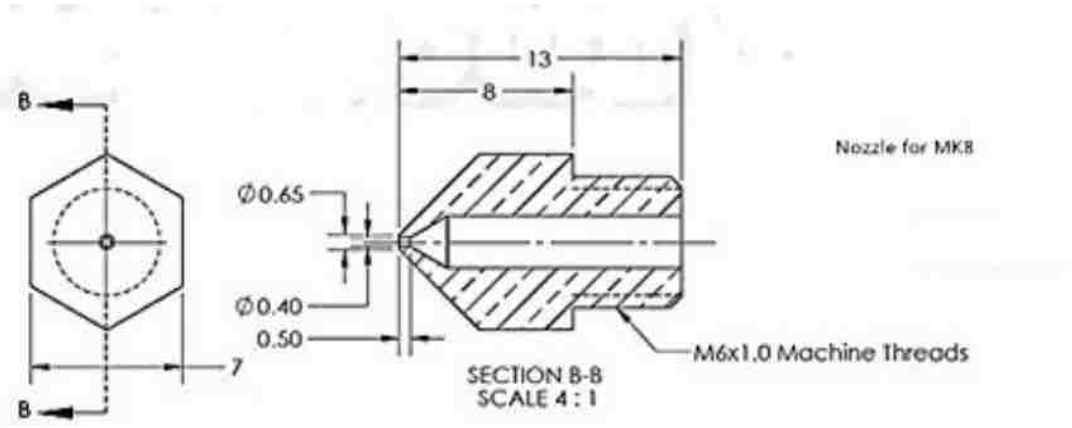

Figure 5-1:Drawing of nozzle.

The material that was used in these simulations is poly (lactic acid), PLA 3052D manufactured by *NatureWorks LLC*. The property data for this material was imported from *Autodesk Moldflow*.

ANSYS Fluent was used to conduct the simulation since it supports transient motion (rotational and translational). The equation the software uses to calculate shear rate is Cross Law model (Equation 1). The zero shear viscosity (η_0) is calculated using Equation 2 [33]:

$$\eta = \eta_0 /(1 + (\eta_0 \dot{\gamma}/ \tau^*)^{1-n} \ldots\ldots\ldots (1)$$

$$\eta_0 = D_1 \exp[((-A_1(T - T^*))/(A_2 + (T - T^*))] \ldots\ldots (2)$$

Where:
η: melt viscosity (Pa-sec)
T : Temperature (K)
T*: Glass Transition Temperature determined by curve fitting
$T^* = D_2 + D_3 p$
P: Pressure (Pa)

The data for the Non-Newtonian fluid was obtained from the *Moldflow* database Table 5-1. These values were then input into Ansys Fluent.

Moldflow Data for PLA 3052D
Power Law index (n) = 0.3846
τ^* = 129000 Pa
D_1= 2.045e+007 Pa-s
D_2= 373.15 K
D_3= 0 K/Pa
A_1= 16.71
A_2= 51.6 K

Table 5-1: PLA 3052D data taken from MoldFlow

Simulations were performed at two different printing speeds 30 mm/s and 90 mm/s, each of these speeds were simulated at 4 angular velocities of the nozzle 0, 100, 250 and 500 RPM. The temperature of the nozzle was set to 420 F which is the recommended nozzle temperature for this material according to NatureWorks. Two cross section planes were chosen at the nozzle to be investigated as shown in Figure *5-2*.

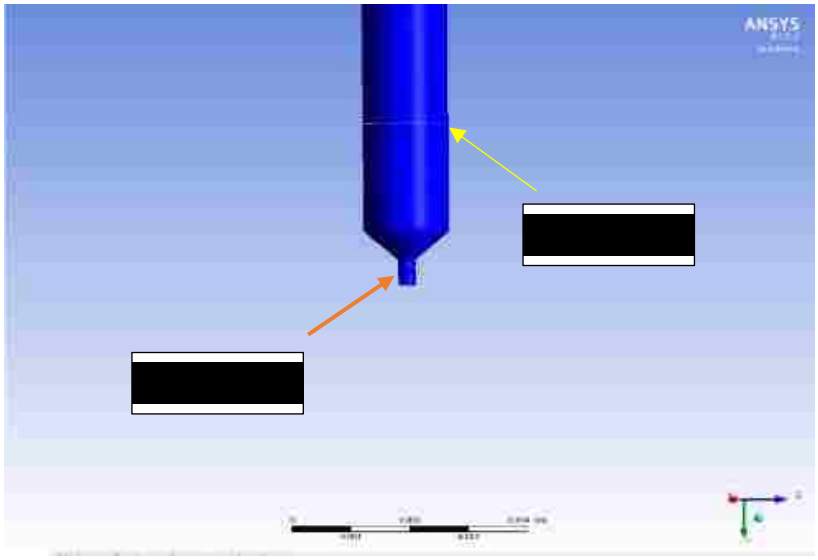

Figure 5-2: Nozzle Geometry.

Numerical Simulations at plane 1 were conducted. The nozzle was rotated at different angular velocities and shear rate was investigated. The results of shear rate that the polymer experiences inside the nozzle at different rotational speeds are shown below in Figure *5-3*Figure *5-4*Figure *5-5*. The results also compare the influence of printing speed on shear rate. The results of printing speeds of 30 and 90 mm/s are documented below.

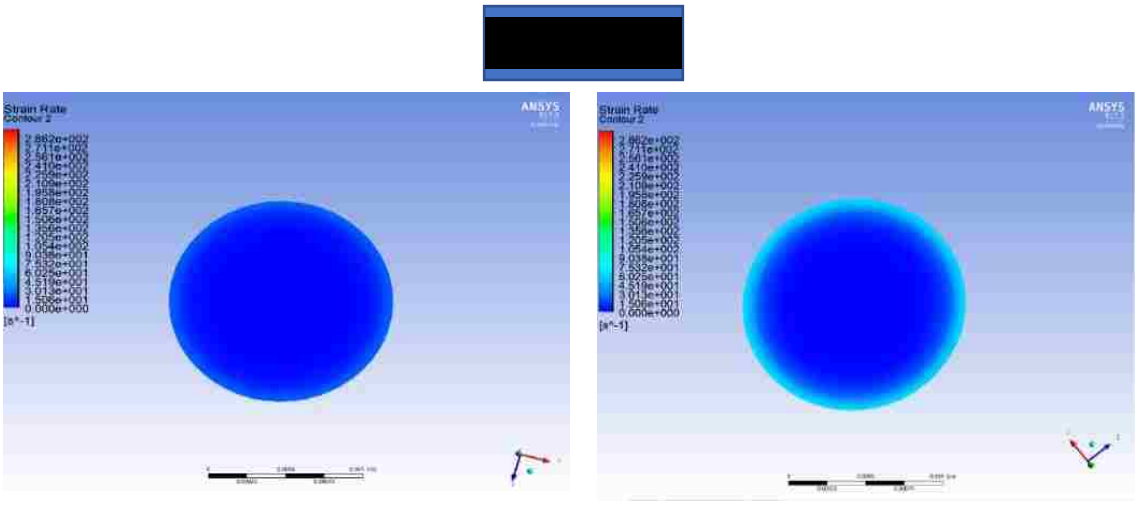

Figure 5-3: Left V= 30mm/s, Right V= 90mm/s.

[redacted]

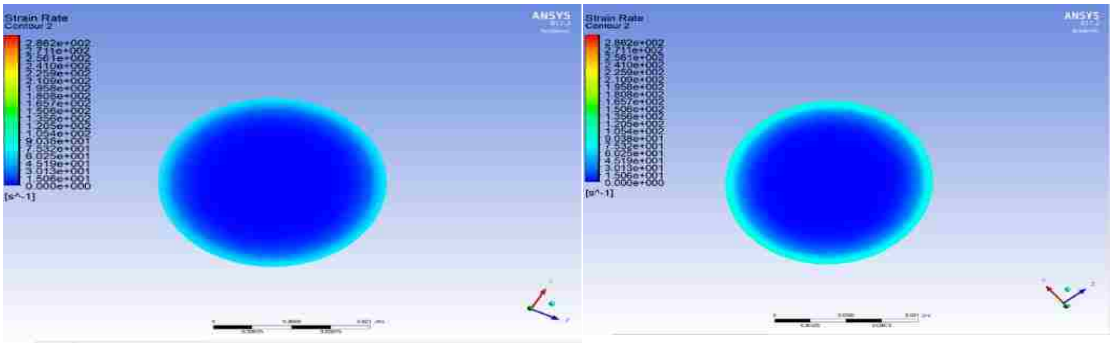

Figure 5-4: Left V= 30mm/s, Right V= 90mm/s.

[redacted]

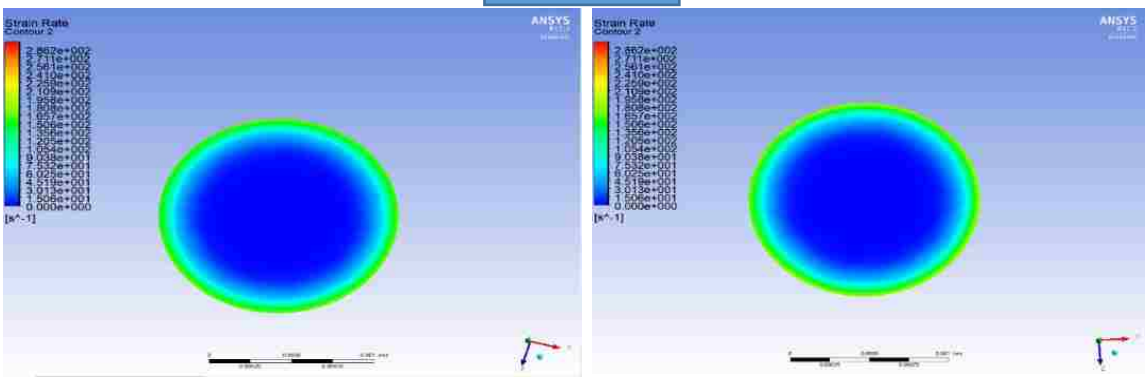

Figure 5-5: Left V= 30 mm/s, Right V= 90 mm/s.

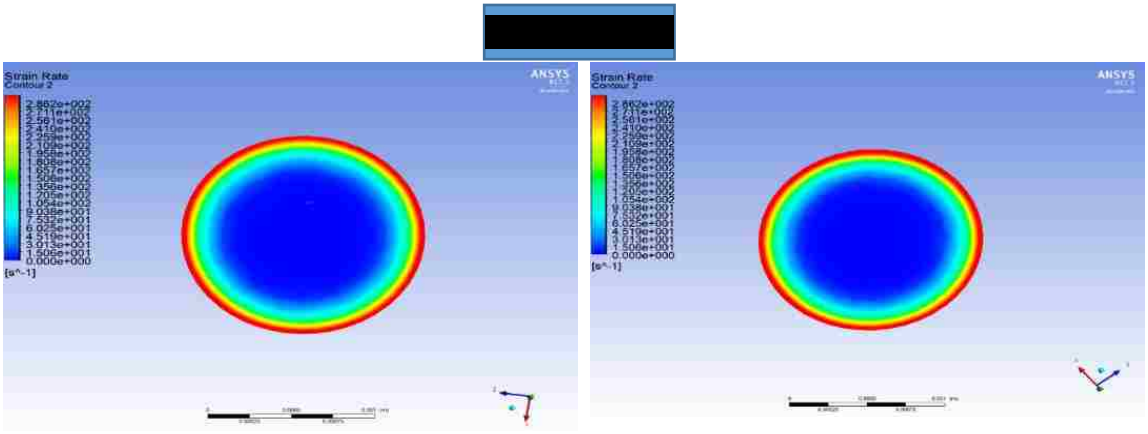

Figure 5-6: Left V= 30 mm/s, Right V= 90mm/s.

As shown in Figure *5-3*, which represents shear rate simulations without rotating the nozzle, this is the typical shear rate that molten polymer experiences at the nozzle of conventional 3D printers such as FDM. Figure *5-3* shows also that printing speed of 90 mm/s increases shear rate slightly more than that of 30 mm/s. As the rotational speed of the nozzle increases in Figure *5-4*, Figure *5-5*, and Figure *5-6* shear rate increases significantly compared to the non-rotating nozzle, which proves that the rotating nozzle is significantly effective when it comes to inducing shear rate.

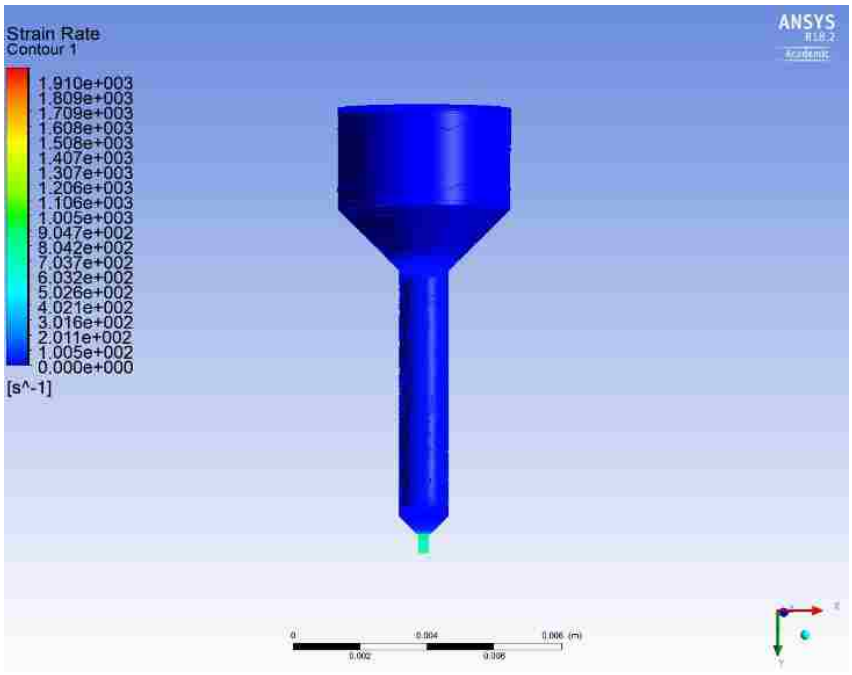

Figure 5-7: shear rate results of printing speed of 30 mm/s & nozzle not rotating

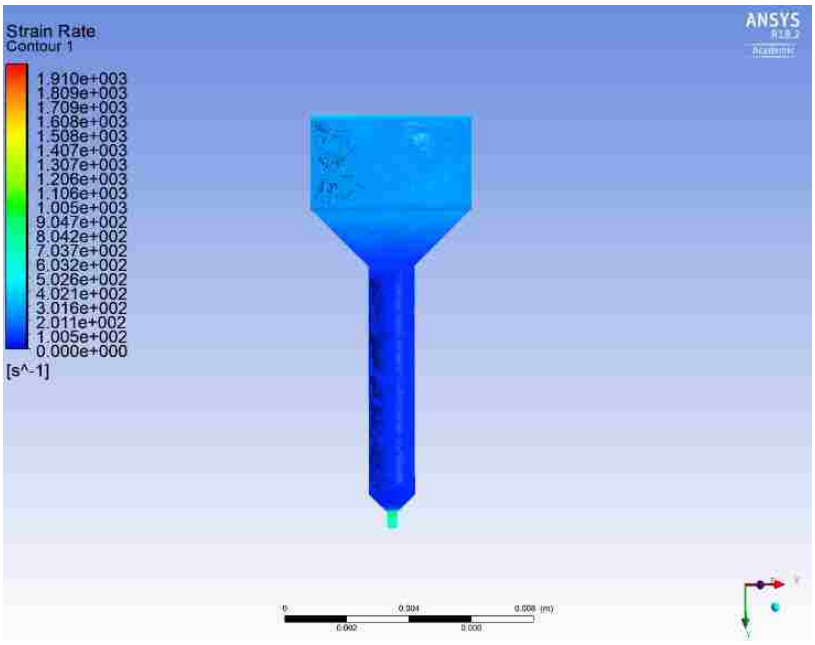

Figure 5-8: shear rate results of printing speed of 30 mm/s & nozzle rotating at 100 RPM.

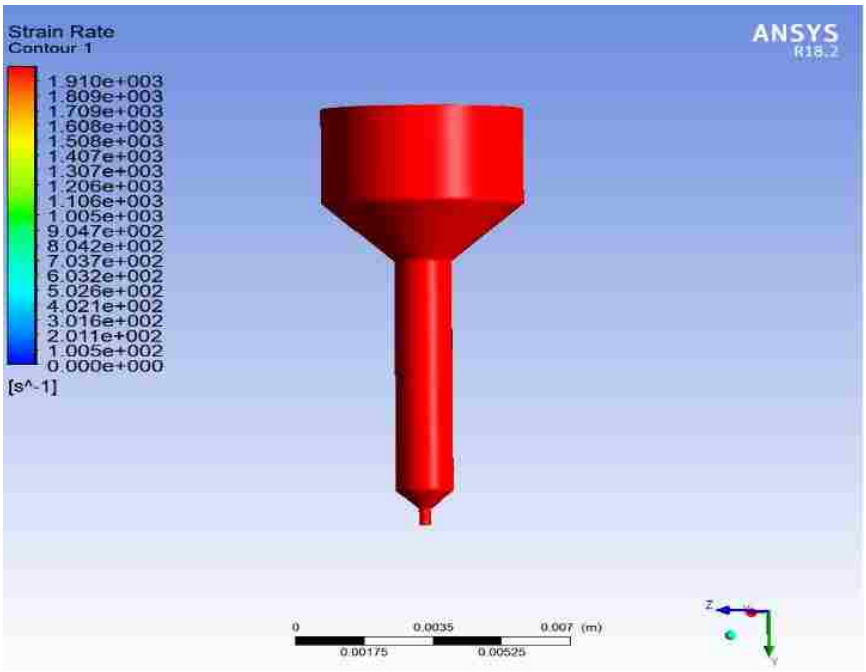

Figure 5-9: shear rate results of printing speed of 30 mm/s & nozzle rotating at 1000 RPM.

Figure *5-7*, Figure *5-8*, and Figure *5-9* show shear rate results of the nozzle at 0, 100 and 1000 RPM. Applying rotation showed significant effect on shear rate throughout the whole nozzle. Comparing the shear rate results at the tip of nozzle that were shown previously in Figure *5-7*and Figure *5-8*, the two cases show similar shear rate at the tip of the nozzle although one was conducted without rotating the nozzle and the other one was at a rotating nozzle of 100 RPM. The reason due to the smaller diameter of the tip of the nozzle which causes the shear to be high and the smaller diameter along with the velocity turned to dominate the influence of shear at low rotational speed of the nozzle. On the other hand, when the nozzle was rotated at 1000 RPM, the shear rate increased significantly at the tip which is shown in Figure *5-9*.

The results of average shear rate at different rotational speed of the nozzle (RPM) taken at plane 1 and plane 2 that were indicated previously are shown in Figure *5-10* and Figure *5-11*. Plane 2 shows the shear rate results the material experiences at the tip of the nozzle, while plane 1 shows the shear rate in the middle of the nozzle, which has slightly larger diameter.

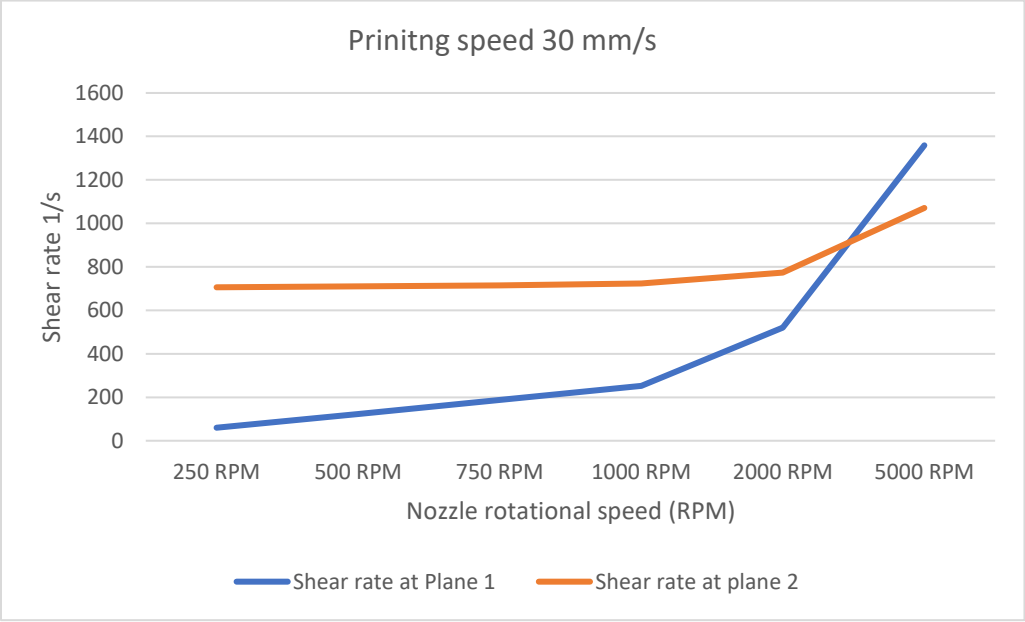

Figure 5-10: Average shear rate at different nozzle RPM and at printing speed of 30 mm/s investigated at two different planes of the nozzle.

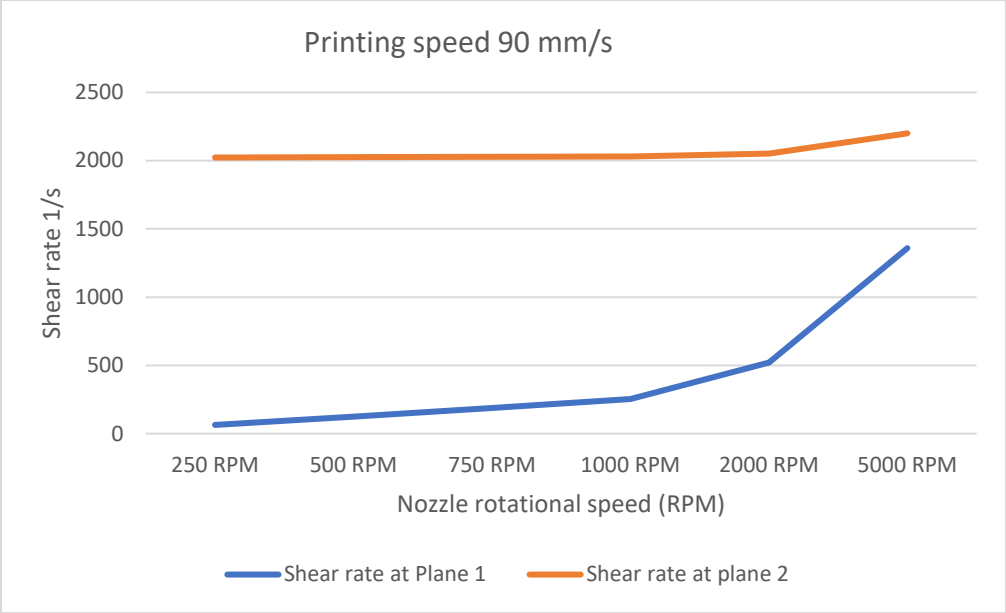

Figure 5-11: Average shear rate at different nozzle RPM and at printing speed of 90 mm/s investigated at two different planes of the nozzle.

By analyzing the results shown in Figure *5-10* at a printing speed of 30 mm/s. At low nozzle RPM, shear rate at plane2 is much higher than plane1 due to the smaller diameter of plane2. As the nozzle RPM increases, shear rate at plane1 increases, while shear rate at plane 2 stays constant. The reason is due to the smaller of plane 2 is dominating the influence of shear rate. For ease of explanation, let's assume that there is a particle going down the nozzle at a speed of 30 mm/s, the length of the nozzle is 30 mm. So, it will take the particle 3 seconds to exit the nozzle. Let's also assume that the nozzle is rotating at 1 RPS, so, the particle will experience just 3 revolution per seconds, and the slower the speed of the particle the longer the particle will experience rotation which means more shear in our experiment. Also, the larger the diameter as in plane1, the more the influence of rotation on shear rate. At very high RPM, the shear rate at plane 1 became higher than plane 2.

In the case of printing speed of 90 mm/s as shown in Figure *5-11*, the results at low RPM are similar to the one with printing speed of 30 mm/s, except that shear rate of plane2 is much higher compared to the previous case at 30 mm/s. At high nozzle RPM, shear rate at plane2 was still higher than that shear rate at plane1. The reason is due to the velocity is dominating the influence of shear rate and it requires much higher rotation to induce more shear.

5.3 Viscosity versus shear rate and temperature.

Viscosity of Pseudo Plastics non-Newtonian fluids decreases with increasing shear rate. The reduction in viscosity due to the polymer chains orienting from shear rate which allow them to pass freely around each other. Temperature also reduces viscosity of plastic materials. The effect of shear rate and temperature on viscosity of PLA was investigated analytically and it is shown in Figure *5-12*. The cross model was chosen equation (1) and (2) to be utilized in this analysis over power law model since it is not limited to a linear relationship between viscosity and shear rate [33]. It is also important to note that each material behaves differently under shear and this investigation was conducted using PLA grade 3052D provided by NatureWorks.

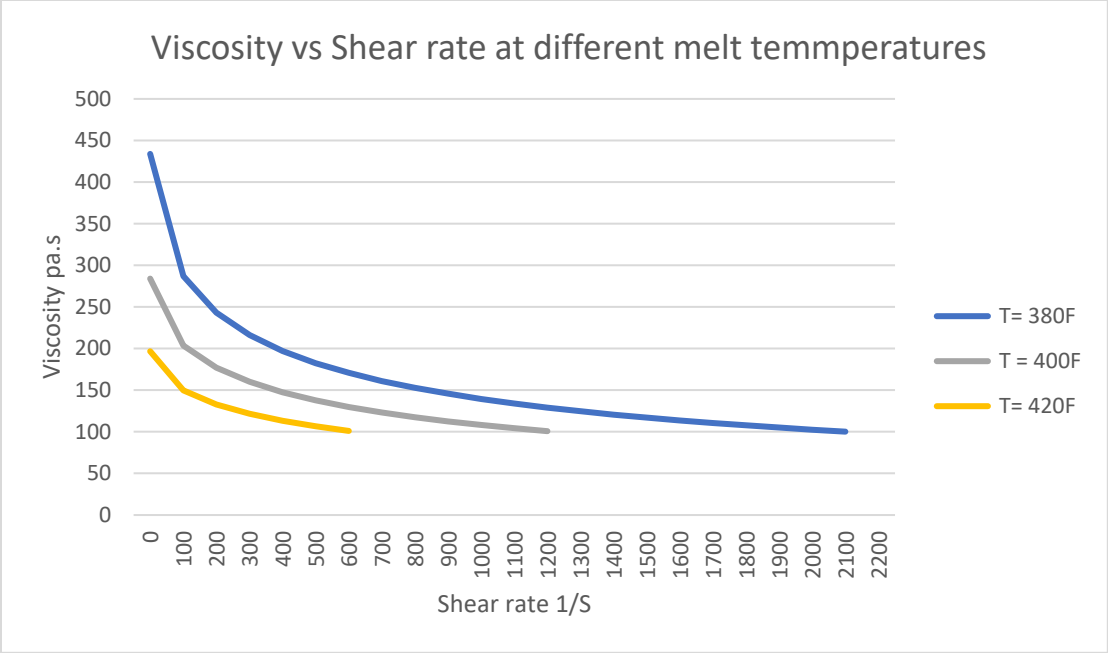

Figure 5-12: Calculated Viscosity at different shear rate and temperatures of PLA using cross model.

Figure *5-12* show the investigation results that was conducted to study the effect of shear rate and temperature on viscosity of PLA. The recommended melting temperature of this material according to NatureWorks is 400F, at this temperature the zero shear viscosity was around 284 pa.s. Let's assume that the optimum melt viscosity is 284pa.s, which is the viscosity at the recommended melting temperature. At a temperature of 380F, the viscosity was 433pa.s. The optimum melt viscosity at a temperature of 380F was achieved by applying shear rate of 150 1/s. These results indicate the shear rate sensitivity of the used material.

The viscosity changes with the rotating nozzle (RPM) for both amorphous PLA and semi crystalline PLA were investigated numerically through Ansys Fluent as shown in Figure *5-13*.

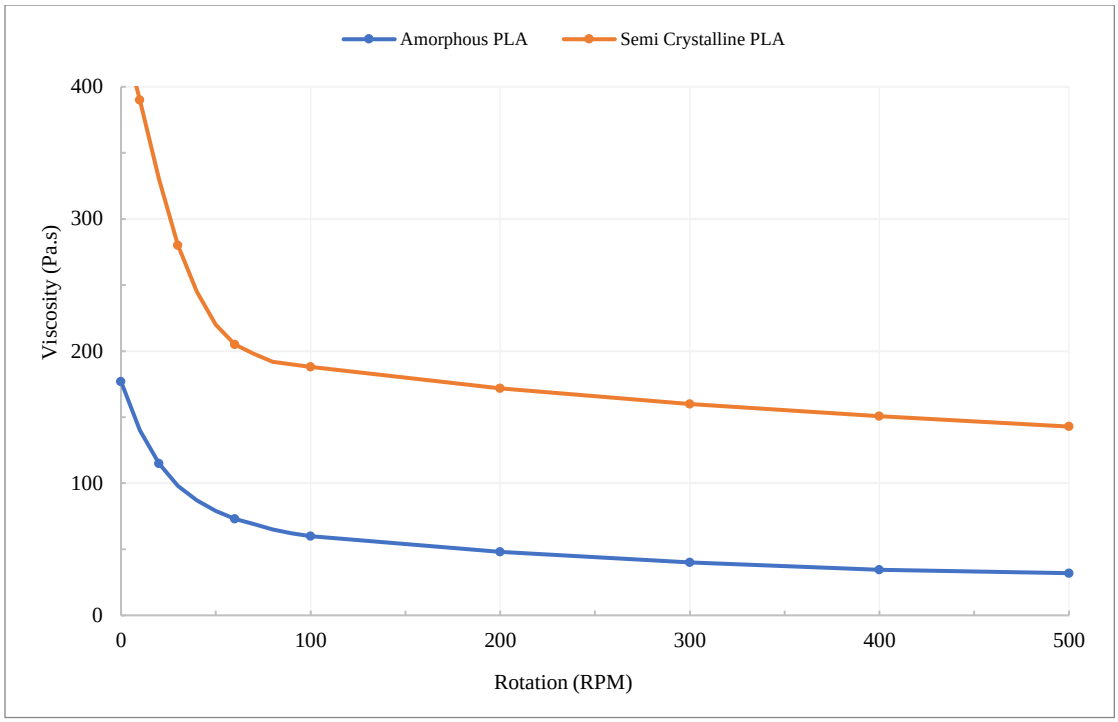

Figure 5-13: Numerical results of average viscosity at different rotational speed of the nozzle at plane 1

The results shown above show the effect of the rotational nozzle on the viscosity of both amorphous and semi crystalline PLA. At 0 RPM, there is shear rate already acting on the material due to the flow rate. So, the viscosity at 0 RPM is not the zero shear viscosity. It is clear and expected that the viscosity of the Semi crystalline PLA to be higher than that of the amorphous PLA at the same temperature. The results indicate the capability of the rotating nozzle to reduce viscosity of PLA. The viscosity of both materials were reduced dramatically using the rotating nozzle.

5.4 Molecular relaxation analysis

After the material exists the nozzle the control of the ambient temperature and cooling rate will enable continued influence over molecular orientation and crystallinity. A fast cooling rate will freeze in more of the molecular orientation induced by shear at the rotating nozzle into the part, while a slow cooling rate will allow the molecular orientation to relax. In the case of semi crystalline materials, a fast cooling rate can limit crystallinity and growth causing the crystallites to remain small, while slow cooling rate will allow more crystals to grow to achieve higher end crystallinity. So, ambient temperature and cooling rate should be adjusted according to the final required part's properties and to the material that are being used.

Doi Edward model was used to investigate the relaxation time of PLA, the relaxation time is calculated using the following formula as motioned previously in chapter 3:[47]

$$\tau = \frac{15Me\eta 0}{\pi\ 2\rho RT}$$

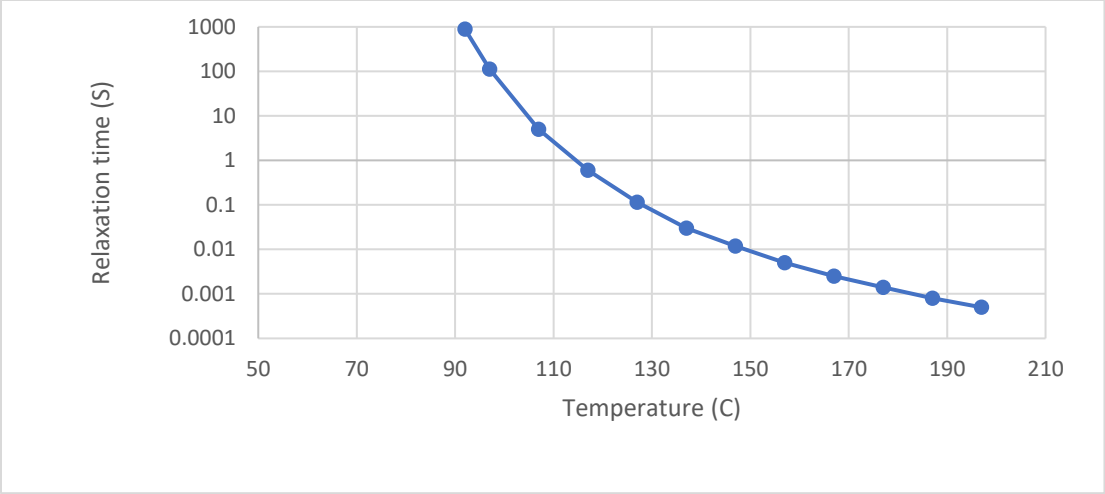

Figure 5-14: Relaxation times of PLA.

Figure *5-14* shows relaxation times of PLA at different temperatures, it shows how fast the molecular chains will relax and go back to their original state after being stretched by shear rate. At a temperature of 115, the relaxation time was around 1 second which is still quiet fast. As the temperature goes down, the relaxation times become slow. One of the advantages of the 4D Rheo-printing technology is its ability to extrude polymers at lower temperatures since it can reduce viscosity for extrusion by introducing shear rate at the nozzle. This characteristic will allow molecular chains to relax slower when extruded at lower temperature, thus, better control of frozen molecular orientation into the printed parts can be achieved.

5.5 Crystallization kinetics

Avrami equation was used to calculate the non-isothermal crystallization kinetics. The crystallization kinetics of PLA was calculated using Avrami equation at different cooling rate as shown in *Figure 5-15*.

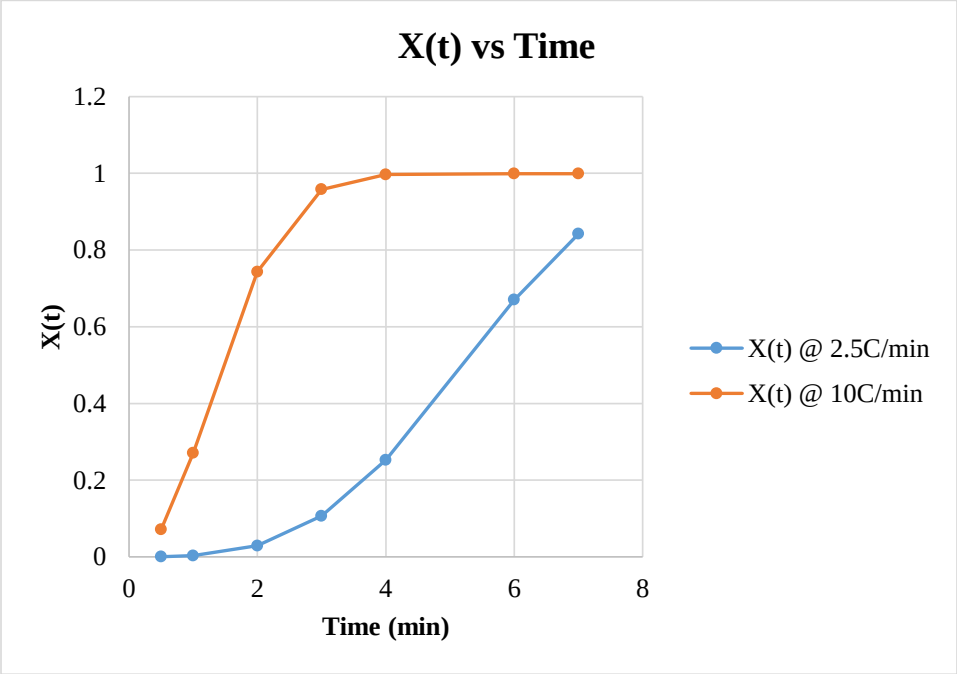

Figure 5-15: Crystallization kinetics of PLA at different cooling rates.

The results show that as the cooling rate can influence the crystallization kinetics. As the cooling rate increases the crystallization kinetics increases as well.

5.6 Conclusion

Numerical simulations using Ansys Fluent were conducted to validate the proposed concept and to establish a baseline of the parameters to be used in the experimental work. The results showed the capability of the 4D Rheo-Printing concept (the rotating nozzle) to induce and tune shear rate of the polymer melt. Therefore, the entanglement of the chain molecules get reduced, which allow the chains to slip past each other. As a result, the viscosity becomes lower which was proved numerically and analytically.

CHAPTER 6: Experimental Investigation

6.1 Introduction

This chapter includes three parts,

The first part includes crystallization analysis investigation of the materials to be used in the experimental work. Non isothermal crystallization analysis under quiescent conditions were conducted using DSC. The reason to conduct this investigation was to understand the crystallization behavior of the materials and to establish a baseline of the parameters to be used in the experimental work.

The second part includes the work that was conducted to investigate the influence of various processing factors such as melt temperature, stage temperature and shear rate on the final properties of PLA parts. This is the first test of its kind in 3D printing to investigate the influence of shear rate incorporating a rotating nozzle.

The third part includes the investigation that was conducted to investigate the capability of the 4D Rheo-printing system to enable multi material printing with single extrusion head.

6.2 An investigation of polymer crystallization under quiescent conditions

6.2.1 Introduction

The crystallization behavior of different grades of PLA was investigated under quiescent conditions. The investigation was conducted using thermal analysis DSC. This investigation was conducted to understand the different grades of PLA materials and to establish a baseline of what crystallinity can be achieved for each material. For polymer processors, this investigation along with the next study conducted next in this chapter can help to identify the optimum processing conditions such as bed temperature and surrounding temperature in the case of 3D printing, mold temperature and cooling rate in the case of injection molding. Therefore, high performance products can be manufactured and tuned based on the consumer's needs. Also, this study was conducted to be able to understand and distinguish between the final properties driven by the isothermal crystallization and non-isothermal crystallization which will be discussed later in this chapter.

6.2.2 Materials

This investigation was conducted on three grades of PLA using DSC. Figure 6-1 shows the materials that were used in this investigation which are 3052D, 2500HP and 2500HP with additives. PLA 2500HP with additives contains >85% Ingeo™ 2500HP and <15% proprietary blend of additives that include a nucleating agent, an accelerant, an impact modifier, and a mold flow agent.

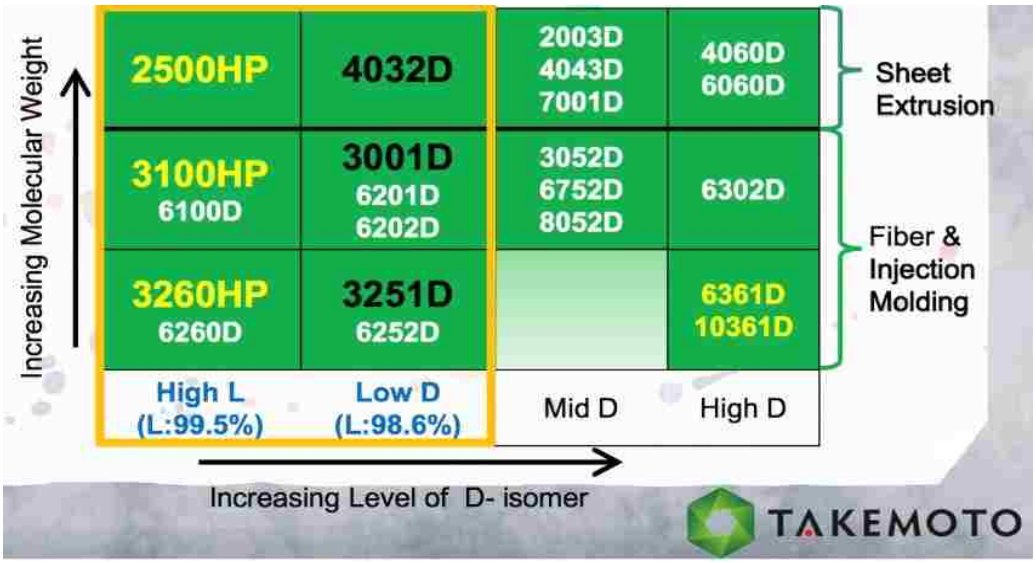

The three materials that are being investigated were studied under the same conditions in order to understand them and be able to compare them next to each other. The test procedure was set as follows:

1. Heat the material to 200°C at a rate of 10°C/min.
2. Cool down to 100°C at a rate of 25°C/min.
3. Isotherm for 5 minutes
4. Cool down to 25°C at a rate of 25°C/min.
5. Isotherm for 2 minutes
6. Heat the material again to 200°C at a rate of 10°C/min.

The results presented in Figure 6-2 is showing the last heating cycle to investigate the effect of cooling rate, isotherm temperature and isotherm time on the crystallinity and crystal structure of different grades of PLA. The procedure process along with calculated crystallinity and melting temperature are shown in Table *6-1*.

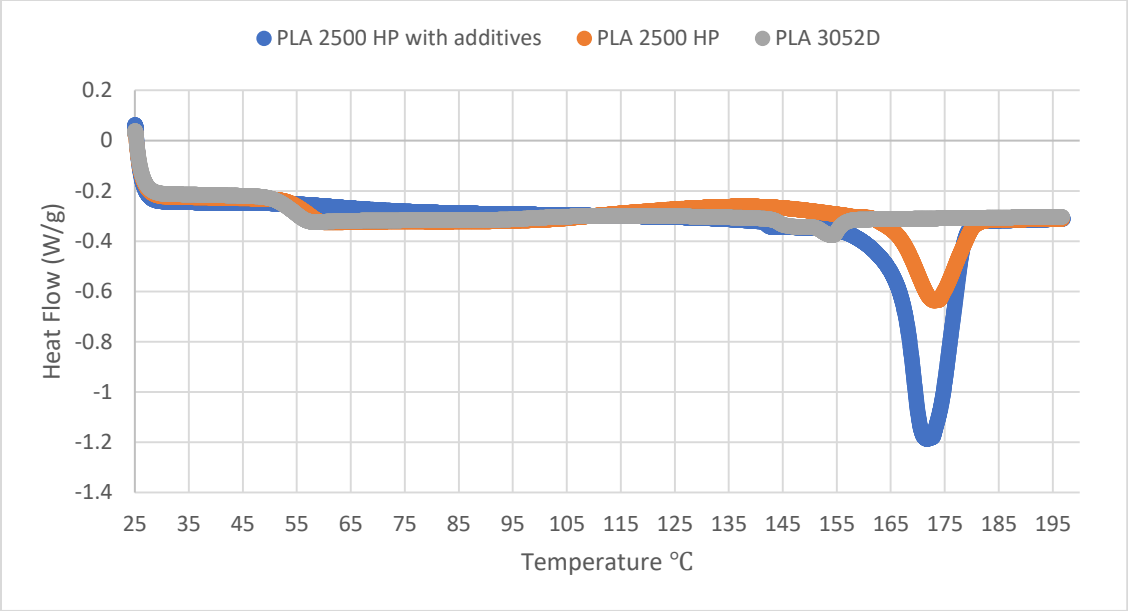

Figure 6-2: DSC results of different PLA grades indicated above.

	PLA 3052D	PLA 2500HP	PLA 2500HP with additives
Isothermal Temp.	100°C	100°C	100°C
Isothermal Time	5 minutes	5 minutes	5 minutes
Crystallinity	0%	2%	55%
Melting Temp.	154°C	173°C	171°C

Table 6-1: Summary of DSC Results

The results show that Amorphous PLA grade (3052D) acquired totally amorphous structure, and it also got a melting temperature of 154°C. The semi crystalline PLA grade (2500HP) got a crystallinity of 2% and a melting temperature of 173°C, and lastly semi crystalline PLA with additives grade (2500HP with additives) showed a crystallinity of 55% and a melting temperature of 171 °C. It is clear that the semi crystalline PLA with additives didn't need much time to crystallize, as it acquires near the maximum crystallinity for this grade. It also crystallized at a temperature of 120°C during cooling before it was isotherm for 5 minutes at 100°C as discovered by looking at the cooling cycle which is shown in Figure 6-3. In other words, it didn't need to be isotherm to achieve high crystallinity as the crystallization kinetics are so fast due to the addition of additives. On the other hand, regular PLA 2500 HP didn't show any cold crystallization peak during cooling as shown in Figure 6-4.

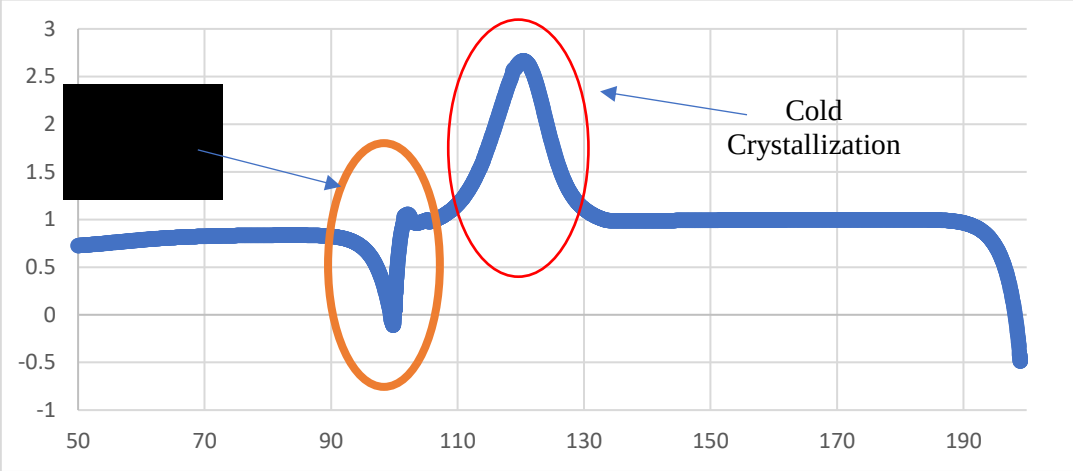

Figure 6-3: DCS results showing cooling cycle of PLA 2500HP with additives.

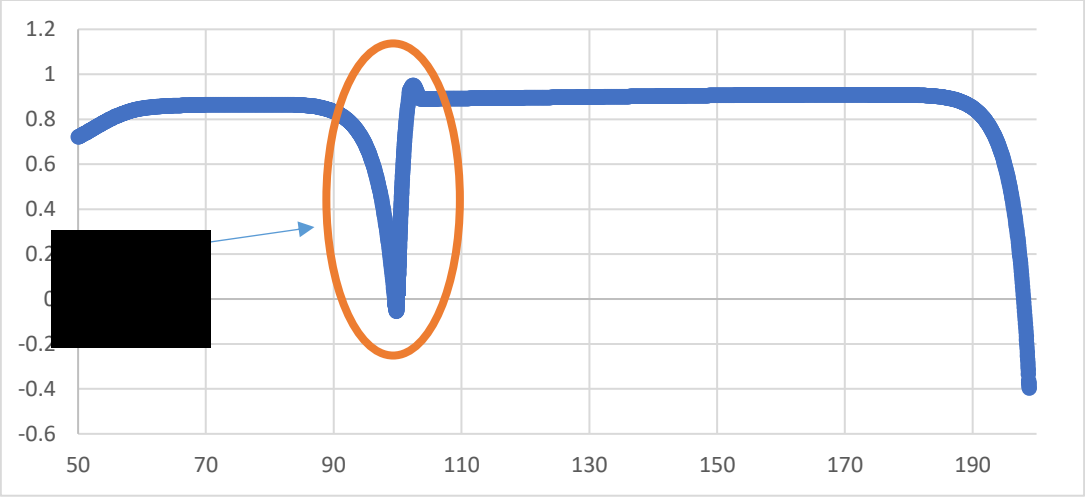

Figure 6-4: DSC results showing cooling cycle of PLA 2500HP.

The cooling cycles shown in Figure 6-3 and Figure 6-4 are the first cooling cycles after the first heating cycles. The cooling rate was 25 ℃/min in both cases. The cooling cycle of amorphous PLA grade 3052D showed similar behavior as PLA 2500HP which is shown in Figure 6-4 where there is no noticeable cold crystallization peak during cooling, which means that the material didn't crystallize during cooling. Comparing the melting temperature of the PLA 2500HP to the PLA 2500HP with additives, the latter achieved lower melting temperature although it has higher crystallinity. The reason might be due to the additives that were added to it, which increased the formation of nuclei and as a result more crystal spherulite are form. So, crystal spherulites becomes smaller since they don't have much space to grow compared to the PLA 2500HP where the crystal spherulites have more space to grow. The larger size of crystal spherulite might explain the increase in the melting temperature of the PLA 2500HP compared to the PLA 2500HP with additives.

6.2.3 Effect of isothermal time and temperature

The material that was chosen to be investigated was PLA 2500 HP since its properties have great potential to be influenced by tuning the processing conditions compared to the amorphous PLA and the PLA 2500 HP with additives. The amorphous PLA didn't show any sign of crystallization when isotherm for 20 minutes, and the PLA 2500 HP achieved almost the maximum crystallinity level for this material.

Isotherm time and temperature were tuned in order to investigate their effect on the crystallization of this material. In order to study the effect of each factor independent of one another, each test was conducted with one factor being held constant and the other one was variable.

The first test procedure was conducted to investigate the influence of isotherm time on PLA thermal properties using DSC and the procedure was as follows:

1. Heat the material to 200°C at a rate of 10°C/min.
2. Isotherm for 2 minutes
3. Cool down to 110°C at a rate of 25°C/min.
4. Isotherm for
    a. Case 1, 20 minutes
    b. Case 2, 40 minutes
5. Cool down to 25°C at a rate of 25°C/min.
6. Isotherm for 2 minutes.
7. Heat the material again to 200°C at a rate of 10°C/min.

The DSC results for the previous procedure to investigate the influence of isotherm time are shown in Figure 6-5. The second heating cycles are shown in the results.

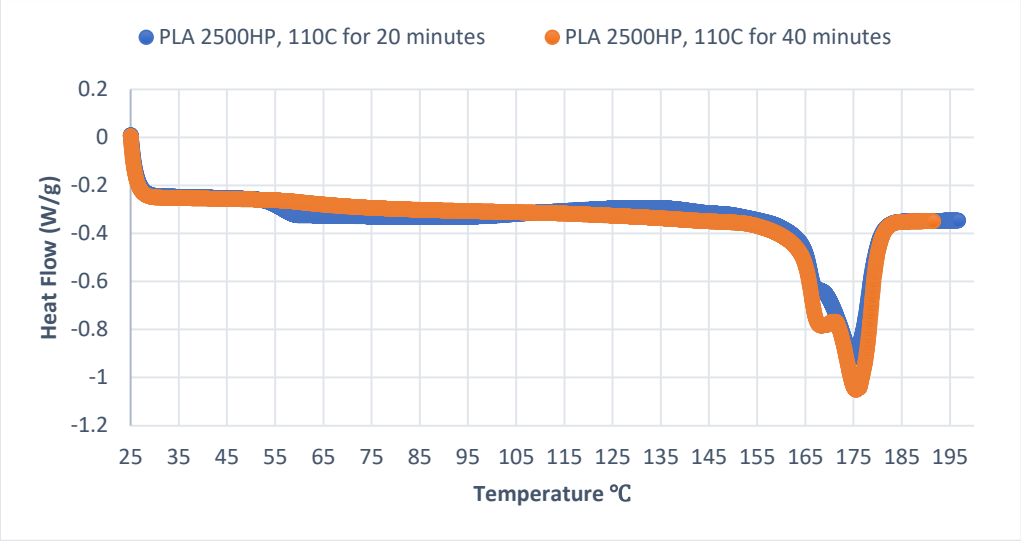

Figure 6-5: DSC results showing the effect of isotherm time on PLA 2500HP.

The second test was conducted to investigate the influence of isotherm temperature on PLA thermal properties using DSC and the procedure was as follows:

1. Heat the material to 200°C at a rate of 10°C/min.
2. Cool down at a rate of 25°C/min to.
    a. Case 1, 110°C.
    b. Case 2, 90°C.
3. Isotherm for 20 minutes
4. Cool down to 25°C at a rate of 25°C/min.
5. Isotherm for 2 minutes
6. Heat the material again to 200°C at a rate of 10°C/min.

The DSC results are shown in Figure 6-6 where the second heating cycle is viewed to investigate the influence of isotherm time on PLA properties.

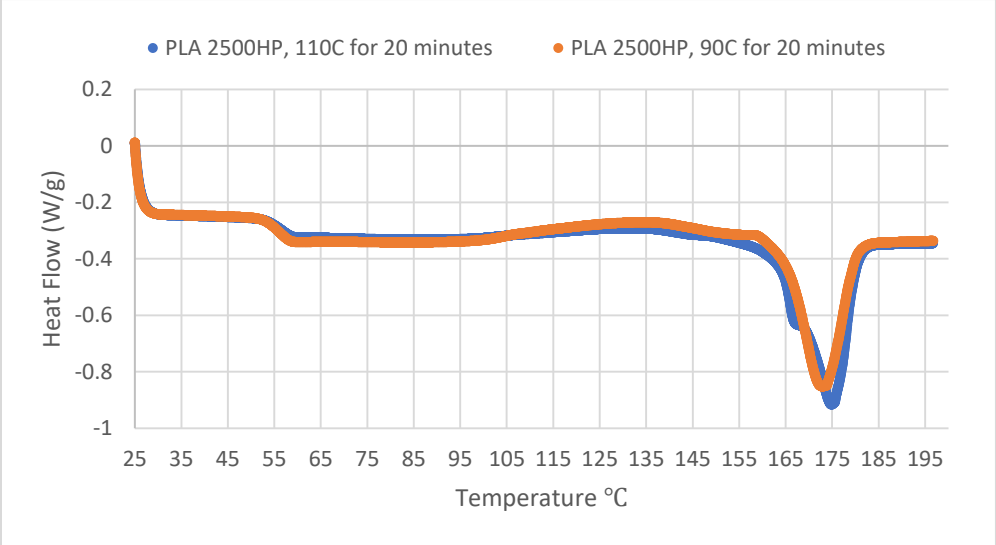

Figure 6-6: DSC results showing the effect of isotherm temperature on PLA 2500HP

The calculated crystallinity and melting temperature of each case that was investigated previously in Figure 6-5 and Figure 6-6 are shown in Table *6-2*.

	PLA 2500HP	PLA 2500HP	PLA 2500HP	PLA 2500HP
Isothermal Temp.	90°C	110°C	110°C	100°C
Isothermal Time.	20 minutes	20 minutes	40 minutes	5 minutes
Crystallinity	13%	27%	50%	2%
Melting Temp.	172.8°C	174.78°C	175.48°C	173.1°C

Table 6-2: Summary of DSC results shown in the previous two figures

The results show that both isotherm temperature and isotherm time have significant effect on overall crystallinity. Crystallinity increased by 14% when isotherm temperature was increased from 90°C to 110°C. Previous literatures have shown that the crystallization temperature of PLA is around 100℃ and it slightly varies based on the processing conditions [78,79]. Crystallinity increased by 23% when isotherm time was raised from 20 to 40 minutes at 110°C. According to a literature study [78], the half crystallization time of PLA is 20 minutes at 100℃. So, PLA should fully crystalize when isotherm for 40 minutes at 100℃. In this case, the material didn't achieve the potential over all crystallinity when isotherm at 110℃ for 40 minutes. Crystallinity up to 60% has been achieved with this material.

The isotherm temperature is shown to influence the melting temperature. The higher the isotherm temperature the higher the melting temperature which indicates the formation of larger crystals [78].

6.2.4 Effect of cooling rate

The effect of cooling rate on crystallinity and crystallization structure was investigated. Faster cooling rate results in lower processing time, and slower cooling rate results in higher processing time. Although faster cooling rate can reduce processing time, it might not allow enough time for crystalline and semi crystalline parts to crystallize. As a result, low performance parts will be generated. On the other hand, slower cooling rate will result in longer cycle time and will allow crystals to grow. Depending on the application, fully crystallized parts might be desirable or undesirable. So, the cooling rate should be optimized precisely based on the desired outcome. In this study, the influence of

cooling rate on the overall crystallinity and melting temperature of semi crystalline PLA is investigated. The influence of different cooling rates on PLA thermal properties were investigated with and without holding the material at isotherm temperature.

6.2.4.1 Effect of cooling rate with isotherm

1. Heat the material to 200°C at a rate of 10°C/min.
2. Cool down to 110°C at a rate of
    a. Case1, 10°C/min.
    b. Case2, 25°C/min.
    c. Case3, 40°C/min.
    d. Case4, 80°C/min.
3. Isotherm for 20 minutes
4. Cool down to 25°C at a rate of
    a. Case1, 10°C/min.
    b. Case2, 25°C/min.
    a. Case3, 40°C/min.
    c. Case4, 80°C/min.
5. Isotherm for 2 minutes
6. Heat the material again to 200°C at a rate of 10°C/min.

The results are shown in Figure 6-7 and Table *6-3*.

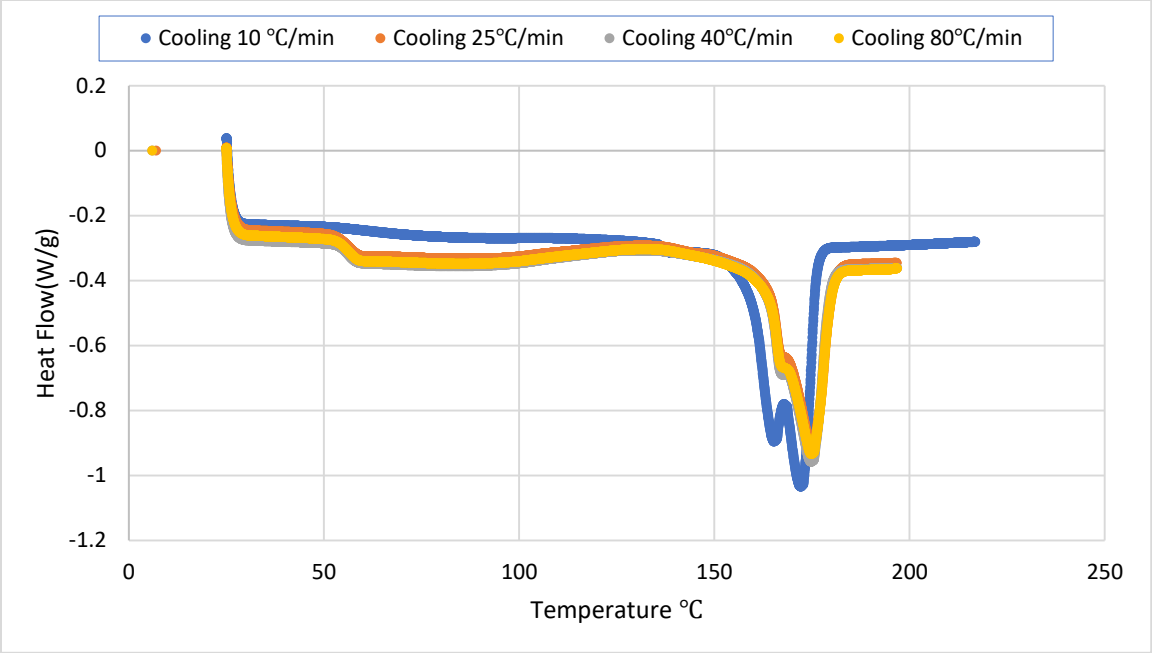

Figure 6-7: DSC results showing the effect of cooling rate on PLA 2500 HP.

	PLA 2500HP	PLA 2500HP	PLA 2500HP	PLA 2500HP
Cooling rate	10 °C/min	25 °C/min	40 °C/min	80 °C/min
Isothermal temp.	110 °C	110°C	110°C	110°C
Isothermal time.	20 minutes	20 minutes	20 minutes	20 minutes
Crystallinity	61%	27%	21%	28%
Melting temp.	172.1	174.9°C	174.8°C	174.9

Table 6-3: Calculated Crystallinity and melting temperature for the samples proceeded at different cooling rates with isotherm.

The sample that was processed at slowest cooling rate of 10°C/min showed the highest crystallinity of 56.8%. As cooling rate increased to 25°C/min, crystallinity decreased to around 27%. When cooling rate was increased further to 40 °C/min, crystallinity dropped to 21%. Then, at cooling rate of 80 °C/min, crystallinity was 28%.

Regarding melting temperature, samples proceeded at faster cooling rates of 25, 40 and 80°C/min resulted in higher melting temperature than the sample that was proceeded at lower cooling rate of 10°C/min. This indicates that the melting temperature is not just driven by overall crystallinity. Also, it might indicate that faster cooling rate causes crystal structures to be more ordered which caused the melting temperature to increase.

According to literature [57], the longer the isotherm time, the less effective the influence of cooling rate on the material. The longer isotherm time allows crystal spherulite to grow larger and demolish the influence of cooling rate on nuclei formation. In this study, at isotherm time of 20 minutes, the results look quite the same for the samples proceeded at cooling rates of 25℃/min and higher. The significant difference occurred when cooling rate was increased from 10℃/min to 25℃/min. The literature suggests that isotherm time of around one hour can cause the demolishing of the influence of cooling rate on the final properties of polymeric parts.

6.2.4.2 Effect of cooling rate without isotherm

In order to deeply understand the effect of cooling rate on PLA final properties free from other influences, an investigation was held at different cooling rates without isotherm. The samples were cooled at a rate of 5, 10, 30 and 60℃/min. The test procedure was set as follows:

1. Heat the material to 200°C at a rate of 10°C/min.
2. Cool down to 25°C at a rate of
    a. Case1, 5°C/min.
    b. Case2, 10°C/min.
    c. Case3, 30°C/min.
    d. Case4, 60°C/min.
3. Isotherm for 2 minutes at 25°C.
4. Heat the material again to 200°C at a rate of 10°C/min.

The results are shown in Figure 6-8 and Table *6-4*.

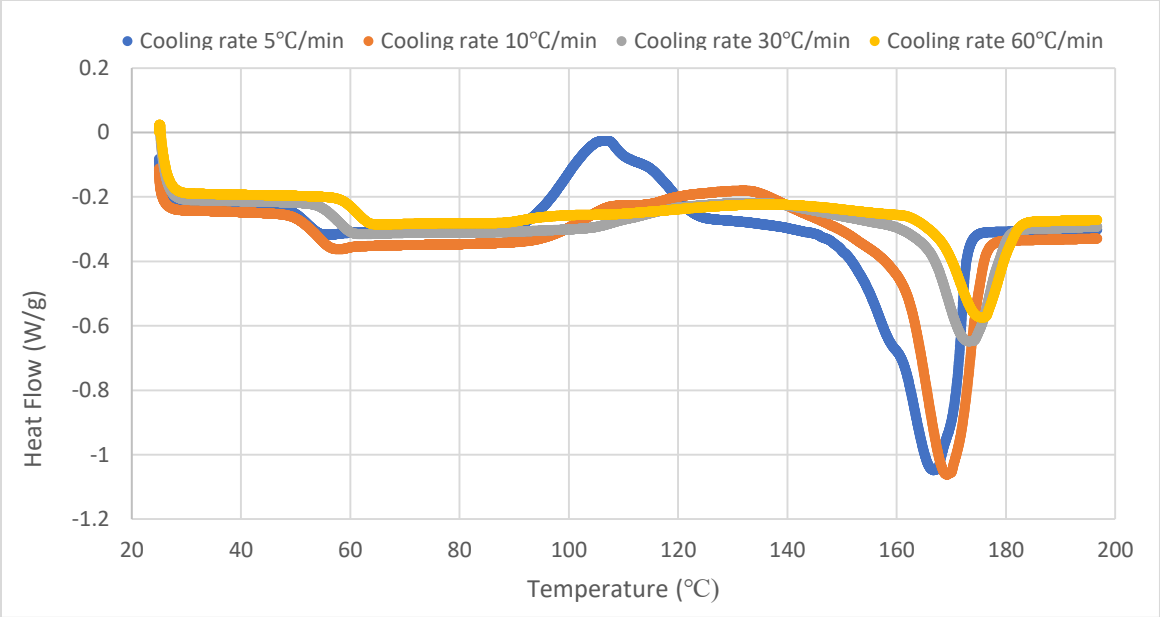

[redacted]

	PLA 2500HP	PLA 2500HP	PLA 2500HP	PLA 2500 HP
Cooling rate	5 (°C/min)	10 (°C/min)	30 (°C/min)	60 (°C/min)
Crystallinity	29.77%	7%	0.4%	0.7%
Tm	168.08°C	170.45°C	173.41°C	175.44°C
Tg	53.61°C	55.72°C	58.53°C	61.33°C

Table 6-4: PLA properties obtained from the previous figure.

As seen from the results above, the crystallinity dropped with increasing cooling rate which is expected sine PLA is known to have slow crystallization kinetics. Sample proceeded at a cooling rate of 5 ℃/min achieved overall crystallinity of 29.77%. Then, crystallinity dropped significantly by 20% when cooling rate was increased by 5%. At cooling rates of 30 and 60 ℃/min, the overall crystallinity was less than 1%. It should also be noted that the cooling rates of 30 and 60 ℃/min didn't show any crystallization exothermic peaks during cooling from the first melt. Unlike cooling rates of 5 and 10 ℃/min. Figure 6-9 and Figure 6-10 show DSC first cooling cycle of cooling rates of 5 and 10 ℃/min respectively. The cold crystallization peak observed in the cooling cycle of the sample proceeded at a cooling rate of 5℃/min is sharper than that was proceeded at a cooling rate of 10℃/min. Also, both cases acquired the cold crystallization peaks around the temperature of 100℃.

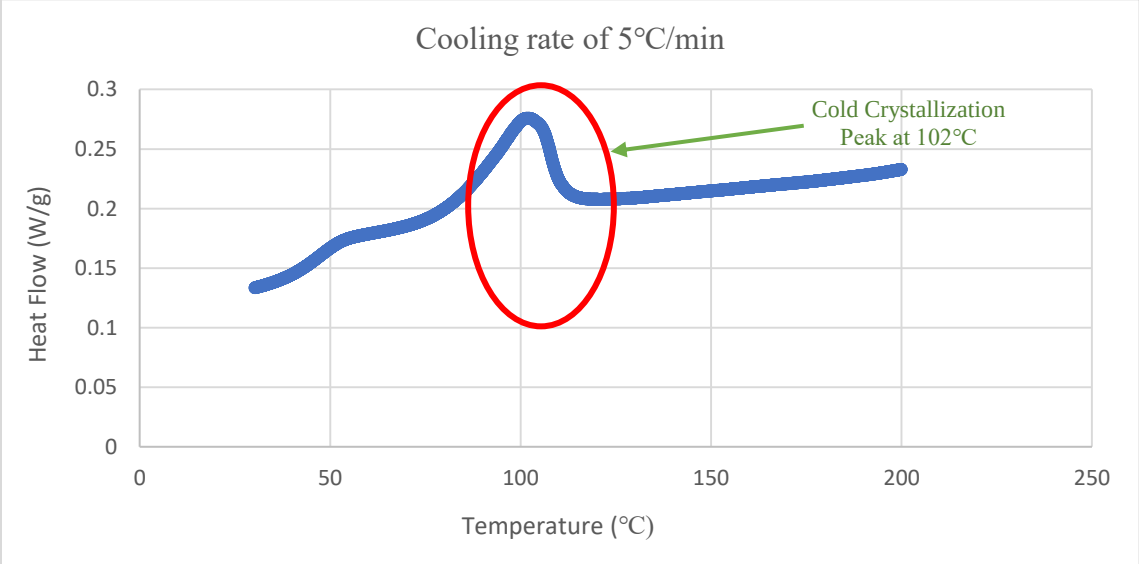

Figure 6-9: DSC results showing the first cooling cycle.

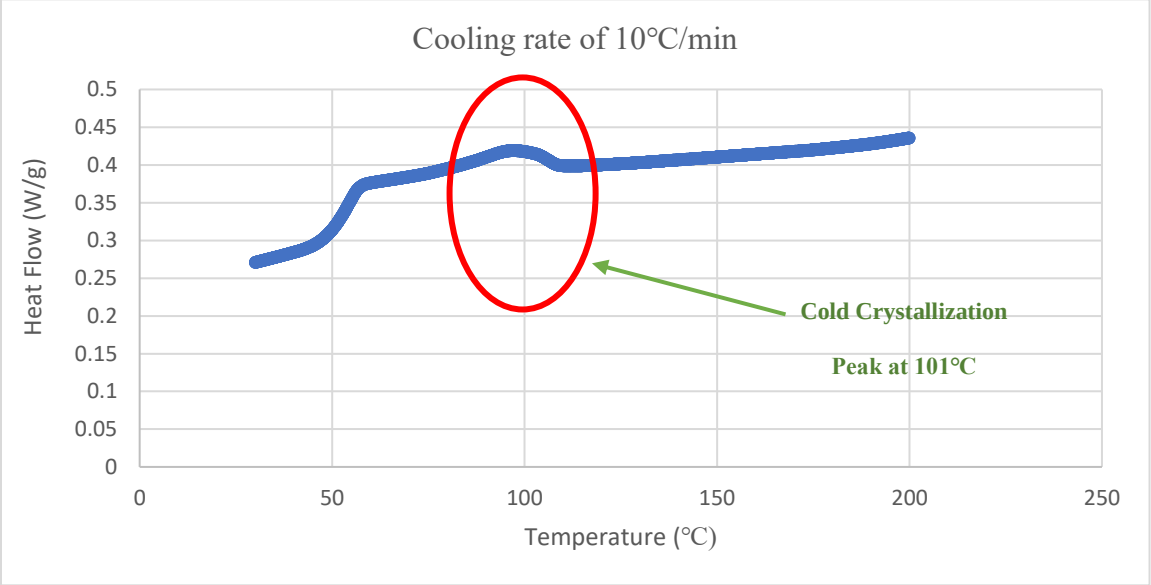

Figure 6-10: DSC results showing the first cooling cycle.

As observed in Figure 6-8, the higher cooling rates caused the crystallization peaks to spread over a wider temperature range which is consistent with a literature study [2]. The melting temperature increased with increasing cooling rate although crystallinity was decreasing.

6.2.5 Results and Discussion

Comparing all the results presented in this study, it is clear that isotherm temperature, isotherm time and cooling rate have significant effect on crystallinity and melting temperature of polymeric samples.

An increase in isotherm temperature from 90°C to 110°C when isotherm time was set for 20 minutes caused the crystallinity to increase by 14%. The melting temperature

increased from 172.8℃ to 174.8℃ when isotherm temperature was increased from 90℃ to 110℃, which indicates the formation of larger crystals [78].

The influence of isotherm times of 20 and 40 minutes at a temperature of 110℃ on crystallinity and melting temperature of semi crystalline PLA were investigated. Crystallinity increased by 23% from around 27% to 50% with increasing isotherm time from 20 to 40 minutes at the same temperature. In this case, total cooling time was increased by 20 minutes from 27 minutes to 47 minutes in order to increase crystallinity by 23%. A literature study has shown that the half crystallization time of PLA is 20 minutes [78]**.** The melting temperature increased by 1℃ with increasing isotherm time from 20 to 40 minutes.

The effect of various cooling rates with and without isotherm was investigated. Cooling rate of 10 °C/min when isotherm for 20 minutes at 110°C resulted in a crystallinity of around 61%, in this case the total cooling time was 37 minutes including the isotherm time. The DSC curve for this sample didn't show glass transition peak, which is expected due to the difference in viscoelastic behavior between amorphous and crystalline polymers. Crystallinity dropped significantly by 34% with increasing cooling rates from 10 °C/min to 25 °C/min, where it decreased from 61% to 27%. Then, with increasing cooling rate to 40 and 80°C/min, crystallinity was 21% and 28% respectively. The total cooling time for all cases that were isotherm were 37, 27, 24, and 22 minutes. The total cooling time is the time it took the temperature to drop from the melting temperature to the room temperature. The melting temperature increased with increasing cooling rate from 10 °C/min to 25

°C/min even though crystallinity was decreased significantly. Then, with further increase in cooling rate above 25°C/min, melting temperature remained constant.

In the cases where the effect of various cooling rates 5, 10, 30 and 60°C/min were investigated without isotherm, crystallinities that were achieved were 29.7%, 7%, 0.4% and 0.7% respectively. The melting temperatures increased with increasing cooling rates although crystallinity was decreasing, this behavior is consistent with the previous study shown in this chapter. The glass transition temperatures increased with increasing cooling rates as well. There are several factors that are known to influence the glass transition temperature such as free volume [80]. It looks that as the cooling rate increases, the free volume between the polymer chains decreases, which results in an increase in the glass transition temperature.

By comparing two cases where both were isotherm at 110℃, the first one when isotherm time was 40 minutes at a cooling rate of 25℃/min and total cooling time was 47 minutes, the second when isotherm time was 20 minutes at a cooling rate of 10℃/min and a total cooling time of 37 minutes. The second case got higher crystallinity of 61% than the first case which got 50%, even though the total cooling time was less by 10 minutes. The reason might be due to the crystallization temperature is not exactly 110℃ and as a result slower cooling rate will allow the crystals to grow more around the crystallization temperature where the crystallization kinetics will be the fastest. The melting temperature was higher in the first case even though the overall crystallinity was lower, which is consistent with literature [78] where a shift to higher temperature can occur with increasing isotherm time when isotherm temperature is above 105℃.

6.2.6 Conclusion

It is well known that final properties of polymeric parts are influenced by thermal history. The influence of isotherm temperature, isotherm time and cooling rates on final properties of semi crystalline PLA were investigated through thermal analysis using DSC. The findings can be summarized as flows:

- PLA 2500HP with additives showed much higher crystallinity than the regular 2500 HP without additives.
- The melting temperature of the one with additives was lower than that without additives although crystallinity was higher, the reason can be attributed due to the spherulite size in the one with additives are smaller which caused the melting temperature to be lower.
- Higher cooling rates resulted in higher glass transition temperature.
- Higher cooling rates caused the cold crystallization peaks to spread over a broad temperature range during the next heating cycle.
- Samples proceeded with slower cooling rates show cold crystallization peak in the cooling cycle.
- Faster cooling rate + isotherm at the crystallization temperate can result in higher crystallinity compared to slow cooling rate without isotherm. Following this strategy can help reduce the processing time while achieving the best parts quality.

This study was conducted to understand the crystallization behavior of PLA, and to investigate the influence of various parameters such as isotherm temperature, isotherm time and cooling rate on the thermal properties of PLA.

In the case of extrusion based additive manufacturing, once the material exits the nozzle it is exposed to cooling until it lands on the heated bed, then, it will be heated at a certain temperature for a specific amount of time until the print finishes. So, according to this study, the theoretical optimum conditions would be to cool the material fast once it exits the nozzle until it reaches the crystallization temperature. Then, set the heated bed at the crystallization temperature and keep the material there until the desired crystallinity is achieved.

6.3 The influence of 4D Rheo-Printing on crystallinity and crystal structure of PLA (Non isothermal crystallization)

Although additive manufacturing has a great potential to make customizable parts quickly and inexpensively to meet unique specifications, its product's general properties are still modest. The properties of additive manufacturing parts are influenced by many factors such as thermal history, shear rate, nozzle diameter and layer thickness, such properties are mechanical, physical, thermal and biodegradation properties. These factors can significantly influence the properties of the final printed parts. Additive manufacturing parts are built layer upon layer from the ground up, and if processing conditions where to be tuned for each single layer, parts with tunable and gradient properties can be produced to provide new functionalities. This characteristic is unique for additive manufacturing, we are taking advantage of this characteristic by tuning shear rate and thermal history of the polymer melt to tune the properties of the final parts. In order to understand and demonstrate the influence of these factors on the properties of 3D printed parts, a series of experiments have been conducted.

6.3.1 Introduction

Additive manufacturing revolutionizes the way in which products are produced. It allowed designer to design complex structures and manufacture what was impossible to be manufactured otherwise. Parts with complex geometries are easily built using additive manufacturing. Despite that, the properties of additive manufactured parts are still considered modest compared to traditional manufacturing techniques. In this project, we

developed a technique not only can enhance the properties of additive manufactured parts but also can tune the properties within one single parts to meet unique specifications.

The 4D Rheo-Printing technique has been primarily implemented to tune the processing conditions of the polymer melt such as shear rate and thermal history. Shear rate and thermal history imposed on the polymer melt during the manufacturing process are known to influence the evolution of molecular orientation and crystallization. Moreover, the performance of polymeric parts is highly dependent on the molecular structure and crystallinity. Therefore, our novel technique introduces a new way to control the molecular structure in 3d printed parts by applying shear rate.

The primary goal of the experiments was to investigate the processing parameters and their impact on 3d printed parts properties, and to validate the use of 4D Rheo-Printing technique. In this section, the details of a couple of experiments are presented. Taguchi design of experiment was used to investigate the influence of the following factors melt temperature, stage temperature and shear rate. In addition, the influence of layer thickness and nozzle diameter on the crystallinity of printed parts was investigated. Two characterization techniques were used to analyze the results. Also, in order to investigate the influence of imposing more ordered molecular structure using the proposed technique compared to traditional FFF on the biodegradability of PLA, samples were characterized again 6 months after the first test.

6.3.2 Materials and Methods

The material that was chosen to be exanimated in this project had to be biodegradable and biocompatible because of the potential applications in the medical sector for this system. Two materials were used which were provided by NatureWorks. The materials are PLA 3052D and PLA 2500HP. The characteristics details of these two materials were mentioned in the previous section.

Taguchi design of experiment was conducted using the PLA 2500HP, since this material properties showed great potential to be influenced by the processing factors according to the study conducted previously in this section. For the material PLA 3052D, this material was tested using a heated stage to investigate if this material can crystallize at all when shear rate is applied to enhance its crystallization kinetics.

All the samples prepared had rectangle shape 0.4 X 0.8 inches, these dimensions were chosen in order to be able to fit the specimens in the XRD rings for testing as shown in Figure 6-11. G code was written in order to print the sample in these dimensions.

Figure 6-11: Sample attached to the XRD ring.

6.3.3 Results

6.3.3.1 The influence of shear rate at different stage and melt temperatures.

- PLA 2500HP

The influence of imposing higher shear rate at different stage and melt temperatures was investigated using PLA 2500HP. First, the stage temperature was set to be at room temperature. Then, at the recommended melting temperature the influence of introducing higher shear rate was examined. Higher shear rate was imposed at the printer head by rotating the nozzle. Based on the results achieved when printing at room temperature stage which are shown below in the DSC and XRD results, it was decided to pursue the experiment with heated bed.

Design of experiment was used with three factors and two levels as shown below in Table 6-5 and Table 6-6:

Parameter	Level 1	Level 2
Shear rate	High shear	Low shear
Stage temperature	85℃	65℃
Melt temperature	210℃	190℃

Table 6-5: Experimental Processing Parameters.

Sample No.	Melt Temp.	Stage Temp.	Nozzle
1	210℃	85°C	0 RPM
2	210℃	85°C	200 RPM
3	210℃	65°C	0 RPM
4	210℃	65°C	200 RPM
5	190℃	85°C	0 RPM
6	190℃	85°C	200 RPM
7	190℃	65°C	0 RPM
8	190℃	65°C	200 RPM

Table 6-6: Modified L8 orthogonal array

6.3.3.1.1 X Ray Diffraction Results (XRD)

X Ray Diffraction is a useful tool to investigate the crystallinity and the crystalline structure. The results of the samples printed at room temperature stage with and without imposing higher shear rate are shown in Figure 6-12.

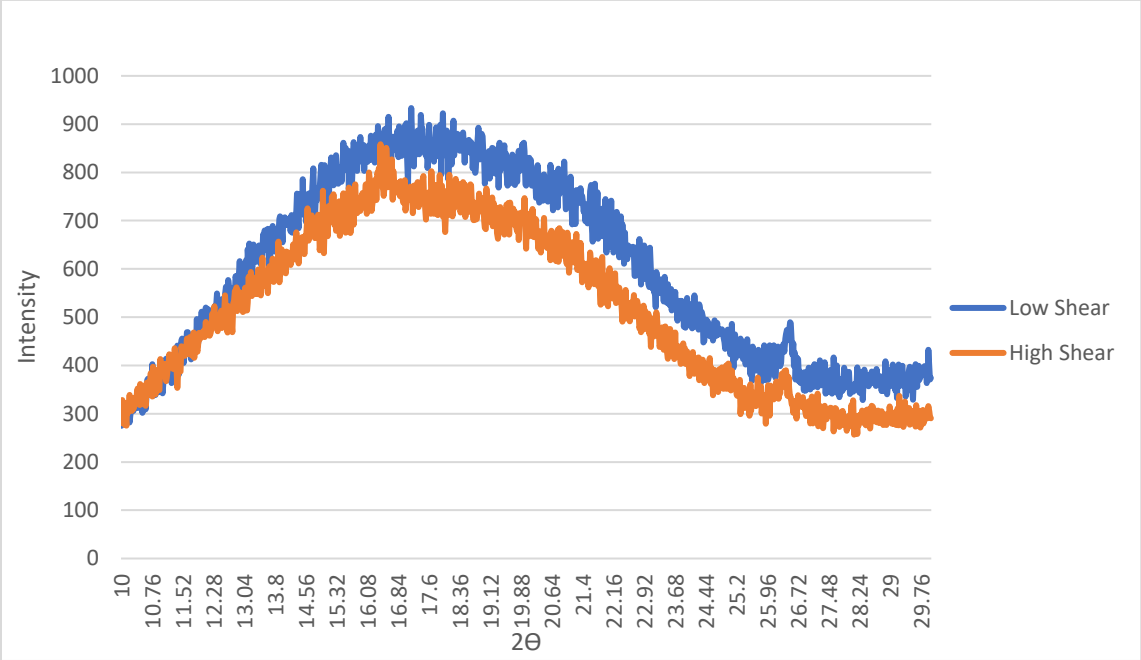

Figure 6-12: XRD results of samples printed at room temperature stage.

The XRD results shown in the previous figure indicates that there is no significant difference in the molecular structure between the two samples printed with low and high shear. Introducing higher shear rate showed no significant effect on the XRD results. In order to investigate if the samples are able to crystallize if given some time, one of the samples that was printed at a room temperature stage was annealed for 5 minutes in the oven at a temperature of 80°C and the results are shown in Figure 6-13.

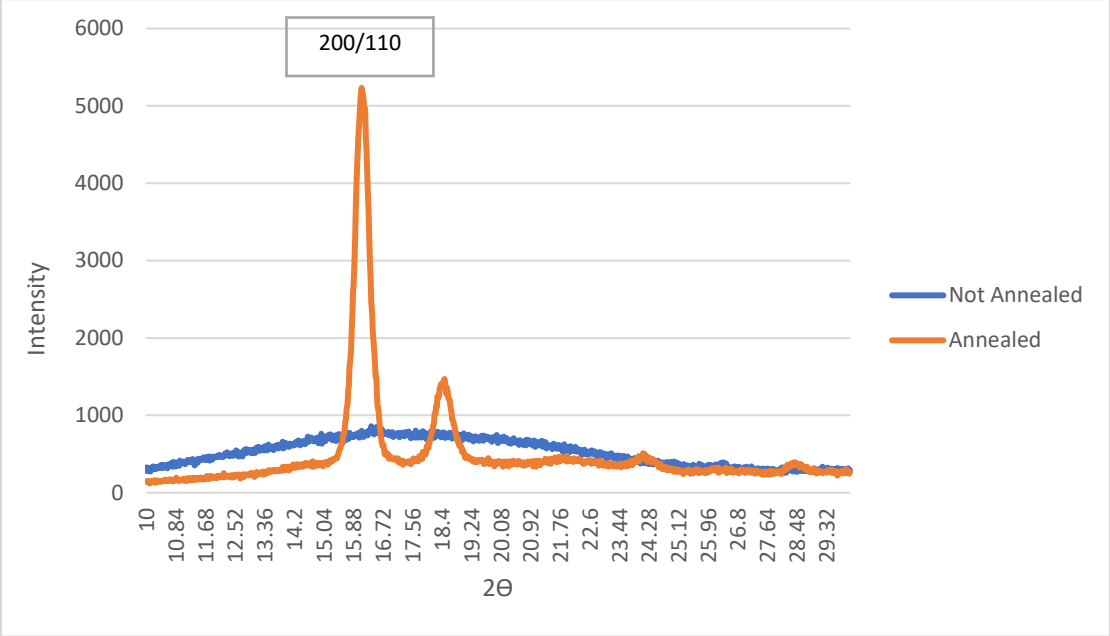

Figure 6-13: XRD results of annealed vs not annealed PLA

The results shown in Figure 6-13 showed the XRD results of annealed and not annealed samples. As seen, the annealed sample exhibit sharp peaks, which indicates higher crystallinity compared to the not annealed one. Before annealing, the sample was transparent and it transformed to be opaque after annealing, which indicated the high crystallinity level. Based on these results, it was decided to use a heated bed and the design of experiment was conducted with just heated bed since PLA has shown to have slow crystallization kinetics.

The XRD results for the design of experiment that was shown in Table 6-6 are shown below in Figure 6-14, Figure 6-15, Figure 6-16 and Figure 6-17. The intensity that

is shown in the results is attributed to the 200/110 plane since it is the most noticeable peak which occurs around 2Θ = 16.5°.

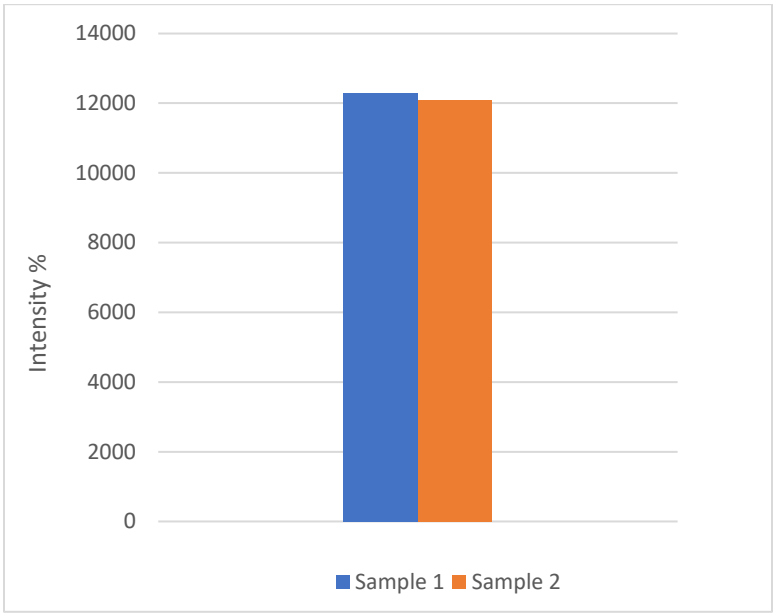

Figure 6-14: XRD intensity of samples 1 (low shear) and sample 2 (high shear) printed under the conditions shown previously.

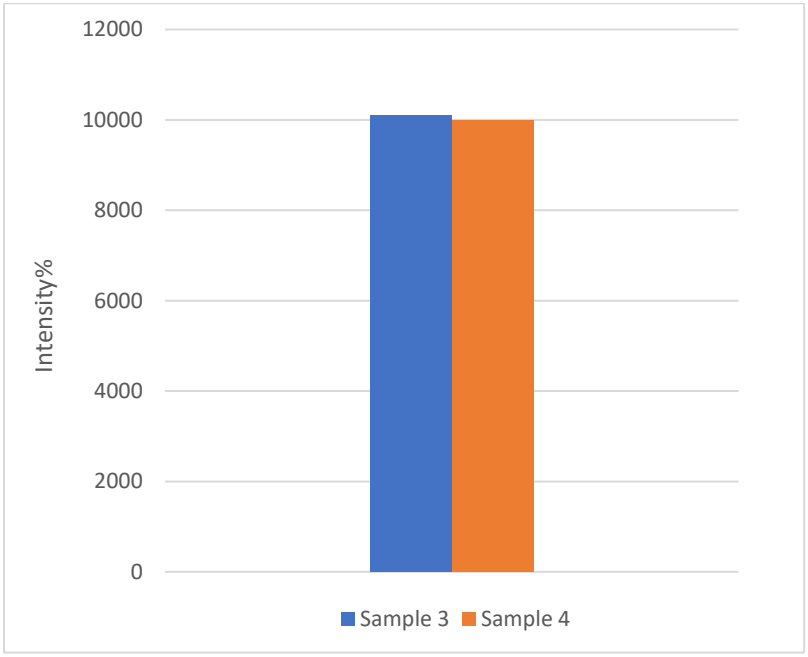

Figure 6-15: XRD intensity of samples 3 (low shear) and sample 4 (high shear) printed under the conditions shown previously.

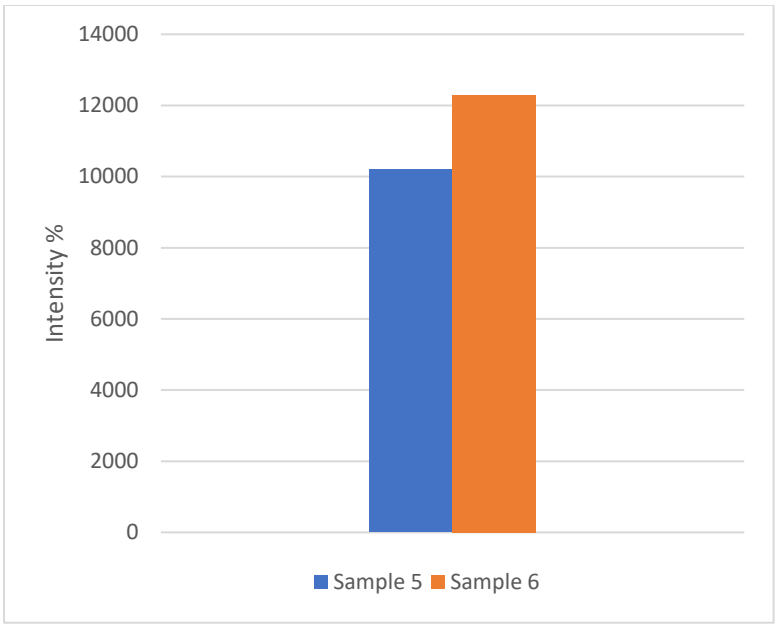

Figure 6-16: XRD intensity of samples 5 (low shear) and sample 6 (high shear) printed under the conditions shown previously.

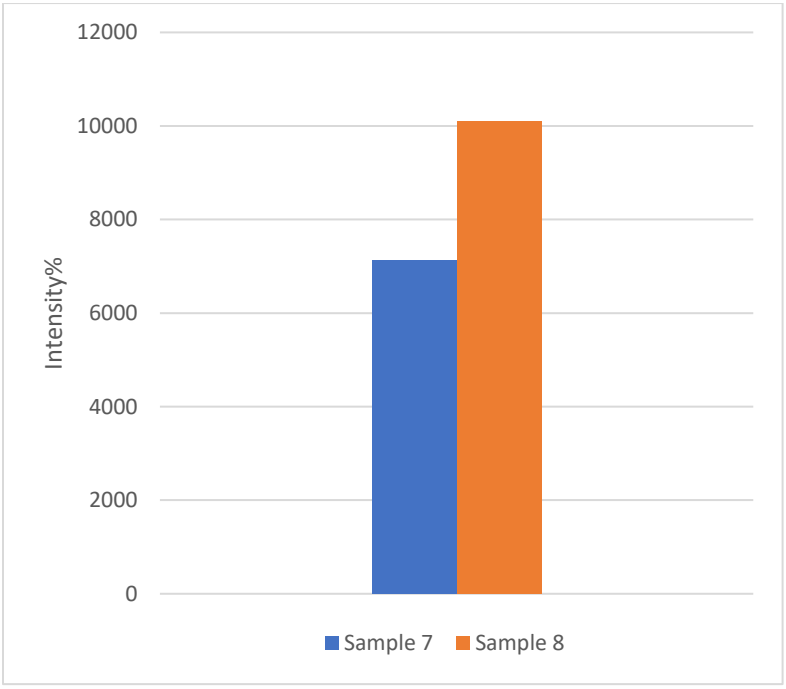

Figure 6-17: XRD intensity of samples 7 (low shear) and sample 8 (high shear) printed under the conditions shown previously.

The above results showed that at the higher range of the melting temperature, shear rate didn't cause any significant difference in the results. While at the lower range of the melting temperature, the higher shear rate that was imposed caused the intensity of the peaks to increase. This indicates higher crystallinity since the crystallinity is calculated through XRD by subtracting the area under sharp peaks from the area under the broad peaks and any increase in the sharpness of the peaks will increase the area of the sharp peak and therefore will result in crystallinity increase.

6.3.3.1.2 Differential Scanning Calorimetry (DSC)

DSC is a useful tool to investigate the crystallinity, the melting temperature and the glass transition temperature. The DSC results of the samples that were printed at room temperature stage are shown in Figure 6-18.

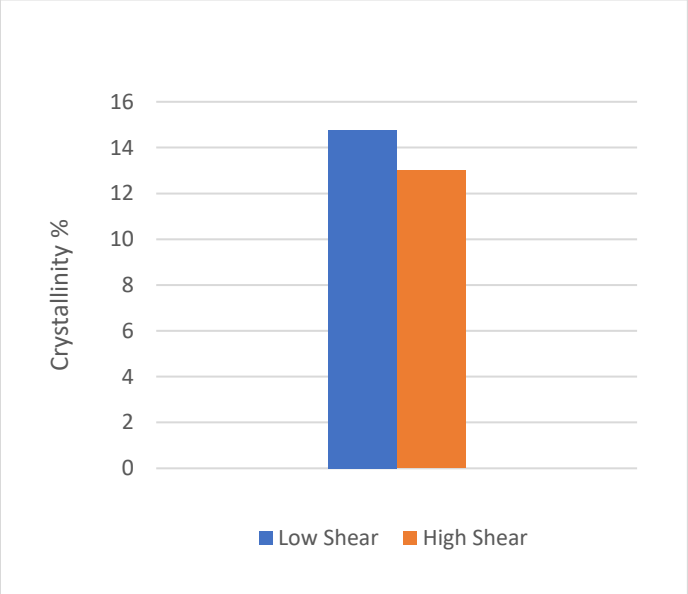

Figure 6-18: Calculated crystallinity from DSC results of samples printed at room temperature stage.

The results shown above indicate that applying high shear rate when printing at room temperature stage caused the crystallinity to drop by 2%. The possible explanation for this could be because of the slow crystallization rate of PLA. So, applying higher shear rate and then cooling the material fast caused the crystallization to be impeded rather than enhanced.

The calculated crystallinity from the DSC results for the design of experiment that was shown in Table 6-5 are shown below in Figure 6-19, Figure 6-20, Figure 6-21 and Figure 6-22.

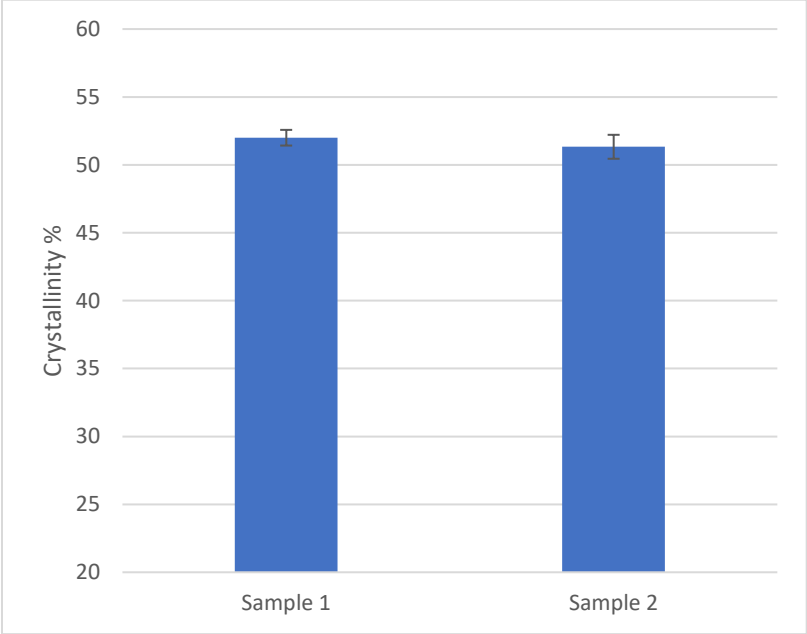

Figure 6-19: Calculated crystallinity from DSC results of sample 1 (Low shear) and sample 2 (High shear) under the conditions shown previously.

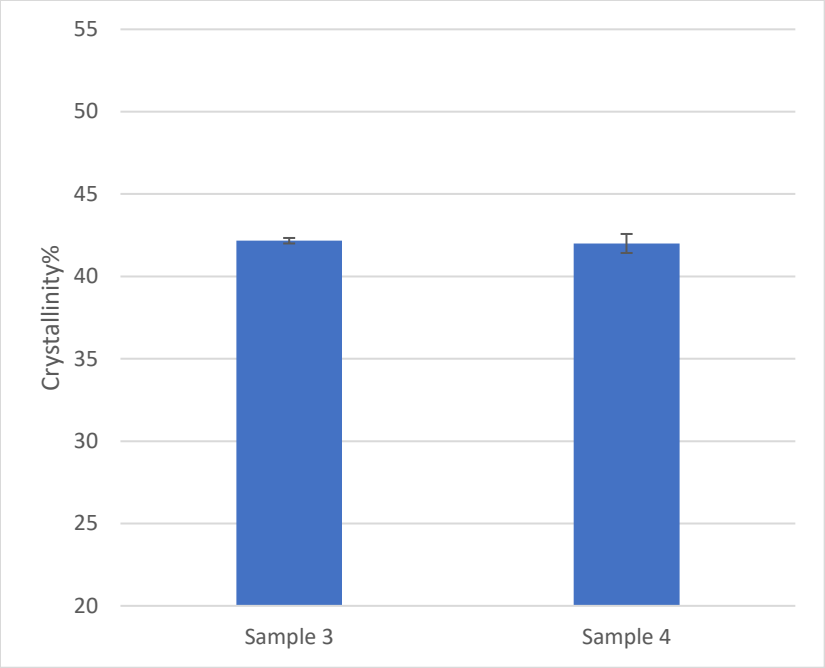

Figure 6-20: Calculated crystallinity from DSC results of sample 3 (Low shear) and sample 4 (High shear) under the conditions shown previously.

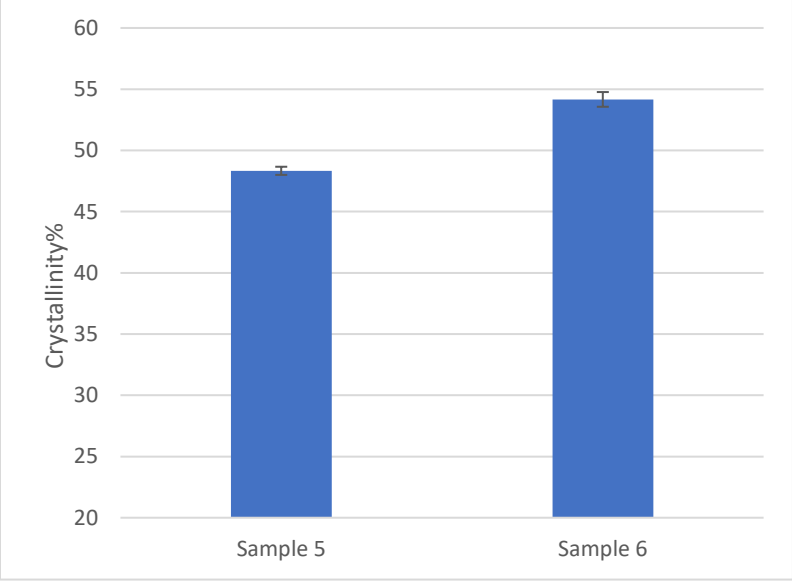

Figure 6-21: Calculated crystallinity from DSC results of sample 5 (Low shear) and sample 6 (High shear) under the conditions shown previously.

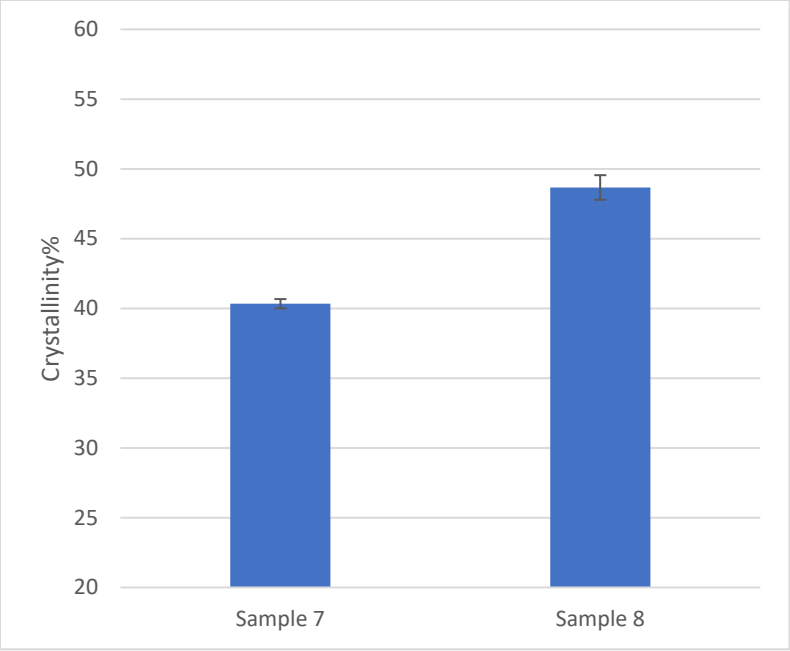

Figure 6-22: Calculated crystallinity from DSC results of sample 7 (Low shear) and sample 8 (High shear) under the conditions shown previously.

Figure 6-19 and Figure 6-20 show the crystallinity of the samples that were printed at the higher range of the melt temperature of 210℃. The results are consistent with the XRD results which indicate than there is no significant changes in the crystallinity when higher shear rate was imposed on the polymer melt. A possible explanation is that as the melt temperature increases the onset of shear rate where it starts affecting the molecular structure of the melt and reducing viscosity increases as well. Also, as the melt temperature decrease, the onset of shear rate where it starts affecting the molecular structure of the melt and reducing viscosity decreases. So, the shear rate applied by the rotational nozzle was not high enough to orient the molecules, and in order to orient the molecules higher shear rate is required. This was proved with the Rheometer study of this material that are shown next in this chapter. Another reason is that as the melt temperature increases the relaxation time of the molecules where they fold back to their original shape becomes faster as well,

which was investigated for this exact material in Chapter 5. The orientations caused by shear at higher temperatures disappear fast and that result in no difference between the samples printed at high or low shear.

Figure 6-19 shows more crystallinity than Figure 6-20 which was expected, since the samples shown in Figure 6-19 were printed to a higher stage temperature. Also, as the stage temperature increases above the glass transition temperature the crystallinity will increase as well, since the viscosity will be low enough to allow the molecules to move and therefore crystals will have sufficient time to grow larger.

Figure 6-21 and Figure 6-22 show the results of the samples that were printed at the lower range of the melt temperature of 190℃. In this case, crystallinity increased with increasing shear rate, which is consistent with the XRD results shown previously where the intensity peaks increased with increasing shear rate. This further proved the assumptions mentioned previously where at the lower melt temperatures the onset of shear rate required to affect the orientation of the molecules becomes lower as well, therefore, the shear rate that was induced was sufficient to enhance the overall crystallinity. Also, the molecular relaxation becomes slower as the temperature decreases, thus, allowing crystals induced by shear to grow. These results are consistent with several literature studies that have shown a correlation between shear rate and crystallinity enhancement [1,3,5,55,58], most of these studies were conducted using Rheometer.

The results in Figure 6-21 show the crystallinity of the samples that were printed to a bed temperature of 85℃. The sample that was printed with higher shear rate achieved around 12% higher crystallinity than the sample that was printed with low shear rate. Moreover, in Figure 6-22 when the stage temperature was 65℃, the sample printed with

higher shear rate achieved 20% higher crystallinity than the sample printed with low shear rate. It is obvious from these results that higher shear rate enhanced the crystallization kinetics which resulted in higher overall crystallinity of the samples. Also, shear induced crystallization

It was shown in Figure 6-18 that applying higher shear rate to the samples printed to a room temperature stage impeded crystallinity. In order to investigate it further, a cooled bed was used, and two samples were printed with and without rotating the nozzle. The results are shown in Figure 6-23.

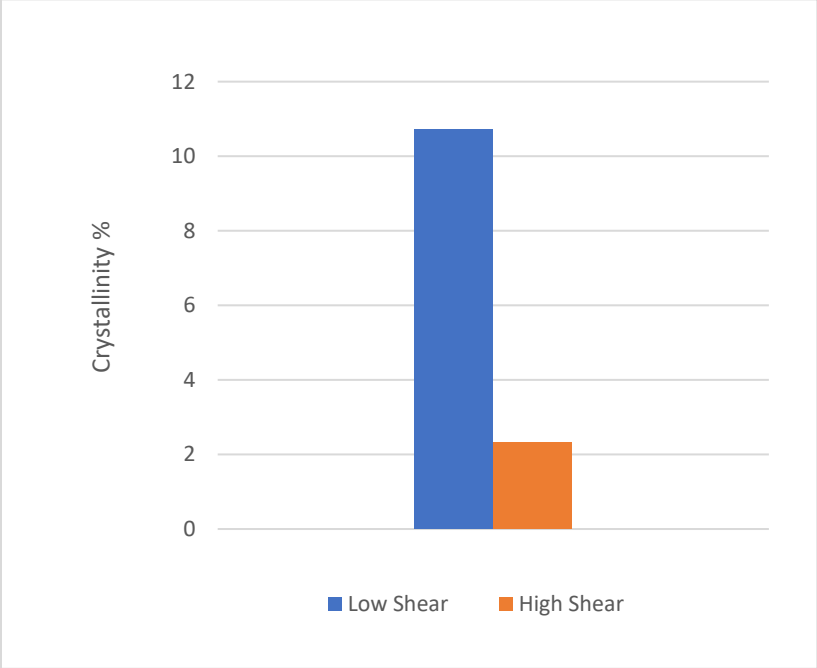

Figure 6-23: Calculated crystallinity from DSC results of samples printed with cooled stage at 18℃.

Figure 6-23 shows the crystallinity of the samples that were printed with cooled bed. Overall crystallinity of the final part dropped when higher shear rate was applied to the

melt. The results shown above further indicates that in order to enhance the crystallization by applying higher shear rate, the stage temperature or the ambient temperature has to be above the glass transition temperature to allow molecules movement and thus crystal growing, otherwise, the crystallinity will be impeded rather than enhanced.

- **PLA 3052D**

X Ray Diffraction technique was used to investigate the samples that were prepared using PLA 3052D. This material has higher D isomer content compared to 2500HP, which means that it has more amorphous structure.

The samples were prepared under the conditions shown in Table 6-7. A stage temperature of 70°C was chosen because it was the maximum stage temperature that we could print on successfully for this specific material. Higher temperatures caused the layers to flatten and increased their width.

Sample name.	Stage Temp.	Nozzle
High Shear	70°C	Rotation
Low Shear	70°C	Without Rotation

Table 6-7: Experimental Processing Parameters.

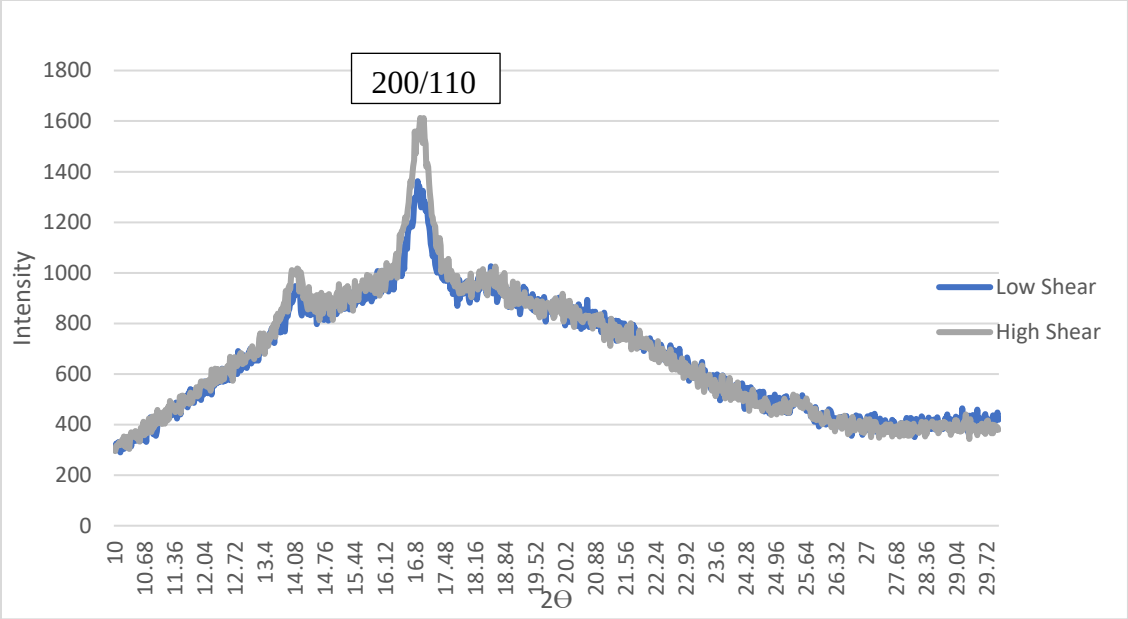

Figure 6-24: XRD results of samples printed under the conditions shown in Table 6-7.

Figure 6-24 shows the XRD results of the samples prepared using PLA 3052D. The sharp peaks are for plane 200/110. It is clear that introducing high shear increased the intensity of the peaks. Also, the D spacing became slightly smaller with higher shear which indicates more compacted crystal planes [58].

The XRD analysis was performed on the same samples again a week later to investigate if any changes have occurred in the molecular structure as shown in Figure 6-25.

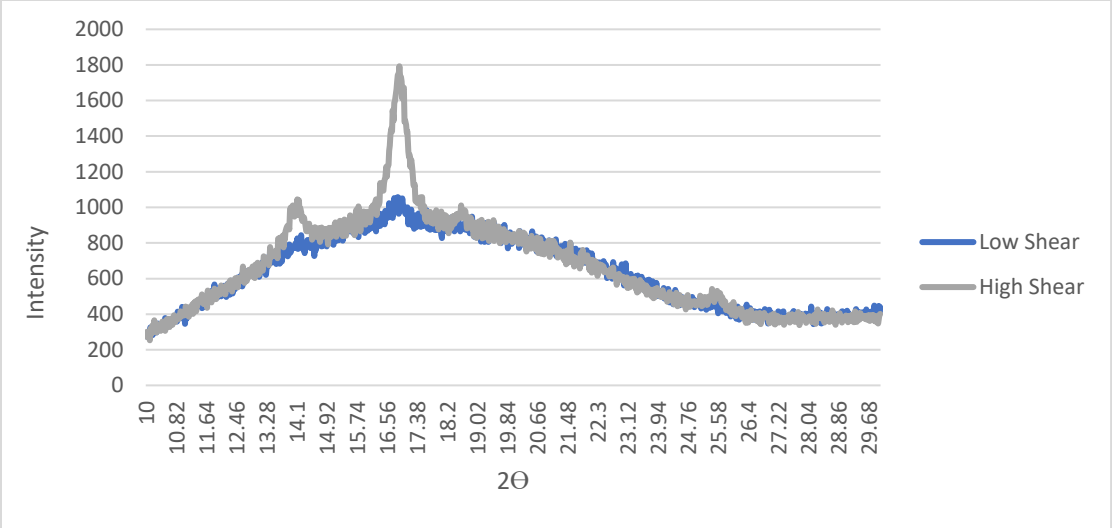

Figure 6-25: XRD results conducted on the samples shown in the previous Figure 6-24, after one week.

Figure 6-25 shows the XRD results conducted a week later after the first test shown in Figure 6-24 of the exact same samples. The intensity of the peak of the sample printed with high shear increased slightly after one week, while the intensity of the peak of the sample printed with low shear decreased. These changes in the results were not expected, since the samples were stored at room temperature, which is less than the glass transition temperature of this material, and below the glass transition temperature the chain mobility is greatly decreased.

The same samples were tested again after two weeks and the XRD results are shown in Figure 6-26.

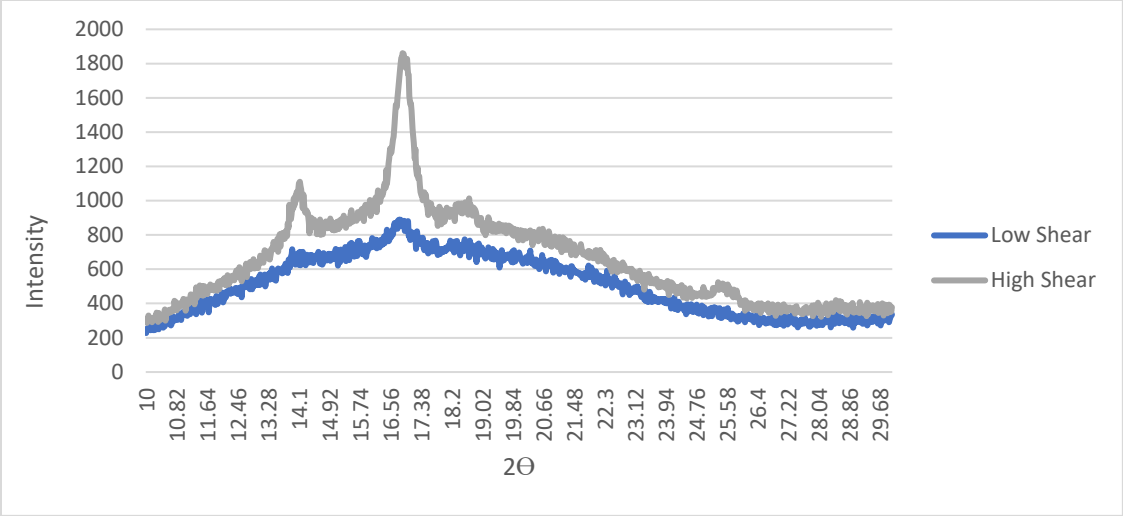

Figure 6-26: XRD results conducted on the samples shown in the previous Figure 6-24, after two weeks.

The XRD peak of the high shear samples increased slightly compared to the previous test that was conducted a week earlier. On the other hand, the XRD peak of the low shear sample dropped slightly. The XRD test was conducted a week later, but this time no noticeable changes were observed. The changes that occurred in the first two weeks to these samples were interesting and not expected. The obvious was that the sample printed with high shear (nozzle rotation) maintained and slightly enhanced their peaks while the one printed with low shear (without nozzle rotation) lost their peaks.

6.3.3.2 Influence of the stage temperature

The influence of stage temperatures on PLA samples have been investigated. Semi crystalline PLA samples were printed at different stage temperatures 18℃, 25℃, 55℃, 65℃ and 85℃. In order to achieve a stage temperature of 18℃, a bag filled with cold water was placed under the stage, and then the temperature was measured constantly during the print with a laser gun. For the temperature of 25℃, no cooling or heating was required, since the room temperature was 25℃. A heated stage was used in order to heat the stage to 55, 65 and 85℃. A glass stage was used to prepare all the samples. It was placed over the heated stage in order to heat it.

The samples were then investigated through XRD and DSC as shown in Figure 6-27 and Figure 6-28 respectively.

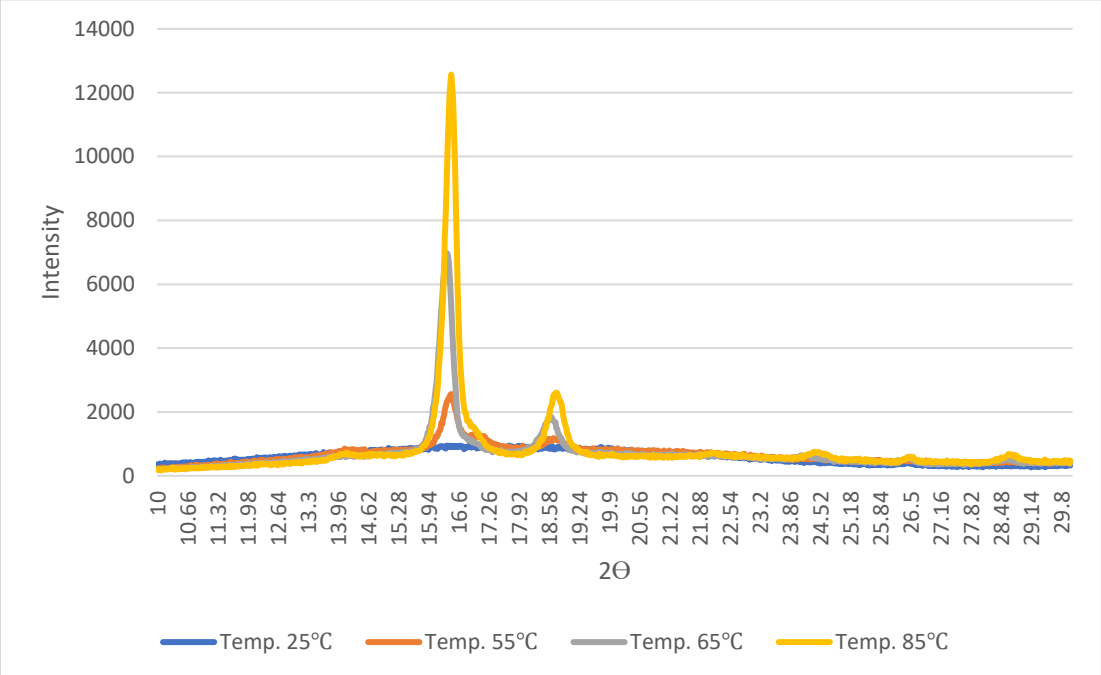

Figure 6-27: XRD results showing the influence of different stage temperatures.

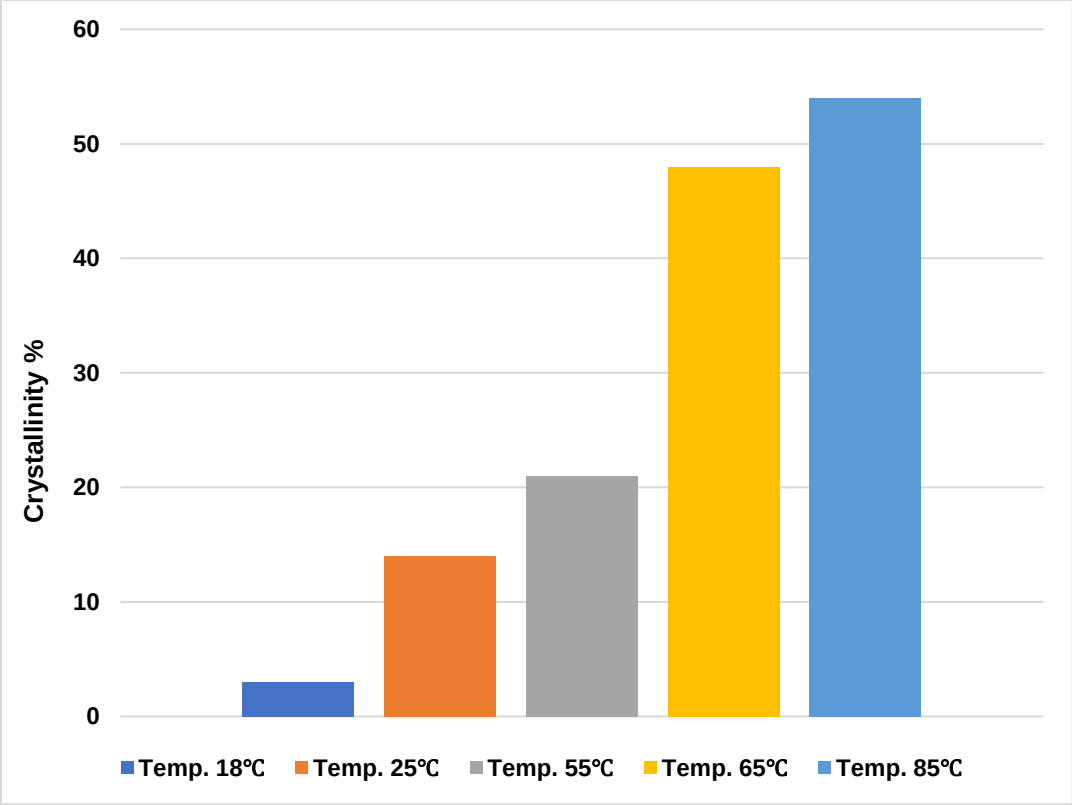

Figure 6-28: Calculated crystallinity from DSC showing the influence of different stage temperatures.

As shown in Figure 6-27, the higher the stage temperature the higher the intensity of the peaks of the XRD results. Figure 6-28 shows the crystallinity which increased with increasing the stage temperature. The crystallinity increased from around 3% to around 52% when the stage temperature was increased from 18℃ to 85℃. The stage allows the samples to crystallize in an isothermal crystallization process and gives molecules more time and energy to crystallize.

The stage temperature also affects the adherences of the parts to the stage. In additive manufacturing, the parts are built layer upon layer from the ground up and each layer has to adhere to the previous layer, and the first layer had to adhere to the stage. A

successful prints were achieved when using 25, 55 and 65℃ stage temperatures. At a stage temperature of 18℃, the part didn't adhere to the stage properly and it was difficult to print them. On the other hand, the elevated temperature of 85℃ caused the parts to shrink and not adhere to the stage as shown in Figure 6-29.

Figure 6-29: Part printed at stage temperature of 85℃, which caused it shrink.

Comparing the results of the samples printed at a room temperature stage to the samples printed with cooled bed, the samples printed with cooled bed achieved higher melting temperature as shown in Figure 6-30 even though it has lower crystallinity. The results were acquired from the DSC thermal analysis.

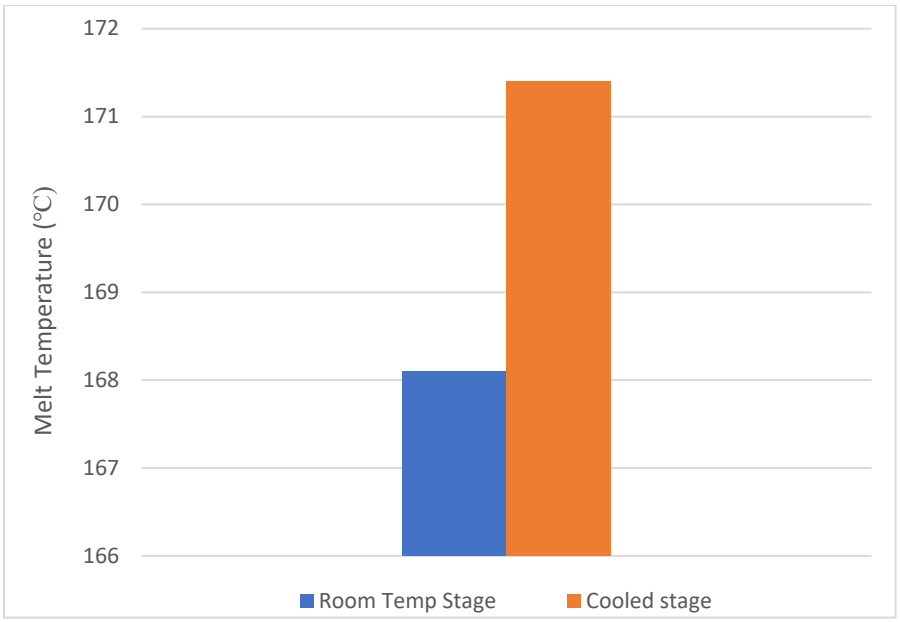

Figure 6-30: Melt temperature acquired from DSC analysis for the samples printed to investigate the influence of different stage temperatures.

The results shown above show that higher cooling caused the melting temperature to increase although crystallinity was decreasing. These results are consistent with the previous results shown previously in this chapter to investigate the effect of cooling rate using DSC. The cooling rate affects the nucleation rate. As the cooling rate increases, the nucleation rate increases as well [57]. Moreover, crystals will not grow at fast cooling rates, thus, the overall crystallinity will be less in the sample proceeded with high cooling rate compared to the one proceeded with low cooling rate.

6.3.3.3 Influence of the melt temperature

The melt temperature is found to be a complicated factor, since an increase of the melt temperature will increase the temperature of the nozzle, and the nozzle acts as a thermal source for the previous laid layers, which causes their crystallinity to slightly increase.

Comparing the influence of the melt temperature on the crystallinity of the parts printed without introducing nozzle rotation, an increase in the melt temperature from 190℃ to 210 ℃ resulted in an increase in crystallinity by around 2 to 4 %. This might be due to the nozzle being close to the printed part and acting as a thermal source, therefore, the higher melt temperature will keep the printed part at elevated temperatures which allows crystals to grow. On the other hand, by looking at the influence of melt temperature on crystallinity of the samples printed with nozzle rotation. In this case, crystallinity dropped with increasing melt temperature. A possible hypothesis is that introducing rotation (high shear) at lower melt temperatures enhances the crystallization kinetics more when compared to the higher melt temperature. In other words, the onset where shear rate starts influencing the viscosity of the melt becomes lower at lower temperatures. As a result, applying the same amount of shear rate at low and high melt temperature will affect the viscosity of the low melt temperature case more than the high temperature case, thus, resulting in greater molecular stretching. Moreover, at lower processing temperatures, the relaxation times according to Doi Edwards model increases, which allow the crystals induced by shear (shear induced crystallization) to grow larger and therefore result in higher overall crystallinity.

6.3.3.4 Influence of the nozzle diameter and the thickness of layers

Different nozzle diameters were used to investigate their influence on the crystallinity of the printed samples. It is clear that as the nozzle diameter increases, the thickness of the layers increases as well if all settings remain the same. The test was conducted using two nozzle diameters 0.4 mm and 1mm, and the temperature of the stage were kept at room temperature. The sample printed with the bigger nozzle achieved larger layer thickness of the print. It was found that the part printed with the bigger nozzle achieved slightly higher crystallinity by 1% to 2%.

The influence of the thickness of the layer was also tested using one diameter nozzle. The layer thickness was increased by increasing the flow rate relative to the speed of the stage movement. Crystallinity also increased slightly by 1 to 2% with increasing the layer thickness.

In both cases mentioned previously, the crystallinity increased with increasing the layer thickness regardless of the method used to increase the thickness. A possible explanation is that the larger the thickness, the slower the material will be cooled, which allow them to stay for a longer time at elevated temperatures above the glass transition temperature compared to the smaller layer thickness. As a result, crystals will have more time to grow.

6.3.3.5 Investigation of the samples after 6 months

Samples were tested again 6 months after they were tested the first time. Two samples were prepared with and without introducing higher shear rate through rotation, and all the other factors were kept constant. Figure 6-31 shows the XRD result of the first test which was conducted right after preparing the sample. Figure 6-32 shows the XRD result of the second test which was conducted 6 months after the first test.

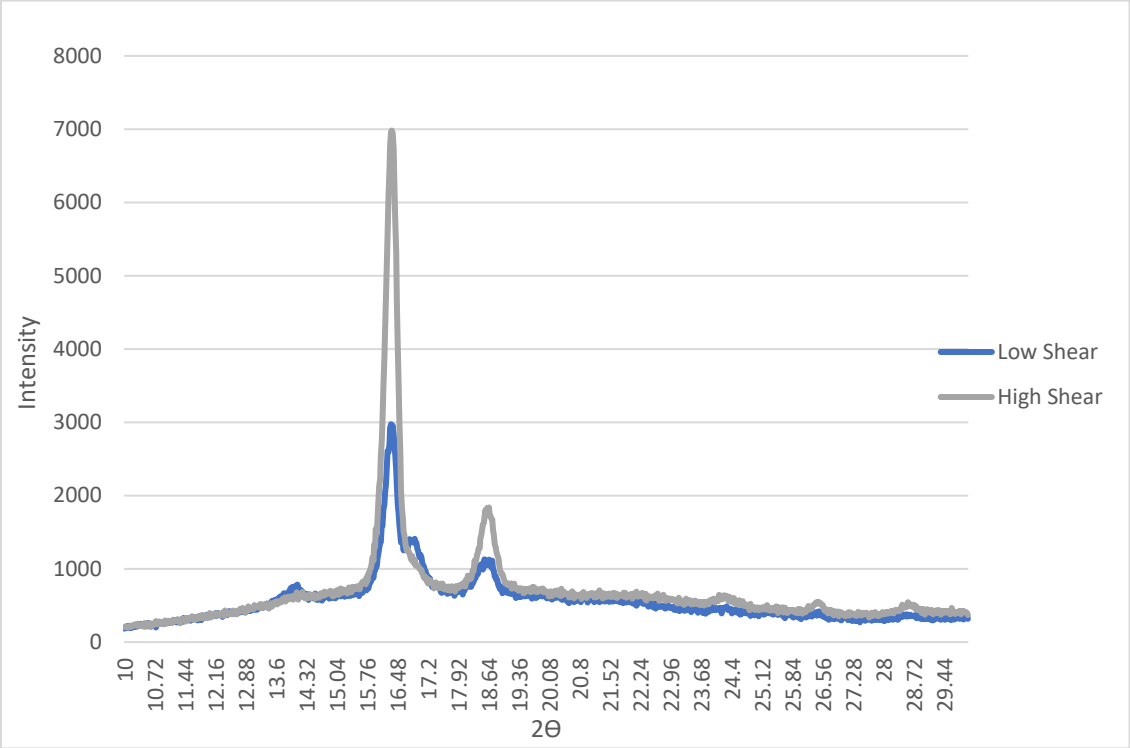

Figure 6-31: XRD results of the samples prepared with and without rotation.

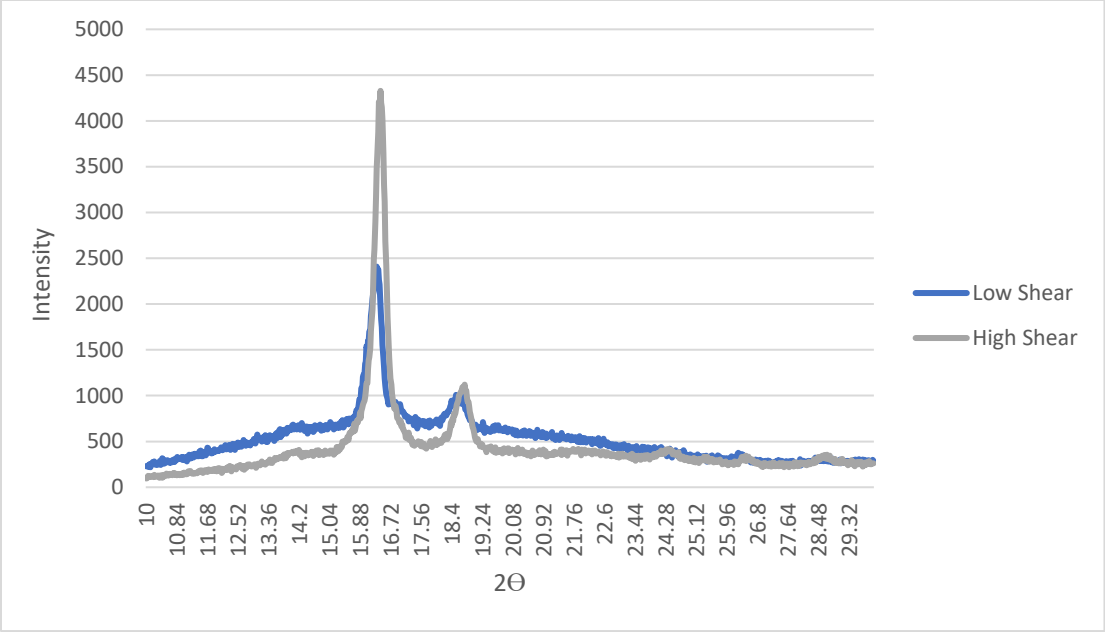

Figure 6-32: XRD results conducted 6 month later of the same samples shown in the previous figure.

As shown in the previous two figures, after 6 months the intensity of the peaks for the two samples printed with and without rotation have dropped slightly. The samples were stored in a zip lock at room temperature. The rate at which the peaks and crystallinity dropped is not clear and it requires further investigations with controlled humidity levels and temperatures.

6.3.3.6 Microscope

Figure 6-33 and Figure *6-34* show a comparison in the physical appearance between two samples that were printed with and without nozzle rotation. It is clear that the rotation affected the physical appearance of the sample. The sample printed with rotation was looked at under the microscope and the results are shown in Figure 6-35, these pictures show the effect of nozzle rotation in a single road.

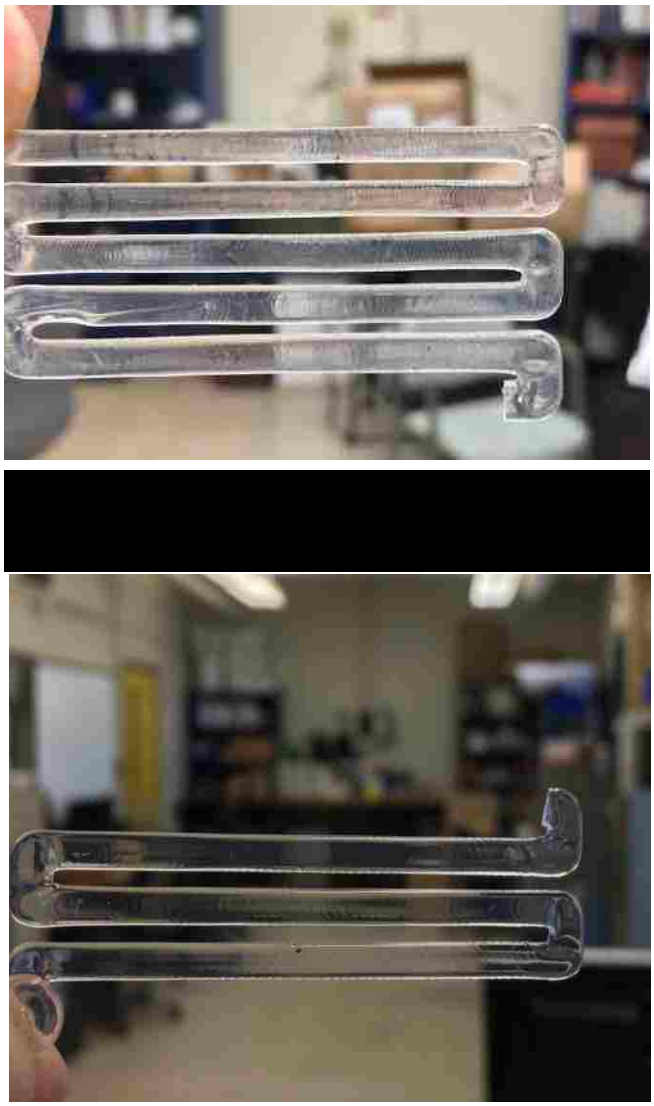

Figure 6-34: Clear sample printed without nozzle rotation

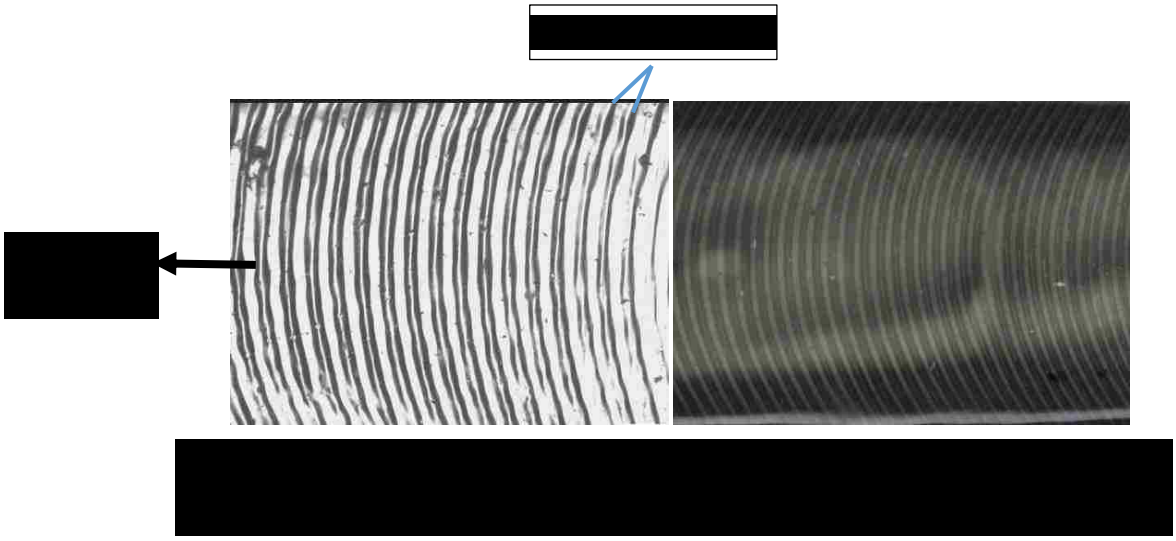

The distance between two roads of rotations shown in Figure 6-35 can be tuned by controlling the nozzle rotational speed relative to the stage speed. This can be useful when using this technique to align short fibers to tune the mechanical properties of the printed parts.

Figure 6-36 shows a layer of an ASTM D638 Type V dog bone specimen printed using the prototype AM device. The printed sample shows that the device is capable of printing roads with different processing history within a single construct. Inset (A) shows an enlarged cross polarized optical image of a printed road.

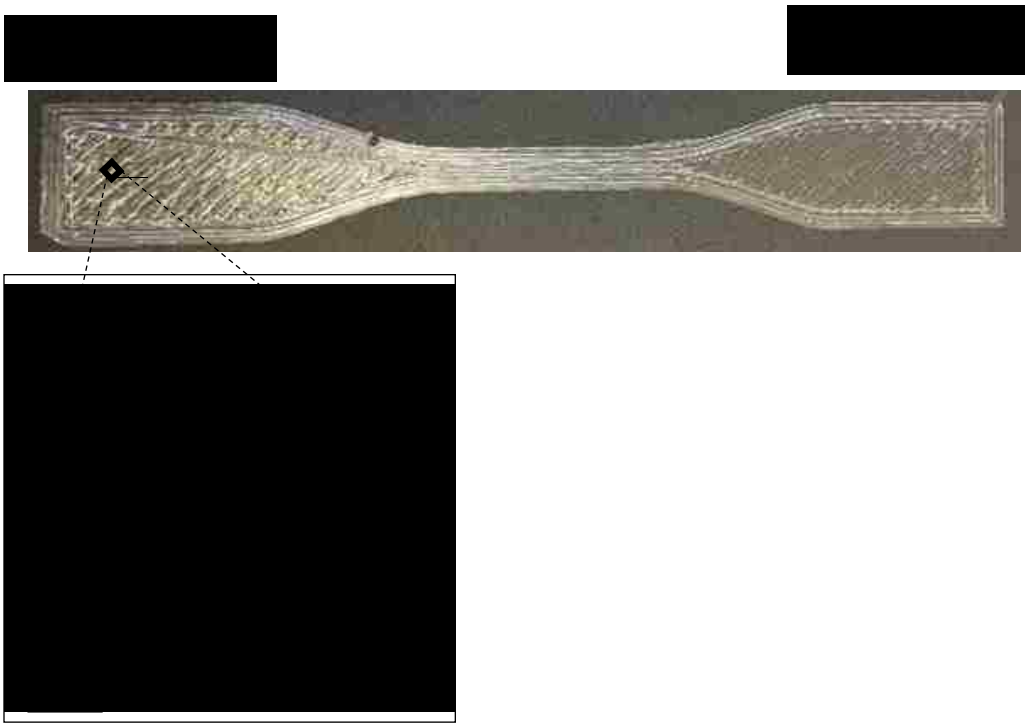

Figure 6-36: An ASTM D638 Type V dog bone specimen printed with the novel AM device. Two regions, as indicated, were printed with and without nozzle rotation. Inset (A) shows an enlarged polarized optical image of a printed road.

6.3.3.7 Discussion and Conclusion

Several conclusions can be drawn from the results:

- The influence of the melt temperature turns to be a complicated factor since it elevates the temperature of the nozzle, and the nozzle acts as a thermal source for the printed part. In a regular FFF printer, the increase of the melt temperature might result in an increase of crystallinity of the printed parts. In our experiment when no rotation was being applied, the increase of melting temperature increased crystallinity by around 2%.

- The Stage temperature have shown to significantly influence the crystallinity of the printed parts. A range of different stage temperatures were tested starting from 18℃ to 85℃. The crystallinity increased from around 10% to 52% with increasing the stage temperature. The stage temperature also influences the adherent of the parts to the stage which is necessary to achieve good quality print, otherwise, the parts will not adhere to the stage and the print will be ruined. For this material, a range of temperatures between 25℃ and 65℃ resulted in a successful print. These results show that controlling crystallinity by controlling the stage temperature is an effective technique where the crystallinity can be increased dramatically.
- The layer thickness was found to affect the crystallinity of the printed samples. It was found that the larger the layer thickness the higher the crystallinity. The reason for this increase might be due to that the part with larger layer thickness will cool slower compared to the smaller ones, which will allow the material to stay for a longer time at elevated temperatures and therefore allowing crystals to grow larger. Also, this experiment was conducted when the stage temperature was set to room temperature. According to literature study[26], the larger layer thickness resulted in a significant enhancement of maximum stress.
- The rotating nozzle was found to influence crystallinity in different ways:
    - At the upper limit of the melt temperature, introducing higher shear rate didn't result in any changes of crystallinity regardless of the stage temperature.
    - At the lower limit of the melt temperature, introducing higher shear rate resulted in an enhancement of crystallinity within one part by around 20%

when heated stage was used. A possible explanation is that at the lower limit of the melt temperature, the onset of shear rate where it starts affecting the alignment of the molecules becomes lower as proved in the next section on this chapter. So, the introduced shear rate by rotating the nozzle was enough to enhance the crystallization process compared to the previous case. Also, at the lower melt temperature, the relaxation time becomes slower and, thus, the shear effect on the molecular orientation can have sufficient time to cause nuclei formation and therefore spherulites grow from there.

- The rotating nozzle can also be used to align fibers by controlling the stage speed relative to the nozzle rotational speed. As a result, it can enhance the mechanical performance of the printed parts.

6.4 Multi Material Printing with Single Extrusion Head incorporating the 4D Rheo-Printing system

6.4.1 Introduction

Multi material 3D printing is of great interest as functionally gradient products with tunable mechanical, thermal, electrical and biodegradation properties can be fabricated to desired specifications. It allows for designing and manufacturing objects that were impossible to fabricate with other manufacturing processes. The focus of this study will be on multi material extrusion based 3D printers.

There are two types of extrusion based 3D printers. The first one, which is the most common, is called Fused Deposition Modeling (FDM) which uses material in form of filaments. The second one, which is the one developed in this study, has a mini extruder mounted on its head, and it uses the material in form of pellets instead of filaments. The majority of the multi material printers currently available are dual extrusion fused deposition modeling printers [81], where each extruder feeds one material, and the melt temperature for each extruder is set to the melting temperature of the material being used.

Multi material printing with single extrusion head has an advantage over multi extrusion heads since it allows the mixing of two different materials to tune product's properties. However, it requires instantaneous control of melting temperature which is not feasible since polymers are known to be poor conductors [31,82]. Otherwise, problems such as under extrusion and over extrusion will arise. Under extrusion occurs when the melting temperature is set too low, which causes the material to not melt properly and the viscosity to be high. As a result, the extruder is not able to supply the right amount of

material, which causes under extrusion [83]. On the other hand, over extrusion occurs when the melt temperature is set too high which causes the viscosity of the material to be too low and as a result increases the layer thickness of the print. So, it is important when dealing with multi material printing with single extrusion head to be able to have rapid control over viscosity of the melt in order to achieve desirable quality print.

Most polymers are non-Newtonian shear thinning materials, which belongs to a class of pseudo plastic materials fluids [35]. The viscosity of pseudo plastics non-Newtonian fluids decreases with increasing shear rate. Since shear rate causes the polymer chains to orient, leading to reduced entanglement, thus allowing them to slip past each other easily [84]. The end result is reduction of viscosity of the polymer melt. Once shear rate disappears, polymer chains will return to their entangled high viscosity conditions.

In this report, the "4D Rheo-Printing" technology is utilized where the viscosity of a polymer melt can be controlled precisely and instantaneously by tuning shear rate. Additionally, we demonstrate that this strategy enables 3D printing of dissimilar polymers (with distinct melting temperatures and viscosities) utilizing a single extrusion head and provides a path for fabricating functionally gradient materials.

6.4.2 Method

The "4D Rheo-Printing" is an extrusion based printer. The printer head consists of a screw extruder and a heated extruder barrel, which allows it to process different variety of materials in their granulated form. The nozzle of the printer can be rotated at different speeds to control several properties of the polymer including molecular orientation and

crystallization kinetics as discussed previously [85]. The primary focus of this study is to understand and exploit the impact of "4D Rheo-Printing" on melt rheology.

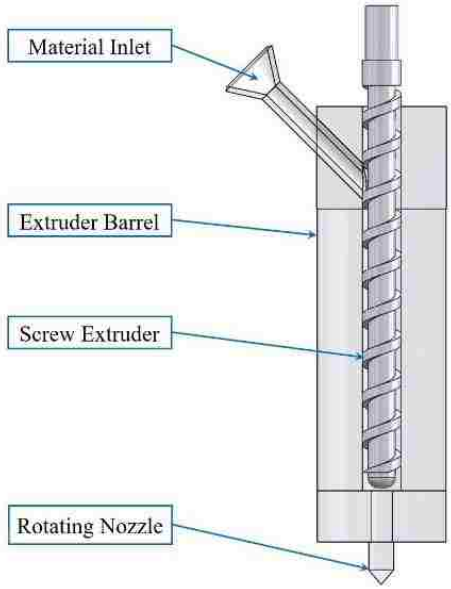

Figure 6-37: A schematic of the novel extrusion based 3D printer utilized in this study.

Shear rate of the polymer melt is controlled precisely by the spinning nozzle. As the RPM of the nozzle increases, shear rate increases and as a result viscosity of the polymer melt decreases. Generally, when feeding two materials with two different melting temperatures, the temperature at the nozzle will be set to the lowest melt temperature. Then, just before the material with the higher melting temperature arrive to the nozzle, the nozzle will be rotated in a controlled fashion to reduce the viscosity of the melt to allow it to pass through the small passage of the nozzle for extrusion.

6.4.3 Materials

The materials that were used in this experiment are two grades of PLA, Ingeo 2500HP and Ingeo 3052D, both materials were supplied by NatureWorks LLC. Ingeo 2500HP is designed for extrusions applications and it is also designed to crystallize during processing, and the amount of crystallinity depends on the processing conditions [86]. On the other hand, Ingeo 3052D is an amorphous clear material.

6.4.4 Rheometer of the Materials

A parallel plate Rheometer was used to investigate the shear thinning behavior of the two aforementioned grades of PLA at different temperatures. The results for the semi crystalline PLA and the amorphous PLA are shown in Figure *6-38* and Figure *6-39* respectively.

As shown in the figures, at low shear rate, both materials acted as Newtonian fluids. The viscosity started to decline sharply at higher shear rate exhibiting a pseudo plastic behavior.

It was also observed that the onset of shear thinning for both materials occurs at a lower shear rate as the temperature is decreased. For the semi-crystalline PLA, the onset of shear thinning was at a very low shear rate of 3 s^{-1} at 180°C, while at 200°C viscosity didn't start declining until shear rate reached 30 s^{-1}.

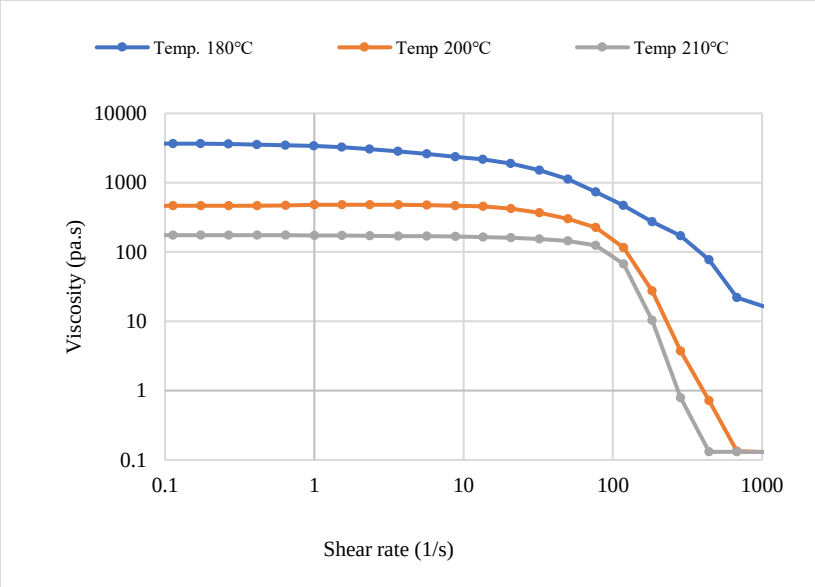

Figure 6-38: Shear rate dependence of viscosity of Semi Crystalline PLA (Ingeo 2500HP) at various temperatures as indicated in the plot.

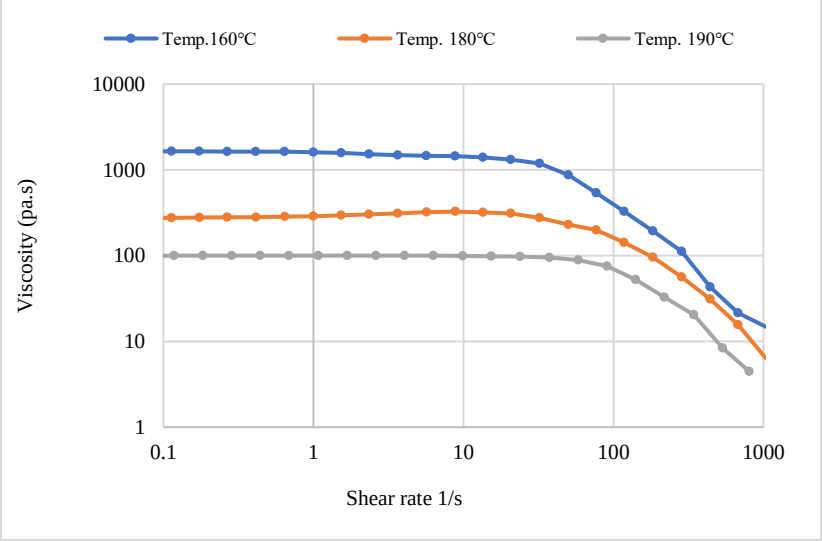

Figure 6-39: Shear rate dependence of viscosity of Amorphous PLA (Ingeo 3052D) at various temperatures as indicated in the plot.

The shear thinning behavior of the amorphous Ingeo 3052D PLA at 180°C is compared with that of the semi-crystalline Ingeo 2500HP PLA in Figure *6-40*.

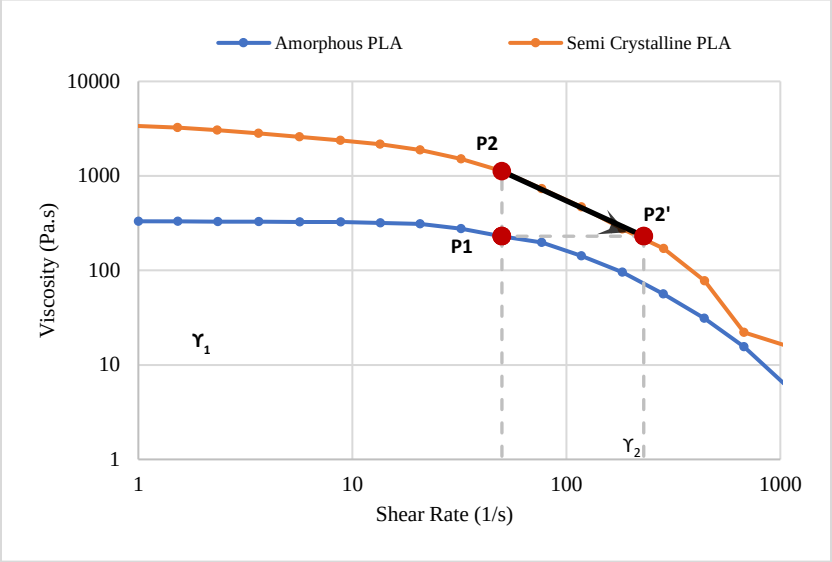

Figure 6-40: A comparison of the shear rate dependent viscosity of Amorphous PLA (Ingeo 3052D) and Semi Crystalline PLA (Ingeo 2500HP) at 180°C.

At 180°C, the semi crystalline Ingeo 2500HP PLA had higher viscosity compared to amorphous Ingeo 3052D PLA due to differences in their micromolecular structure. The zero shear viscosity of amorphous PLA was around 330 pa.s, while for semi crystalline PLA the viscosity was 3400 pa.s. Shear rate of 155 s^{-1} was needed in order to reduce the viscosity of the semi crystalline PLA to match that of the amorphous PLA at zero shear.

Let us assume that a viscosity of p1 shown in the previous figure would be ideal for extrusion. As indicated in the previous figure by employing a shear rate of Υ_1, the amorphous Ingeo3052D can be extruded at 180°C. The viscosity of the semi-crystalline Ingeo 2500HP would be p2 under the same conditions. If the two materials were to be printed at the same time using a single extruder head, the parts fabricated from Ingeo 2500HP will be under-extruded. This issue could be resolved by changing the shear rate.

A shear rate Υ_1 could be applied to the amorphous PLA to be extruded at viscosity of p1, and a shear rate of Υ_2 to the semi crystalline PLA to be extruded at the same viscosity without changing the temperature.

6.4.5 Numerical Simulations

Numerical simulations through ANSYS Fluent were conducted in order to investigate the effect of the rotating nozzle on viscosity for the amorphous and semi crystalline PLA. The purpose of this study was to gain an understanding of the effect of angular velocity on the viscosity, in other words, to correlate shear rate and angular velocity. It is an important study because it guides the user of the printer about the required rotation in order to extrude the semi-crystalline PLA without increasing the temperature of the extruder, but by reducing its viscosity.

To set up the simulation, a CAD model representing the passage through the nozzle is modeled. The model is then imported to perform the simulation analysis. Zero shear viscosities of both amorphous and semi crystalline PLA were calculated using the cross model in order to input the properties of the materials to set up the simulation analysis correctly. A number of analyses where done to represent the relation between shear and viscosity at different rotation per minute angular velocities.

The average viscosities at different angular velocities are presented in Figure 6-41 below. The two lines represent the amorphous Ingeo 3052D PLA and the semi crystalline Ingeo 2500HP PLA. The dashed line in the figure matches the required nozzle rotation for the semi crystalline to achieve amorphous viscosity at fixed nozzle. In other words, the

nozzle has to be rotating at around 170 RPM in order for the semi crystalline PLA to reduce its viscosity to 177 Pa-s, which is the fixed nozzle viscosity of the amorphous PLA.

It is worth noting that the fixed nozzle viscosity of the amorphous PLA is much lower than the zero shear viscosity of the material itself due to the velocity and wall friction effects on the viscosity. Because of that, the viscosity behavior we see in acts as non-Newtonian fluids at zero nozzle RPM. Otherwise, if there is no velocity effect, the viscosity will behave as Newtonian at low shear rate as shown in Figure *6-40*.

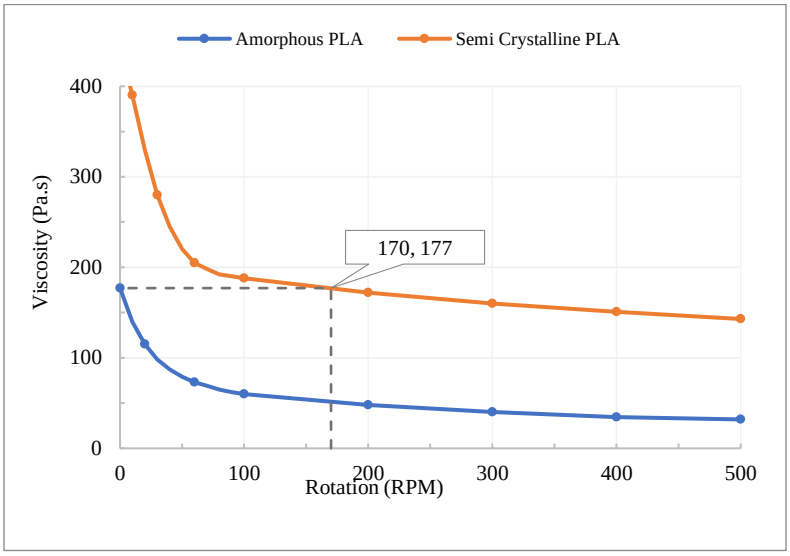

Figure 6-41: Simulation results of amorphous and semi crystalline PLA at 180℃.

6.4.6 Experimental

6.4.6.1 Sample Preparation

The extrusion was performed at two different inlet temperatures, 140° and 80°C. For the extrusion, the amorphous PLA was fed first, followed by a mixture of the amorphous and the semi crystalline PLA. After that, the semi crystalline PLA was fed into the inlet.

6.4.6.2 Differential Scanning Calorimetry

DSC was performed using a TA Instruments Q2000 DSC. Only the first heating scan, at 10 °C /min, was collected to obtain the influence of the printing process on the material. The degree of crystallinity (X_C) was calculated using Equation (1) [87].

$$Xc = \frac{\Delta \mathrm{Hm} - \Delta \mathrm{Hc}}{\Delta Hm^{\circ}} \times 100 \ldots\ldots.(1)$$

Where ΔHm is the melting enthalpy, ΔHc is the enthalpy of crystallization, and ΔHm° is the melting enthalpy of 100% crystalline PLA which is (93 J/g) [88].

6.4.6.3 Results and Discussion

In the beginning, the temperature of the nozzle was set at the melt temperature of the amorphous polymer, and the temperature of the inlet was set to be 140 ℃ which is close to the recommended feeding temperature. Under these conditions the amorphous polymer resin started to soften at the inlet and then got stuck and didn't move into the

extruder. These issues didn't occur with the semi crystalline polymer. That can be explained due to the different viscoelastic behavior of amorphous and crystalline polymers.

Amorphous and crystalline materials behave differently when undergo different temperatures. Amorphous polymers go through glass transition temperature, where the material will start transitioning from glassy to rubbery [37]. On the other hand, a fully crystallized polymer doesn't go thorough glass transition temperature, it will act as elastic solid until the temperature reaches the melting temperature.

In order to solve this problem, the inlet temperature was reduced to around 80℃. Also, since the temperature is still higher than the glass transition temperature, we try to not let the material stay for too long at the inlet so it doesn't start softening. First we fed the amorphous PLA, then a mixture of the amorphous and the semi crystalline PLA was fed. After that, the semi crystalline PLA was fed into the inlet.

In this study, the ability to 3-D print two different materials using one extrusion head is investigated. Also, the ability of tuning 3-D printed parts properties by mixing two materials is investigated as well.

DSC results of the samples that were prepared at the same temperature are shown in Figure 6-42. Amorphous and semi crystalline PLA were printed at a melting temperature of 180℃. Amorphous PLA was extruded easily at that temperature. On the other hand, without imposing higher shear rate to the melt through nozzle rotation, 180 ℃ was not a high enough temperature to extrude the semi crystalline PLA. So, higher shear rate was imposed in order to reduce viscosity of semi crystalline PLA to match that of the amorphous PLA for extrusion.

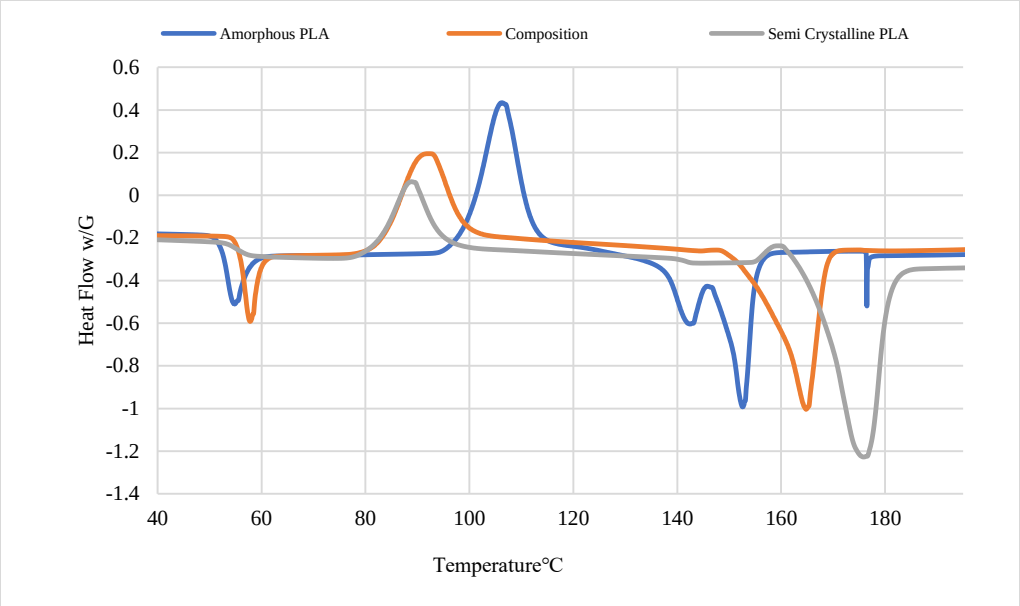

Figure 6-42: DSC results of samples that were prepared by the "4D Rheo-Printing technique.

	Tg (℃)	Tc (℃)	Tm (℃)	Crystallinity %
Amorphous PLA	54.6	106.28	152.64	0
Composition	57.9	91.78	164.58	12
Semi Crystalline PLA	-	89.10	174.95	41

DSC can show glass transition temperature (Tg), cold crystallization temperature (Tc), and melting temperature (Tm).

By observing the three curves shown in Figure 6-42. The first observed distinction is on the glass transition temperature, as discussed in the sample preparation section, amorphous materials show glass transition temperature unlike crystalline materials. On the other hand, semi crystalline polymers will show glass transition depending on the amount of crystals and amorphous phase on them.

Cold crystallization is caused by the ordering of molecular chains [79]. Semi crystalline PLA showed lower crystallization temperature compared to amorphous PLA, which can be attributed to an increase in the mobility of the molecular chains and caused lower Tc compared to amorphous PLA.

By observing the endothermic melting peaks. Amorphous PLA showed double peaks compared to semi crystalline PLA. The double peaks can be attributed to the melting of the lamellae of different thickness [79].

These results show the capability of the "4D Rheo-Printing" technology not only to extrude different materials with distinct temperatures and viscosities, but also to mix different materials together in order to come up with precise desirable properties.

6.4.7 Conclusion

Multi material printing is one of the key capabilities of additive manufacturing that could significantly increase their potentials, since products with performance improvements in definable locations can be manufactured. In this paper, multi material printing with single extrusion head is demonstrated. A novel technique "4D Rheo-Printing" is proposed in order to successfully print and mix different materials together. This proposed system creates a unique control of melt rheology and it enables advanced functionally gradient multi material printing with single extrusion.

CHAPTER 7:Market Analysis

7.1 Introduction

The use of additive manufacturing has been growing rapidly. It has been used more and more to produce final products instead of prototypes due to its many capabilities and advantages. The most significant advantages of additive manufacturing over traditional manufacturing processes are [10]:

- The ability to build customizable parts.

  Parts with complex geometries can be built with additive manufacturing easily due to the nature of the process where parts are built layer upon layer from the ground up.

- The elimination of material waste.

  Unlike traditional manufacturing processes, additive manufacturing has minimal material waste since there is no subtraction in the process.

- The increase of efficiency by producing parts in demand.

  Additive manufacturing can produce parts in demand efficiently. This characteristic is mostly beneficial for industries where mass production is not needed. Also, there is no mold needed to be made in order to build a new part, which saves time and energy.

In addition to the advantages mentioned above, additive manufacturing has the potential to increase its customizable capabilities to include microstructure customization.

With that being said, the 4D Rheo-printing was developed to take additive manufacturing customization capability to a new level.

It is important to understand the market's needs to be able to make it in the market place. A new technology has to provide value for others whether its industries or people to success. This chapter investigates the market size of additive manufacturing, the applications of additive manufacturing and the potential applications for the 4D Rheo-printing system.

7.2 Market Size

Additive manufacturing is growing at a high rate. The global market for additive manufacturing is expected to grow to reach 20.5 billion U.S dollars by 2020 as shown in Figure 7-1 [89].

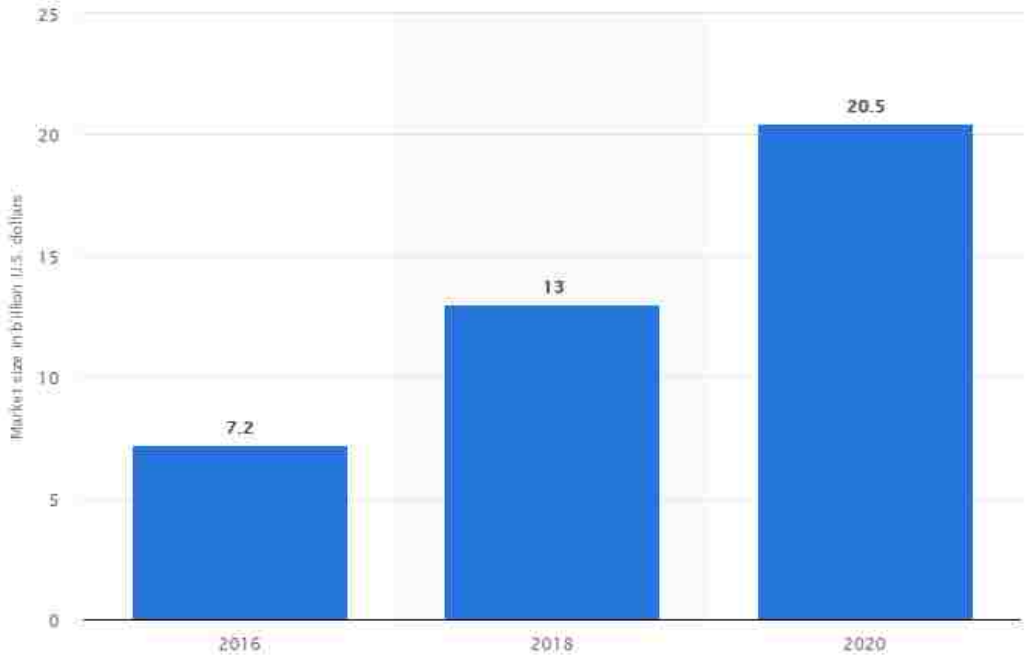

Figure 7-1: Global additive manufacturing market size.

The industries where additive manufacturing is growing the fastest are medical, aerospace and automotive. These industries are expected to account for 51% of the additive manufacturing market by 2020. The reason additive manufacturing is flourishing in these industries especially the aerospace and the medical industries is that the parts are not mass produced and because of the precise customization capabilities of additive manufacturing. Although, additive manufacturing have never been about mass production, some industries are starting to use them to mass produce parts since they are able to reduce the number of parts needed to make a final product such as the fuel nozzle that was mentioned previously in CHAPTER 2.

7.3 Potential applications for the 4D Rheo-Printing system

Additive manufacturing market is big and growing. There are variety of additive manufacturing machines and materials. This research was focused on extrusion based type of 3D printing of polymers.

Currently the 4D Rheo-Printing system can be used to

1. Tune and enhance molecular orientation and crystallinity throughout 3D printed products.
2. Enable multi material printing with gradient properties using one extrusion head.
3. Align fillers to tune and enhance the mechanical properties.
4. Prevent nozzle clogging by reducing viscosity of the melt by inducing higher shear rate.

With that being said, the 4D Rheo-Printing system can be used to achieve one or multiple of the previous goals.

The industries where the proposed system can be of great advantages are any industry that require properties tuning or enhancement, such properties are mechanical, thermal, electrical and biodegradation properties.

In the medical industry, the proposed technique can be used to tailor the products to meet the individual needs and therefore can play a significant role in personalized health care. Examples of products that can be printed are tissue scaffolds, medical implants, screws…etc. With our understanding of the effect of molecular orientation and crystallinity on mechanical, thermal and biodegradation properties and according to literatures, the

proposed technique can tailor the molecular orientation and crystallinity and the mix of multi materials to find a balance between physical, mechanical and biodegradation properties. Balancing all the previous factors can help medical devices to biodegrade at the appropriate rate while transferring the stress to surrounding tissues to assure successful healing.

It is known that natural composites have outstanding mechanical properties. The proposed system can be used to align short fibers composites, without incorporating the rotating nozzle, the alignment of fibers will be random instead of desired distribution.

A common problem with 3D printers are nozzle clogging due to many causes. One of the main causes of nozzle clogging is the temperature not being high enough to reduce viscosity for extrusion. Also, when using additives, the additives might cause the nozzle to clog due to a poor mix with the material. The rotating nozzle can be used to prevent the nozzles from being clogged by inducing higher shear rate to reduce the viscosity of the melt to allow smoother extrusion. Also, when using additives, the nozzle can be used to enhance the mix and ensure better extrusion.

CHAPTER 8: Summary and Conclusion

8.1 Research Summary

Additive manufacturing (AM) has the potential to create parts with tailored properties to meet consumer's needs. It is known that additive manufacturing parts are built from the ground up layer upon layer. Inspired by this mechanism, we have created a system that enables melt rheology control of each single layer. This system provides an intelligent manufacturing process where it locally controls the melt flow for each single layer and adjust the stage and melt temperature accordingly to control part qualities. Thus, parts with tunable properties were produced and demonstrated using this system.

The investigation demonstrated that the 4D Rheo-Printing technique was capable of inducing shear rate to the polymer melt by rotating the nozzle. Shear rate influences the molecular orientation and crystallization kinetics of polymeric materials. Also, molecular orientation and crystallinity is known to influence the mechanical, thermal and biodegradation properties.

At the beginning of this project, the 4D Rheo-Printing technique was just an idea. I have investigated the feasibility of the idea analytically and numerically. Then, I developed the 4D Rheo-Printing system. After that, samples were collected and characterized to assure the system is working as expected. When I started this project, the main goal of the 4D Rheo-printing system was to control molecular orientation and crystallinity of the final parts, now we know that this system is capable of doing more than that. It can be used to 3D print parts using multi materials using one extrusion head. As a

result, functionally gradient multi material printing is enabled and a new products with gradient properties can emerge. The 4D Rheo- printing can also be used to align fillers to enhance the mechanical properties of the final parts.

According to NASA technology readiness level scale shown in Figure 8-1, the current readiness is TRL 4 [90].

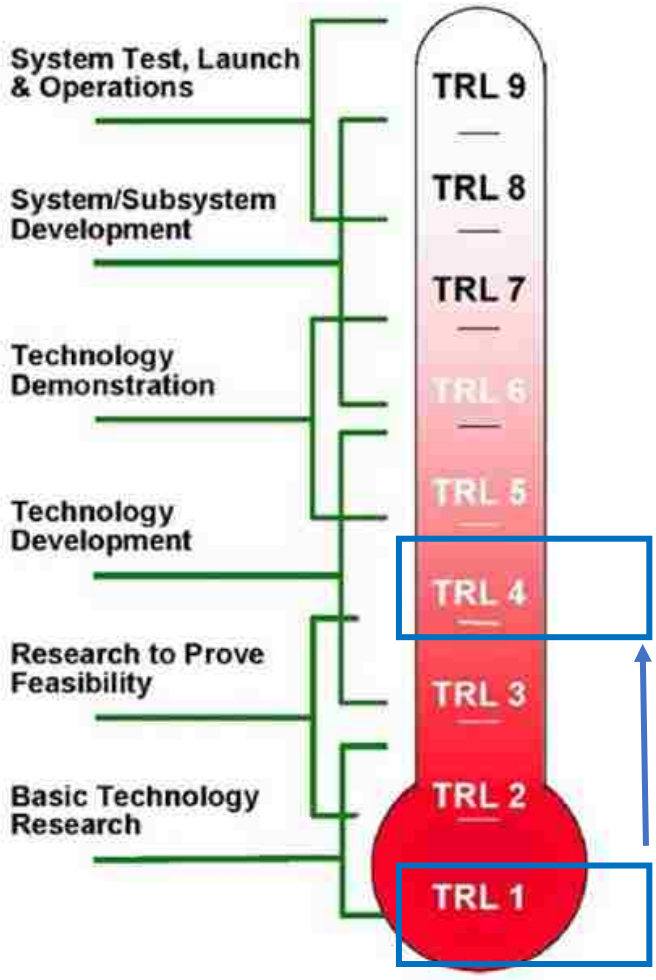

Figure 8-1: NASA readiness levels

The key objectives of this research was as follows:

- Understanding in details the challenges remained to be solved in additive manufacturing. (CHAPTER2)
- Investigate the related scientific fundamentals of melt rheology and morphology, and understand the ways in which they can be manipulated. (CHAPTER3)
- Design the 4D Rheo-Printing technique. (CHAPTER4)
- Investigates numerically the capability of the 4D Rheo-Printing system to tune the melt rheology of polymeric materials. (CHAPTER5)
- Investigate analytically the molecular relaxation times. (CHAPTER5)
- Develop the 4D Rheo-Printing technique. (CHAPTER4)
- Develop the extrusion based 3D-printer, in which the new technology will be assembled to. (CHAPTER4)
- Establish a base line of the parameters to be used in the experimental work by performing non isothermal crystallization analysis under quiescent conditions. (CHAPTER6)
- Conduct experimental testing of the 4D Rheo-Printing system to investigate the validity of the concept, and compare the results of the samples made with and without using the rotating nozzle. (CHAPTER6)
- Investigate the capability of the 4D Rheo-Printing system to print multi materials into one part using one extrusion head. (CHAPTER6)

All the objectives mentioned in the top were completed. As I mentioned earlier, we are still understanding all the capabilities of this machine. Some of the objectives such as

the one concerned with multi material printing was recognized and investigated at the end of the project.

8.2 Impact of dissertation research

Lehigh University has a strong research capabilities, and the area of manufacturing is one of which Lehigh has produced many advancements. The 4D Rheo-Printing system is completely a new technology that has been developed to couple the flexibility of additive manufacturing with in situ control of material and physical properties throughout the product. This is a big step in advancement of additive manufacturing technology. There are four types of innovations as shown in Figure 8-2 [91].

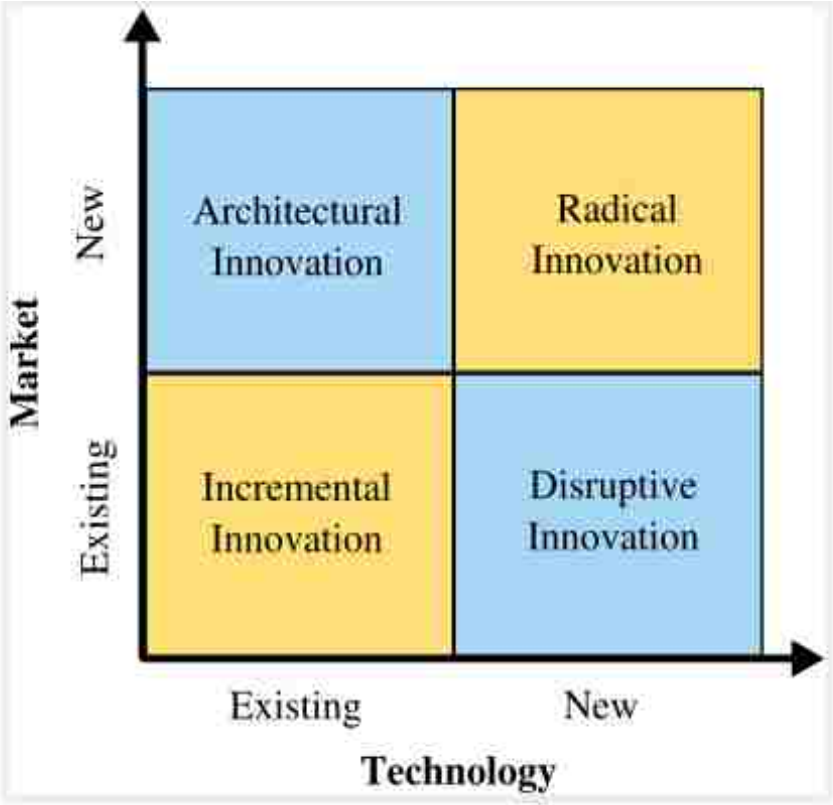

Figure 8-2: Types of innovations.

Radical innovation is the type of innovation that create new technologies or new product lines, which is what the 4D Rheo-printing is doing. This project open a new market for additive manufacturing, where they are able not only to precisely customize the geometry but also to locally tune the molecular structure for each single road to achieve high performance capabilities. It allows manufacturers and designers to think of a new ways to design parts and products to precisely meet the consumer needs. To be more specific, in the medical applications when manufacturing a bone scaffold that will be attached to both the cartilages and the bones, each part of the scaffold has to mimic the properties of the part that is attached to it weather it is the bone or the cartilages, the 4D-Rheo printing technique can precisely and locally tune the properties of the scaffold to mimic the part that it is attached to.

In conclusion of this section, the advantages of the 4D Rheo-Printing system can be summarized as follows:

- Induce locally tunable molecular orientation and crystallinity level in 3d Printed parts.
- 3D print two different materials that have distinct melting temperatures into one part.
- Allow 3D printing of functionally gradient multi material polymer component with single extrusion head.
- Control helical fiber alignment to enhance mechanical properties.
- Prevent nozzle clogging by reducing viscosity for extrusion.

Regarding the impact in the personal level, I have learned so much since I started working in this project. I have developed so many skills by working in this project and by interacting with professor coulter and the group member of the manufacturing lab. Skills and experiences can be summarized as:

- Critical thinking
- Writing proposals and scientific papers
- Additive manufacturing
- Designing software (SolidWorks)
- Numerical simulations (ANSYS FLUENT)
- Numerical simulations (MoldFlow)
- Polymer processing
- G coding
- Characterization (DSC)
- Characterization (XRD)

The most important thing is the friendship relations that I have developed with my advisor and with the previous and current group members. I have developed a friendship with people from all around the world at Lehigh, people form the US, Malaysia, India, China, Kuwait, Saudi, Iraq and Turkey.

The PhD is a long journey and it requires having the skills to both work individually and as a team, and a team work cannot be productive without communication, respect, collaboration and having a common goal. During my time in the manufacturing laboratory at Lehigh, we have learned how to work as a team and individually.

8.3 Proposed future work

The current 4D Rheo-Printing system was simply designed to be retrofitted with existing extrusion based 3d printers. Currently, the hardware part of the new technology regarding the rotating nozzle is ready to be field tested. Regarding the whole printer, the weight might be reduced to make it easier to be commercialized. Also, the inlet of the extruder (The Hopper) should be cooled or insulated with material that has poor thermal conductivity to prevent the polymer from getting stuck and to allow continuous feeding rate. Also, the current version of the system has manual controllable parameters. So, a software that can support the new system and have it work harmonically with the movement of the printer is necessary to develop.

8.4 Conclusions

It is well established that processing factors such as melt temperature, stage temperature and shear rate can significantly impact the final properties of the polymeric parts. These factors influence the crystallization process in semi crystalline polymers, thus, parts with different and desired crystallinity level can be produced by controlling them purposely. Theoretically speaking, higher stage temperature around the crystallization temperature can result in high crystallinity level of additive manufactured parts. But, it was found that a stage temperature higher than 75℃ led to shrinkage of the parts in the case of PLA.

In this project, utilizing the 4D Rheo-Printing technique, the effect of shear rate, stage temperature and melt temperature on the crystallinity of the final printed parts were

investigated. Shear rate was found to influence the crystallinity of final parts by enhancing the crystallization kinetics. Moreover, shear induced crystallization was found to be highly dependent on shear temperature, which is the processing temperature in which shear rate is applied. The stage temperature was found to have a big influence on crystallinity as well.

The ability of the 4D Rheo-Printing system to print multi material with single extrusion head was investigated. This technique was shown to have a great potential to take multi material printing to a new level. The multi material printing techniques that are currently available mostly print one material or the other and they can't mix different materials. The 4D Rheo-Printing system can incorporate the rotating nozzle to induce shear rate to adjust the viscosity of the melt and to mix different materials to enable functionally gradient multi material printing.

The 4D Rheo-Printing technique was successfully developed and validated according to the simulations and experimental work that were conducted during this project. Additive manufactured parts with tunable and gradient properties were produced by physically manipulating shear rate and thermal processing conditions.

References:

[1] E. Koscher, R. Fulchiron, Influence of shear on polypropylene crystallization: morphology development and kinetics, Polymer. 43 (2002) 6931–6942.

[2] M. Boutaous, P. Bourgin, M. Zinet, Thermally and flow induced crystallization of polymers at low shear rate, Journal of Non-Newtonian Fluid Mechanics. 165 (2010) 227–237. doi:10.1016/j.jnnfm.2009.12.005.

[3] S. Huang, H. Li, S. Jiang, X. Chen, L. An, Crystal structure and morphology influenced by shear effect of poly(l-lactide) and its melting behavior revealed by WAXD, DSC and in-situ POM, Polymer. 52 (2011) 3478–3487. doi:10.1016/j.polymer.2011.05.044.

[4] R. Pantani, I. Coccorullo, V. Volpe, G. Titomanlio, Shear-Induced Nucleation and Growth in Isotactic Polypropylene, Macromolecules. 43 (2010) 9030–9038. doi:10.1021/ma101775h.

[5] Z. Wang, Z. Ma, L. Li, Flow-Induced Crystallization of Polymers: Molecular and Thermodynamic Considerations, Macromolecules. 49 (2016) 1505–1517. doi:10.1021/acs.macromol.5b02688.

[6] D.K. Cho, J.W. Park, S.H. Kim, Y.H. Kim, S.S. Im, Effect of molecular orientation on biodegradability of poly(glycolide-co-ε-caprolactone), Polymer Degradation and Stability. 80 (2003) 223–232. doi:10.1016/S0141-3910(02)00402-0.

[7] S. Farah, D.G. Anderson, R. Langer, Physical and mechanical properties of PLA, and their functions in widespread applications — A comprehensive review, Advanced Drug Delivery Reviews. 107 (2016) 367–392. doi:10.1016/j.addr.2016.06.012.

[8] Cao, B., Shepard, T.A., Tollefson, N.M., Sugg, H. (1994), Injection-Spin Process. in ANTEC ’94, Society of Plastics Engineers.: p. 2603-2606., (n.d.).

[9] M. Piazza, S. Alexander, Additive Manufacturing: A Summary of the Literature, (n.d.) 30.

[10] S.H. Huang, P. Liu, A. Mokasdar, L. Hou, Additive manufacturing and its societal impact: a literature review, The International Journal of Advanced Manufacturing Technology. 67 (2013) 1191–1203. doi:10.1007/s00170-012-4558-5.

[11] V. Zukas, J.A. Zukas, An Introduction to 3D Printing, First Edition Design Pub., 2015.

[12] Selective Laser Sintering, Birth of an Industry - Department of Mechanical Engineering, (n.d.). http://www.me.utexas.edu/news/news/selective-laser-sintering-birth-of-an-industry (accessed December 5, 2018).

[13] Stereolithography (SLA) – 3D Printing Simply Explained, All3DP. (2018). https://all3dp.com/2/stereolithography-3d-printing-simply-explained/ (accessed December 5, 2018).

[14] even, SLA 3D Printing: Difference in Laser and DLP Light Pattern Generation, Kudo3D Inc. (2015). https://www.kudo3d.com/sla-3d-printing-difference-in-laser-and-dlp-light-generation/ (accessed December 5, 2018).

[15] Uploading, 3D Printing Processes - Directed Energy Deposition (Part 6/8), (2017). https://www.engineersgarage.com/articles/3d-printing-processes-directed-energy-deposition (accessed December 6, 2018).

[16] MANUFACTUR3D, The 7 Types of Additive Manufacturing Technologies, MANUFACTUR3D. (2018). https://manufactur3dmag.com/7-types-additive-manufacturing-technologies/ (accessed December 6, 2018).

[17] Directed Energy Deposition | Additive Manufacturing Research Group | Loughborough University, (n.d.). https://www.lboro.ac.uk/research/amrg/about/the7categoriesofadditivemanufacturing/directedenergydeposition/ (accessed December 6, 2018).

[18] Mercedes-Benz Is 3D Printing Genuine Replacement Classic Parts - Auto News - Carlist.my, Carlist.My - Malaysia's No.1 Car Site. (n.d.). https://www.carlist.my/news/mercedes-benz-3d-printing-genuine-replacement-classic-parts/53650/ (accessed December 6, 2018).

[19] T. Kellner, How 3D Printing Is Changing Aerospace Manufacturing, GE Reports. (2017). https://www.ge.com/reports/mind-meld-ge-3d-printing-visionary-joined-forces/ (accessed December 9, 2018).

[20] C. Scott, GE Aviation 3D Prints 30,000th Metal 3D Printed Fuel Nozzle at Auburn, Alabama Plant, 3DPrint.Com | The Voice of 3D Printing / Additive Manufacturing.

(2018). https://3dprint.com/226703/ge-aviation-fuel-nozzle-3d-printed-30000/ (accessed December 9, 2018).

[21] 3D Printed Knee Replacement | 3D Printer, (n.d.). http://www.3dprinter.net/3d-printed-knee-replacement (accessed February 12, 2016).

[22] C.L. Ventola, Medical applications for 3D printing: current and projected uses, PT. 39 (2014) 704–711.

[23] B.P. Chan, K.W. Leong, Scaffolding in tissue engineering: general approaches and tissue-specific considerations, Eur Spine J. 17 (2008) 467–479. doi:10.1007/s00586-008-0745-3.

[24] Q. Hamid, J. Snyder, C. Wang, M. Timmer, J. Hammer, S. Guceri, W. Sun, Fabrication of three-dimensional scaffolds using precision extrusion deposition with an assisted cooling device, Biofabrication. 3 (2011) 034109. doi:10.1088/1758-5082/3/3/034109.

[25] D. Hernandez, Factors Affecting Dimensional Precision of Consumer 3D Printing, International Journal of Aviation, Aeronautics, and Aerospace. (2015). doi:10.15394/ijaaa.2015.1085.

[26] What is the influence of infill %, layer height and infill pattern on my 3D prints?, 3D Matter. (2015). http://my3dmatter.com/influence-infill-layer-height-pattern/ (accessed December 2, 2018).

[27] O. Rishi, Feed rate effects in freeform filament extrusion, (2013). http://scholarworks.rit.edu/theses/7833/ (accessed March 22, 2017).

[28] W. Wu, P. Geng, G. Li, D. Zhao, H. Zhang, J. Zhao, Influence of Layer Thickness and Raster Angle on the Mechanical Properties of 3D-Printed PEEK and a Comparative Mechanical Study between PEEK and ABS, Materials. 8 (2015) 5834–5846. doi:10.3390/ma8095271.

[29] L.H. Sperling, Introduction to Physical Polymer Science, Fourth Edition, n.d.

[30] R.J. Young, P.A. Lovell, Introduction to polymers, Second Edition, n.d.

[31] A.B. Strong, Plastics: materials and processing, 3rd ed, Pearson Prentice Hall, Upper Saddle River, NJ, 2006.

[32] Stress-Strain Behavior of Polymers, (n.d.). http://polymerdatabase.com/polymer%20physics/Stress-Strain%20Behavior.html (accessed October 1, 2018).

[33] John P. Beaumont, Runner and Gating Design Handbook, 2nd ed., n.d.

[34] R. Inc, Viscosity of Newtonian and Non-Newtonian Fluids, (n.d.). http://www.rheosense.com/applications/viscosity/newtonian-non-newtonian (accessed October 1, 2018).

[35] Flow Properties of Polymers, (n.d.). http://polymerdatabase.com/polymer%20physics/Viscosity2.html (accessed October 1, 2018).

[36] Week 4, (n.d.). http://www.che.hw.ac.uk/teaching/B11MS1/Material/Week%207/Week75RegionsofViscoelasticity.htm (accessed October 4, 2018).

[37] Rubbery Plateau, (n.d.). http://polymerdatabase.com/polymer%20physics/RubberyPlateau.html (accessed October 4, 2018).

[38] Properties of Materials - ppt video online download, (n.d.). https://slideplayer.com/slide/3503473/ (accessed October 4, 2018).

[39] Plastics Engineering - September 2016 - Plastics – It's All About Molecular Structure, (n.d.). http://read.nxtbook.com/wiley/plasticsengineering/september2016/consultantscorner_plastics.html (accessed October 1, 2018).

[40] R. Pantani, A. Sorrentino, V. Speranza, G. Titomanlio, Molecular orientation in injection molding: experiments and analysis, Rheologica Acta. 43 (2004) 109–118. doi:10.1007/s00397-003-0325-8.

[41] R.H. Somani, L. Yang, B.S. Hsiao, T. Sun, N.V. Pogodina, A. Lustiger, Shear-Induced Molecular Orientation and Crystallization in Isotactic Polypropylene: Effects of the Deformation Rate and Strain, Macromolecules. 38 (2005) 1244–1255. doi:10.1021/ma048285d.

[42] Z. Tadmor, Molecular orientation in injection molding, Journal of Applied Polymer Science. 18 (1974) 1753–1772. doi:10.1002/app.1974.070180614.

[43] Reptation Model, (n.d.). http://polymerdatabase.com/polymer%20physics/Reptation.html (accessed December 17, 2018).

[44] G.S. Layser, An investigation of controlled melt-manipulation based dynamic injection-molding processes, Ph.D., Lehigh University, 2007. http://search.proquest.com/docview/304845099/abstract/AE3533A8ECD1461FPQ/1 (accessed February 12, 2016).

[45] Reptation, Wikipedia. (2018). https://en.wikipedia.org/w/index.php?title=Reptation&oldid=846744879 (accessed December 17, 2018).

[46] D. M, Introduction to polymer physics, 1996.

[47] Delay John M and K.F. Wissburn, Melt Rheology and its role in plastic processing, Kluwer Academic publishers, 1999.

[48] N. N, Crystalline vs. Amorphous Polymers, (n.d.). https://www.mcpolymers.com/library/crystalline-vs.-amorphous-polymers (accessed October 1, 2018).

[49] Q. Li, Biodegradation Study of Polymeric Material with Various Levels of Molecular Orientation Induced via Vibration-Assisted Injection Molding, (2012). http://preserve.lehigh.edu/cgi/viewcontent.cgi?article=2130&context=etd (accessed February 12, 2016).

[50] DoITPoMS - TLP Library Phase diagrams and solidification - Free energy curves, (n.d.). https://www.doitpoms.ac.uk/tlplib/phase-diagrams/freeenergy.php (accessed December 24, 2018).

[51] S. Andjelić, R.C. Scogna, Polymer crystallization rate challenges: The art of chemistry and processing, Journal of Applied Polymer Science. 132 (2015) n/a-n/a. doi:10.1002/app.42066.

[52] E. Clouet, Modeling of Nucleation Processes, ArXiv:1001.4131 [Cond-Mat]. (2010). http://arxiv.org/abs/1001.4131 (accessed December 24, 2018).

[53] Activation energy, Khan Academy. (n.d.). https://www.khanacademy.org/science/high-school-biology/hs-energy-and-transport/hs-enzymes/a/activation-energy (accessed December 24, 2018).

[54] Tangram Technology Ltd. - Polymer-Shrinkage in plastics, (n.d.). https://www.tangram.co.uk/TI-Polymer-Shrinkage_in_plastics.html (accessed December 17, 2018).

[55] X. Li, G. Zhong, Z. Li, Non-isothermal crystallization of poly(L-lactide) (PLLA) under quiescent and steady shear conditions, Chinese Journal of Polymer Science. 28 (2010) 357–366. doi:10.1007/s10118-010-9015-z.

[56] R. Pantani, I. Coccorullo, V. Volpe, G. Titomanlio, Shear-Induced Nucleation and Growth in Isotactic Polypropylene, Macromolecules. 43 (2010) 9030–9038. doi:10.1021/ma101775h.

[57] M. Salmerón Sánchez, V.B.F. Mathot, G. Vanden Poel, J.L. Gómez Ribelles, Effect of the Cooling Rate on the Nucleation Kinetics of Poly(L -Lactic Acid) and Its Influence on Morphology, Macromolecules. 40 (2007) 7989–7997. doi:10.1021/ma0712706.

[58] C. Zhou, H. Li, W. Zhang, J. Li, S. Huang, Y. Meng, J. de Claville Christiansen, D. Yu, Z. Wu, S. Jiang, Thermal strain-induced cold crystallization of amorphous poly(lactic acid), CrystEngComm. 18 (2016) 3237–3246. doi:10.1039/C6CE00464D.

[59] M.L. Di Lorenzo, C. Silvestre, Non-isothermal crystallization of polymers, Progress in Polymer Science. 24 (1999) 917–950. doi:10.1016/S0079-6700(99)00019-2.

[60] M. Zinet, R.E. Otmani, M. Boutaous, P. Chantrenne, Numerical modeling of nonisothermal polymer crystallization kinetics: Flow and thermal effects, Polymer Engineering & Science. 50 (2010) 2044–2059. doi:10.1002/pen.21733.

[61] M. Li, D. Hu, Y. Wang, C. Shen, Nonisothermal crystallization kinetics of poly(lactic acid) formulations comprising talc with poly(ethylene glycol), Polymer Engineering & Science. 50 (2010) 2298–2305. doi:10.1002/pen.21755.

[62] S.J. Huang, P.G. Edelman, An overview of biodegradable polymers and biodegradation of polymers, in: G. Scott, D. Gilead (Eds.), Degradable Polymers:

Principles and Applications, Springer Netherlands, Dordrecht, 1995: pp. 18–28. doi:10.1007/978-94-011-0571-2_2.

[63] A. Göpferich, Mechanisms of polymer degradation and erosion, Biomaterials. 17 (1996) 103–114. doi:10.1016/0142-9612(96)85755-3.

[64] Fig. 68.2 Sequence of polymer-molecular weight, strength, and mass..., ResearchGate. (n.d.). https://www.researchgate.net/figure/Sequence-of-polymer-molecular-weight-strength-and-mass-reduction-over-time-6_fig2_285580293 (accessed January 9, 2019).

[65] C. Shasteen, Y.B. Choy, Controlling degradation rate of poly(lactic acid) for its biomedical applications, Biomedical Engineering Letters. 1 (2011) 163–167. doi:10.1007/s13534-011-0025-8.

[66] X-Ray Diffraction (XRD) - XOS, (n.d.). https://www.xos.com/XRD (accessed December 20, 2018).

[67] C. Rauwendaal, Polymer Extrusion, Hanser/Gardner Publications, Inc, n.d.

[68] T.A. Osswald, Polymer Processing Fundumentals, Hanser, 1998.

[69] Molding Guidelines and Processing Conditions For Complēt Long Fiber Composite Pellets » PlastiComp – Long Fiber Reinforced Thermoplastic Composites, (n.d.). http://www.plasticomp.com/long-fiber-material-processing-guide/ (accessed October 30, 2018).

[70] Basic Screw Geometry: Things Your Extruder Screw Designer Never Told …, (n.d.). http://www.slideshare.net/rbplastics/basic-screw-geometry-things-your-extruder-screw-designer-never-told-you-about-screws (accessed February 13, 2016).

[71] C. Paulson, Plastic Extrusion Training - The Metering Zone of the Screw - Paulson, Paulson Training Programs. (2013). https://www.paulsontraining.com/plastic-extrusion-training-metering-zone-screw/ (accessed October 30, 2018).

[72] General Tolerance Table Charts for Standard Shaft Hole Fits | Engineers Edge, (n.d.). https://www.engineersedge.com/general_tolerances.htm (accessed November 1, 2018).

[73] Bearing fit chart - shaft and housing radial clearance - Pacamor Kubar Bearings, (n.d.). http://www.pacamor.com/technical/shafthousing.php (accessed November 1, 2018).

[74] The 4 Types of FFF / FDM 3D Printer Explained (Cartesian, Delta, Polar), 3Dnatives. (2017). https://www.3dnatives.com/en/four-types-fdm-3d-printers140620174/ (accessed November 4, 2018).

[75] Processing.org, (n.d.). https://www.processing.org/ (accessed November 8, 2018).

[76] https://www.repetier.com/, Repetier Software. (n.d.). https://www.repetier.com/ (accessed November 8, 2018).

[77] 3D Printer Firmware - Which to Choose and How to Change It?, All3DP. (2018). https://all3dp.com/2/3d-printer-firmware-which-to-choose-and-how-to-change-it/ (accessed November 8, 2018).

[78] R. Pantani, F. De Santis, A. Sorrentino, F. De Maio, G. Titomanlio, Crystallization kinetics of virgin and processed poly(lactic acid), Polymer Degradation and Stability. 95 (2010) 1148–1159. doi:10.1016/j.polymdegradstab.2010.04.018.

[79] F.S. Senatov, K.V. Niaza, M.Y. Zadorozhnyy, A.V. Maksimkin, S.D. Kaloshkin, Y.Z. Estrin, Mechanical properties and shape memory effect of 3D-printed PLA-based porous scaffolds, Journal of the Mechanical Behavior of Biomedical Materials. 57 (2016) 139–148. doi:10.1016/j.jmbbm.2015.11.036.

[80] The Glass Transition, (n.d.). https://pslc.ws/macrog/tg.htm (accessed November 19, 2018).

[81] Multi-Material 3D Printing – 2018 Overview, All3DP. (2018). https://all3dp.com/2/multi-material-3d-printing-an-overview/ (accessed October 9, 2018).

[82] X. Xu, J. Chen, J. Zhou, B. Li, Thermal Conductivity of Polymers and Their Nanocomposites, Advanced Materials. 30 (2018) 1705544. doi:10.1002/adma.201705544.

[83] How to fix under-extrusion and improve print quality | Ultimaker, Ultimaker.Com. (n.d.). https://ultimaker.com/en/resources/21477-how-to-fix-under-extrusion (accessed October 9, 2018).

[84] J.P. Beaumont, Runner and gating design handbook: tools for successful injection molding, 2nd ed, Hanser, Munich ; Cincinnati, 2007.

[85] A. Duhduh, A.A. Rajhi, J.P. Coulter, The impact of the “4d-Rheoprinting” additive manufacturing technique on molecular orientation and thermal properties of polymeric parts, (2018) 5.

[86] Ingeo Biopolymer 2500HP Technical Data Sheet, (n.d.) 5.

[87] A.M. Harris, E.C. Lee, Improving mechanical performance of injection molded PLA by controlling crystallinity, Journal of Applied Polymer Science. 107 (2008) 2246–2255. doi:10.1002/app.27261.

[88] L. Běhálek, M. Maršálková, P. Lenfeld, J. Habr, J. Bobek, M. Seidl, STUDY OF CRYSTALLIZATION OF POLYLACTIC ACID COMPOSITES AND NANOCOMPOSITES WITH NATURAL FIBRES BY DSC METHOD, (2013) 6.

[89] Global additive manufacturing market 2018 | Forecast, Statista. (n.d.). https://www.statista.com/statistics/284863/additive-manufacturing-projected-global-market-size/ (accessed February 1, 2019).

[90] nasa trl levels - Google Search, (n.d.). https://www.google.com/search?q=nasa+trl+levels&hl=en&tbm=isch&source=iu&ictx=1&fir=OWyDnI4NGeAsHM%253A%252C_D8YctxGzHb1fM%252C_&usg=AI4_-kR_6b1of7fR6Rwxx9Xii-mktpnNUg&sa=X&ved=2ahUKEwizqM_34JjgAhVLlFQKHVD5AbgQ9QEwAnoECAUQBg#imgrc=OWyDnI4NGeAsHM: (accessed January 31, 2019).

[91] J. Lopez, Types of Innovation, Constant Contact Tech Blog. (2015). https://techblog.constantcontact.com/software-development/types-of-innovation/ (accessed January 29, 2019).

- Appendix

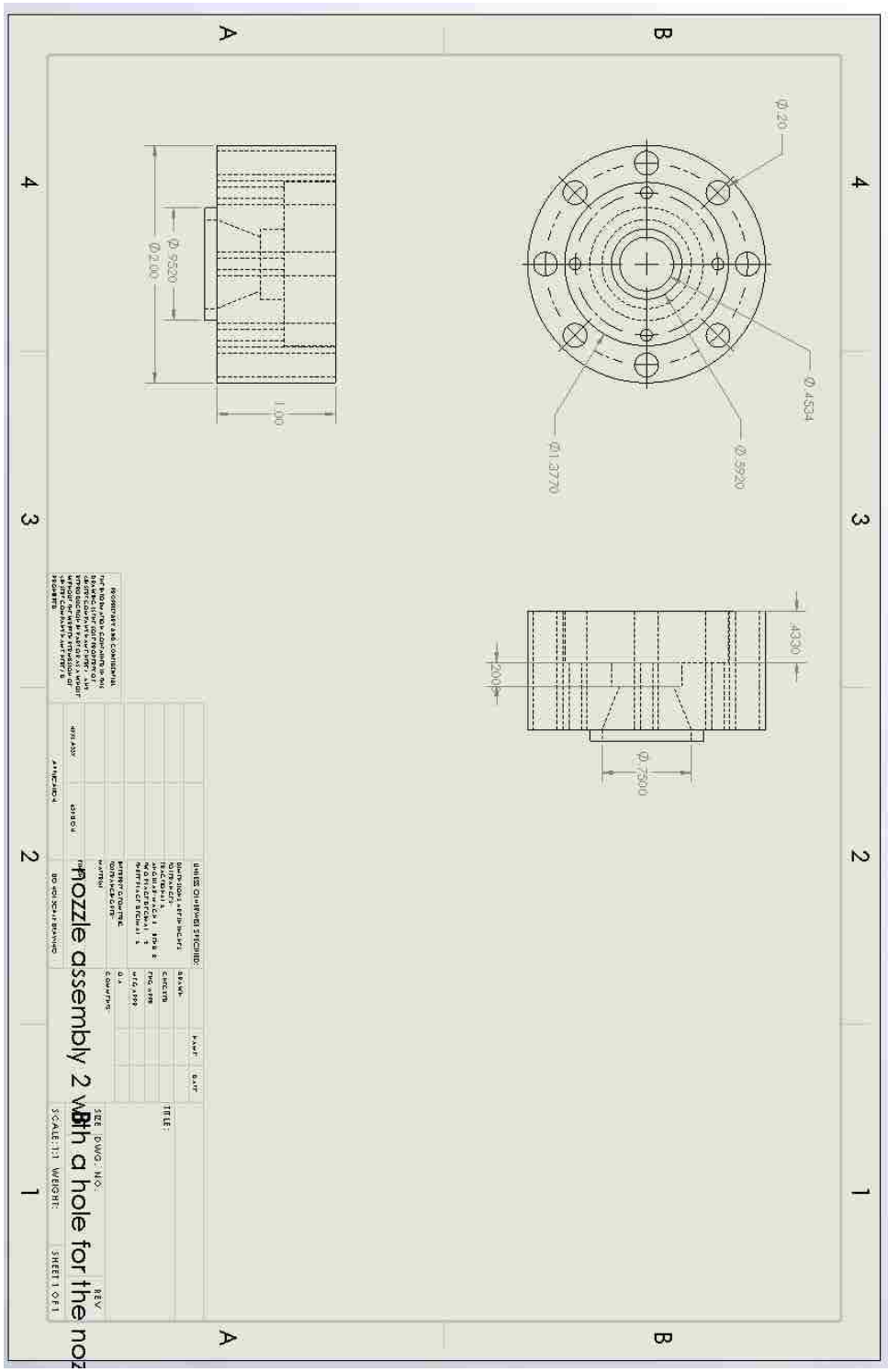
Ø.20
Ø.4534
Ø.3920
Ø1.3770
Ø.9520
Ø2.100
1.100
.4330
.200
Ø.7500
nozzle assembly 2 with a hole for the noz

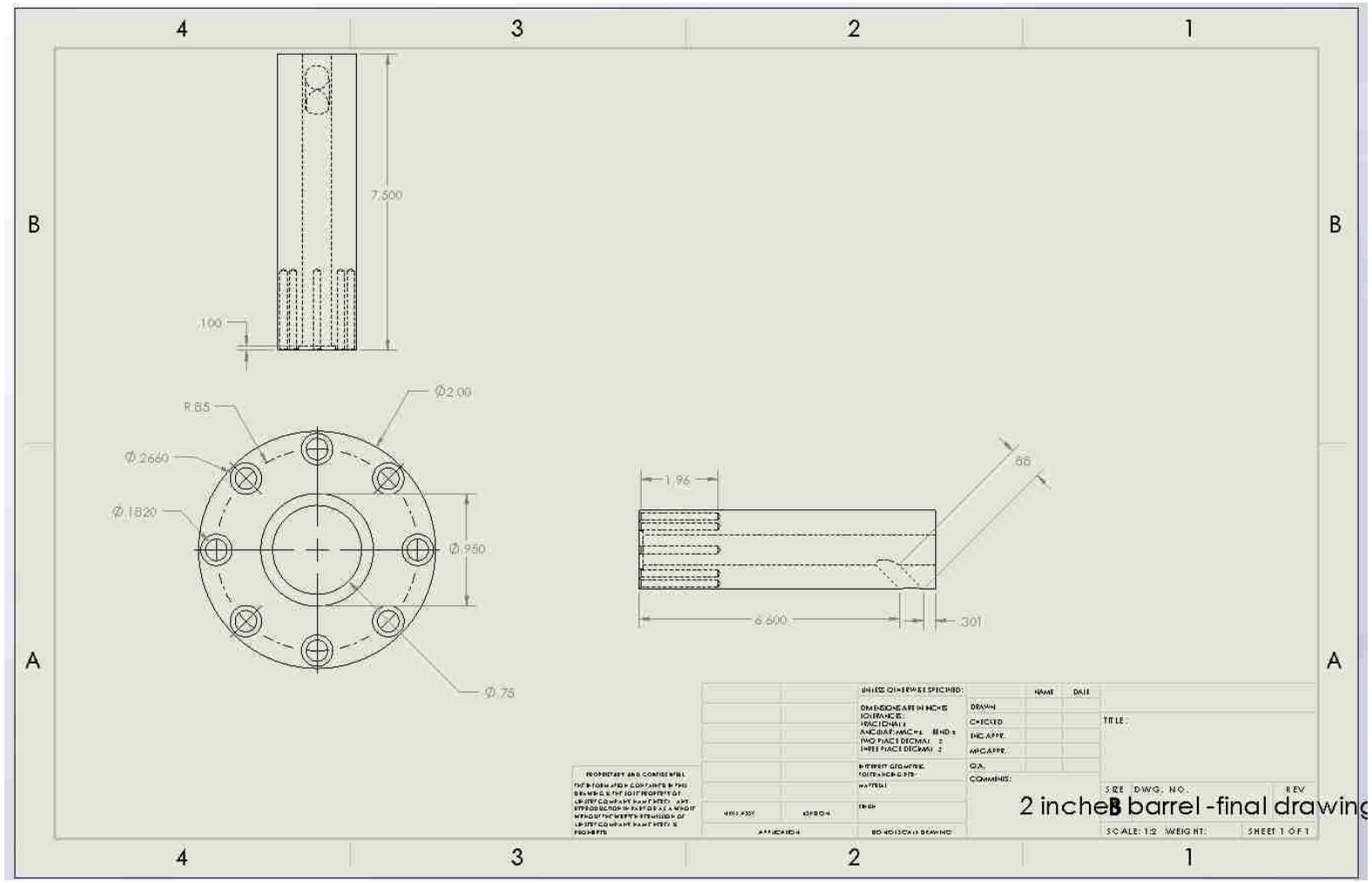
4
3
2
1
B
A
7.500
.100
R.85
Ø2.00
Ø.2660
Ø.1820
Ø.950
Ø.75
1.96
.88
6.600
.301
UNLESS OTHERWISE SPECIFIED:
DRAWN
CHECKED
ENG APPR.
MFG APPR.
Q.A.
COMMENTS:
NAME
DATE
TITLE:
SIZE
DWG. NO.
REV
SCALE: 1:2
WEIGHT:
SHEET 1 OF 1
2 inches barrel -final drawing

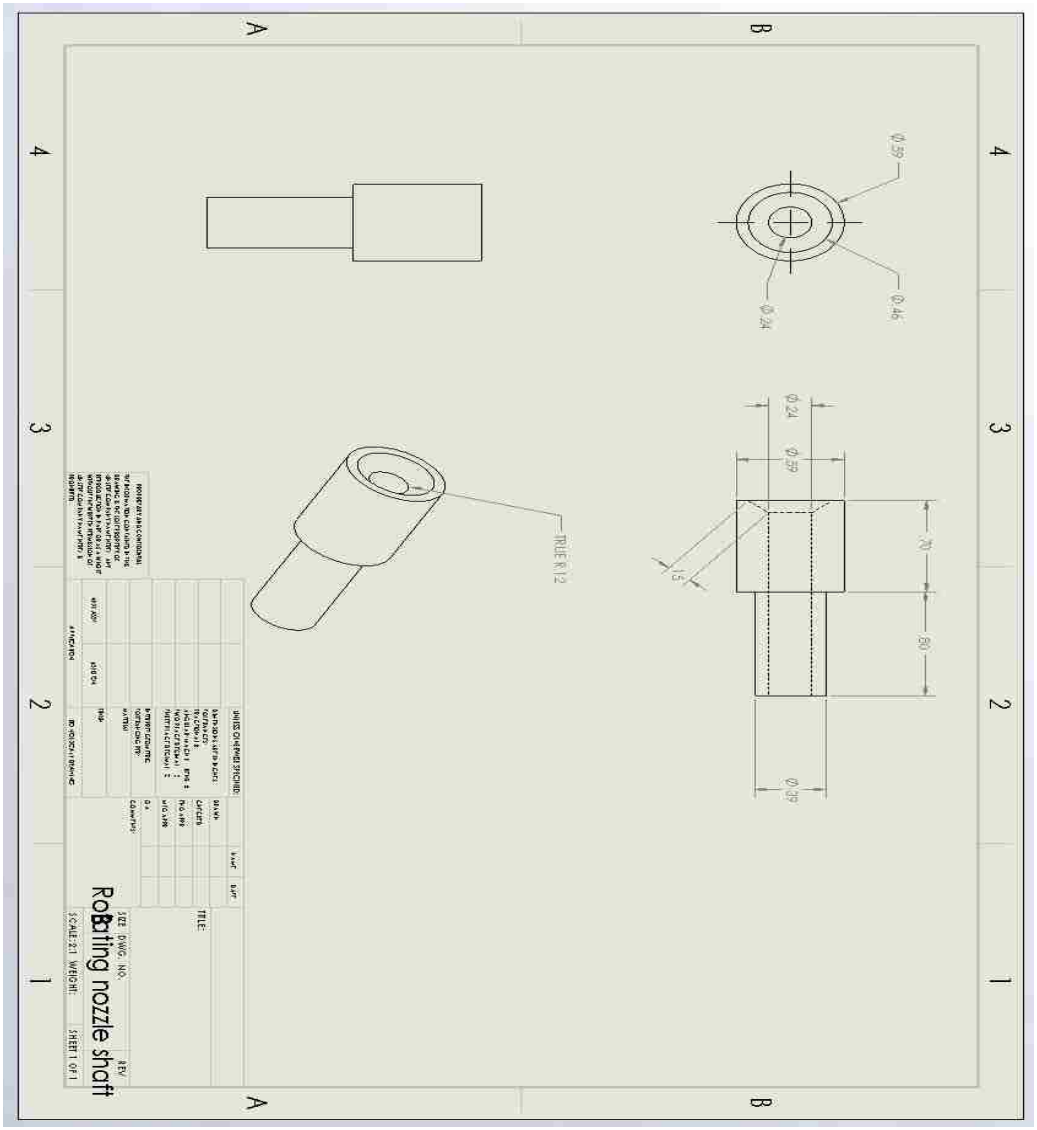
Ø.59
Ø.46
Ø.24
Ø.24
Ø.59
.70
.60
.15
Ø.39
TRUE R 1.2
Rotating nozzle shaft

VITA

Alaauldeen Duhsuh was born in Saudi Arabia. He received his B.S in Mechanical Engineering in 2008 from King Khalid University, and M.S in Mechanical Engineering and Mechanics from University of New Haven in 2011. Alaa has written numerous papers during his PhD. He has also presented his research at multiple professional conferences. During his graduate study at Lehigh, Alaa has served as a departmental graduate assistant in the department of Mechanical Engineering and Mechanics. Alaa was also the president of the Saudi Student Association at Lehigh University from 2016-2018.